ELECTRON MICROSCOPE STUDIES OF THE GROWTH OF CARBON ON METALS

by

BERNARD GRANT

Department of Chemistry, University of Glasgow.

Thesis submitted for the degree of

Doctor of Philosophy.

September, 1972.

ProQuest LLC.
789 East Eisenhower Parkway
P.O. Box 1346
Ann Arbor, MI 48106 – 1346

SUMMARY

The types of carbon formed on iron and nickel surfaces from gaseous precursors have been investigated. At 700°C three categories of carbon were distinguished.

Platelet graphite crystals up to 10 μ in extent were the initial carbon product of the hydrocarbon and acetone decomposition. They were deposited with basal planes parallel to the substrate surface and X-ray measurements of the inter-layer spacing showed that 100% stacking order prevailed. Small metal particles were present throughout the graphite lattice in a fine, possibly atomic, dispersion and it is suggested that these particles were the active catalysts in promoting the production of the highly crystalline platelet graphite at such a low temperature.

When the platelet graphite had covered the whole of the metal surface the crystal edges were observed to distort in order that the basal planes could extend in a non-horizontal direction. This corresponded to the onset of formation of the second type of carbon, termed here " non-oriented carbon" , which gave rise to randomly oriented polycrystalline diffraction patterns. With unsaturated hydrocarbons at high pressure (600 torr) this material resembled non-catalysed solid-phase carbons.

At the point of intersection of several platelet crystals gaps in the graphite matrix often occurred. Surrounding these areas were regions of graphite containing vertically oriented basal planes. It is thought that these sites were the nucleation points of fibrous graphite, the

third type of carbon deposit, which was observed to grow after the deposition process had continued for some time. The fibres had an external carbon wall of constant thickness, whose layer planes were aligned parallel to the fibre axis, surrounding an inner region also of constant diameter containing one or more metal catalyst particles. Minute particles of metal which individually were not visible in the electron microscope even under high resolution conditions were seen to agglomerate during oxidation of the fibrous graphite.

A novel mechanism for the growth of the fibrous material has been presented. It is based on the surface diffusion of individual metal atoms outwards from the central metal particle along the growing tip of the fibre wall. The theory accounts for the presence of metal within the carbon wall of the fibre and also for the observed arrangement of the graphite lattice planes.

At lower temperatures the carbon product of the pyrolyses was less ordered. Smaller crystals of graphite with nodular outcrops of material were formed and thin non-graphitic filaments of carbon often grew out from the nodular deposit.

The kinetics of the reactions were studied and the gaseous products of several interactions were identified by mass spectrometry with a view to obtaining more information on the mode of breakdown of the hydrocarbons on the metal surface.

ACKNOWLEDGEMENTS

This work was carried out in the Electron Microscopy section of the Chemistry Department which is at present under the direction of Professor D. Sharpe.

I would like to express my gratitude to Dr. J.R. Fryer and Dr. T. Baird for their supervision and wholehearted support throughout the course of these studies and during the writing of this thesis and to Dr. S.J. Thompson for the interest he has taken in this topic. I would like to thank my colleagues, past and present, in the microscopy group, especially John Hutchison, Katy Gray and Richard Tedstone, for many academic and non-academic exchanges over the past three years and also Mrs. H. Douglas and Mrs. C. Love for generous aid with the mass of photographic printing required for this thesis.

I wish to express my appreciation to my wife, Doreen, for her unfailing support and encouragement over this period and for her help in arranging the bibliography for this book. I am also indebted to Mrs. E. Callaghan for the typing of the thesis.

My thanks are due to the U.K.A.E.A. for financial assistance and to Mr. J. Wright and other members of the Applied Chemistry Division at A.E.R.E. Harwell for the use of, and their help with, microscopic facilities for a section of this work. I also wish to express sincere thanks to Dr. J.L. Hutchison of the Inorganic Chemistry Department, University of Oxford for his willing and skilful co-operation with the high resolution microscopy and to Mr. G. Mills of the National Engineering Laboratory, East Kilbride, for his help with the scanning microscopy.

BERNARD GRANT.

GENERAL CONTENTS

CHAPTER 1

INTRODUCTION

1. INTRODUCTION

Contents

1. INTRODUCTION

1.1 Carbon

1.1.1 Structure: Perfect graphite consists of layers of hexagonal networks of carbon atoms. The layers can be arranged in the form ABAB... corresponding to hexagonal packing (Hassel and Mark, 1924; Bernal, 1924) or in the form ABCABC... corresponding to rhombohedral packing (Lipson and Stokes, 1942). Both forms exist in natural graphite (Finch and Wilman, 1936; Boehm and Hofmann, 1955) and can be easily interchanged (Laidler and Taylor, 1940; Bacon, 1952) because of the low stacking fault energy of 0.51 ergs cm^{-2} involved (Baker et al., 1961). The distance between the layer planes at room temperature was measured by Nelson and Riley (1945) and found to be 3.3538 Å for natural graphite. However, it is known that basal plane dislocations in graphite corresponding to misalignments between successive layers, can increase the value of this (0002) spacing. Franklin (1951) related the exact value of the spacing to the percentage of disordered layers present; the (0002) spacing varies between 3.35 Å and 3.44 Å as the fraction of disordered layers present, the p factor, varies between 0 and 1. Bacon (1951, 1958) concluded that in graphitic carbons four different environments could exist, each

with its own characteristic c-spacing: (i) between two oriented layers, 3.35 Å; (ii) between two non-oriented layers, both being adjacent to non-oriented layers, 3.44 Å; (iii) between two non-oriented layers one having an oriented layer adjacent to it, 3.408 Å; (iv) between two non-oriented layers both being adjacent to oriented layers, 3.376 Å. The (0002) spacing measured by X-ray or electron diffraction is determined by the relative amounts of the four types of arrangements in any given form of carbon.

1.1.2 Non-Catalysed Carbon Deposition

When a carbon bearing gas is heated to a sufficiently elevated temperature it will decompose and a carbon deposit will result. Studies of the types of carbon formed under a wide variety of reaction conditions are summarised in Table 1.1.

1.1.2.1 Gas Phase Carbons It is found that carbons formed by homogeneous decomposition of gases (gas phase carbons) can be clearly distinguished from those deposited heterogeneously on surfaces (solid phase carbons). Iley and Riley (1948) described gas phase carbon formed at 800–1300°C as a soft, velvet-black pulverulent material whose properties were independent of the hydrocarbon and the formation temperature used. The inter-layer spacing, d_{002},

TABLE 1.1.

Non-Catalysed Carbon Deposition

Authors	Year	Gas	Pressure and Temperature	Surface	Results
Schutzenborger	1890	HCN	red heat	porcelain	a graphite oxide/acid of formula $C_{11}H_6O_6$ was formed, containing filaments.
Smith	1940				gases decompose to carbon via a polymerisation of C_2 species.
Iley et al	1948	various	800° to 1300°C	fused silica	gas and solid phase carbon and filaments formed independently of starting material.
Tesner et al	1952A 1952B	hydrocarbons hydrocarbons	700-1000° 1100-1250°	Pt/C carbon	C surface is catalytic for C deposition C filaments formed, especially in H_2.
Gomer et al	1955	CH_4, C_2H_6	1000-2300° 10^{-2} torr		no gas phase carbon deposits at very low pressures.
Kinney	1956	organic compounds	900-1400°		C deposits divided into 5 types.
Conroy et al	1959		500°C		type of C dependent on gas used.
			900°C		intermediates determine the C formed.

Austin	1959				description of pyrolytic C properties.
Cullis et al	1959	various	850-950° 50 torr	silica	orientation and crystallite size of C reduced by chlorine in reagent molecules.
Frazee	1959	hydrocarbon and additives			physical properties of C formed are independent of additive but chemical reactivity is increased.
Diefendorf	1960	hydrocarbons			pyrolytic carbons formed.
Melik-Zade et al	1960A,B,C. 1961A,B.	hydrocarbons	450°C	AlO_2 and SiO_2	ease of C formation dependent on type of reagent used.
Palmer	1962				review of pyrolytic carbons.
Thomas	1962	aliphatic hydrocarbons			mechanism of carbon formation suggested.
Palmer et al	1965				ease of C formation discussed.
Cullis et al	1965				gas and solid phase carbons compared.
Meyer	1969				irreversible changes in pyrolytic carbons examined.
Lewis et al	1969				type of C formed determined mainly by free radical intermediates.
Saha et al	1969				apparatus for pyrolytic C formation.
Cullis et al	1970,1971		900°C	metal/silica	C contains silica when present as reactor wall.
Tesner	1972	CH_4			kinetics of carbon formation.

was as large as 3.60 Å and the crystallite dimensions were L_C = 12-17 Å and L_A = 29-36 Å. Kinney (1956) obtained gas phase carbon at 900-1400°C and Conroy and co-workers (1959) also found that the gas phase carbon black formed above 900°C was independent of the structure of the original hydrocarbon reagent but was determined by the species intermediate in the carbon deposition process. The review of carbon deposition by Palmer (1962) concluded that gas phase soot-like carbons had low adherence with dimensions, d_{002} = 3.61-3.70 Å, L_C = 12 Å, L_A = 42 Å. Further discussions by Palmer and Cullis (1965) on carbon formation in flames stated that the extent of carbon deposition depended on the type of hydrocarbon being burned. Soot formation increased with degree of unsaturation and with chain branching but decreased with molecular weight except for paraffins. Gomer and Mayer (1955) found, as would be expected, that no gas phase carbon was produced at 1000-2300°C at very low hydrocarbon pressures (below 10^{-2} torr).

1.1.2.2 Solid Phase Carbons Iley and Riley (1948) described the two main types of solid phase deposits formed at 800-1300°C as shiney, vitreous, columnar carbon and filamentous carbon. The filamentous material was also detected by Tesner et al (1952B) around 1200°C but in general it is a minor product in these reactions. As noted for gas phase carbon, the

properties of the solid phase deposits (Iley and Riley, 1948) were independent of the nature of the hydrocarbons used, but the crystallite size increased as the deposition temperature was raised, L_C from 16 Å to 29 Å and L_A from 31 Å to 42 Å. Conroy et al.(1959) and Austin (1959) discussed the properties of pyrolytic carbons and Kinney (1956) classified the types of carbons which are produced:

Type A is a hard, brittle, lustrous material adhering well to surfaces.
Type B is a sooty, poorly adherent gas phase carbon.
Type C is a mixture of types A and B.
Type D is a grey, feathery material appearing to grow out of type A.
Type E occurs with type D but has a brownish, spongy character and is located on its downstream side.

Melik-Zade et al.(1960A,B,C, 1961A,B) have observed that the amount of carbon formed on SiO_2/AlO_2 surfaces at 450°C is dependent on the hydrocarbon used, ease of carbon deposition increasing with molecular weight for paraffins and with degree of unsaturation. Conroy and coworkers (1959) indicated that only below 500°C is the structure of the decomposing gas important in determining the type of carbon formed but Cullis et al.(1959) showed that the presence of chloride in reagent molecules caused a reduction in orientation and in crystallite size of the resultant carbon deposit

at 850-950°C because of the decrease in carbon atom mobility. Oxygen-rich chars produced totally amorphous deposits below 1200°C (Gibson et al., 1946) proving that the product was determined by the character of the starting molecules. It is evident that only for hydrocarbon decomposition is the structure of the carbon independent of the starting material above 500°C.

Cullis and Norris (1970, 1971) discovered that the silica surface often used in reaction vessels is not completely inert during the pyrolysis process and up to 1% Si can be detected in the carbon deposits. If $SiCl_4$ is added to decomposing CH_4, silicon can form β SiC in the deposits. At 900°C silica readily diffuses into graphite and even just about 650°C some diffusion is evident during prolonged experiments (Fryer, 1970).

The nature of the intermediates formed by hydrocarbon decomposition is of crucial importance in determining the mechanism of pyrolytic carbon formation. It has long been thought that polymerisation of C_2 species was involved (Smith, 1940). Gaseous additives are known to affect the chemical reactivity of deposited carbons (Frazer et al, 1959) probably because of the resulting free radicals. Thomas (1962) suggested that free radical polymerisation of C_1 and C_2 species to form conjugated polyene and polybenzenoid

radicals was a stage in the build up of crystallites. The review by Palmer (1962) considered that below 800°C cyclisation and condensation of aromatic molecules resulted in the formation of reagent-dependent carbons. At higher temperatures aromatic rings decompose and hydrocarbons tend to form reagent-independent carbon by the reaction sequence:

$$\text{hydrocarbon} \rightarrow \overset{C_2H_2}{\underset{+\ H_2}{\rightarrow}} C_4H_4 \rightarrow \overset{C_4H_2}{\underset{+\ H_2}{\rightarrow}} \rightarrow \begin{matrix}\text{various radicals}\\ \text{e.g. acetylenic}\\ C_6H_6, C_3 \text{ species etc.}\end{matrix} \rightarrow C$$

1.1.2.3 Investigation of Pyrolytic Carbons It was reported by Debye and Scherrer (1917) that carbons formed by low temperature pyrolyses gave three diffuse bands in X-ray powder photographs. These were recognised to be related to the graphite X-ray pattern and it was suggested that carbon black was similar to graphite but existed in a finer state of subdivision. Warren (1934, 1941), proposed that hexagonally arranged crystals were present in carbon black among disorganised carbon and Hofmann and Wilm (1936) observed that the temperature of formation of the carbon above 1400°C determined the L_A and L_C values and inter-layer spacings of the crystallites. At a deposition temperature of 1000°C no interlayer order was detected (White and Germer, 1941) and hence Biscoe and Warren (1942) used the word " turbostratic" to describe a substance such as carbon black which has only two-dimensional order. The work of Hall (1948),

Mizushima (1959) and Grisdale and coworkers (1951, 1953) established that the crystallites in carbon black had a tendency to rientate with basal planes parallel to their surfaces. This was variously regarded as " tangential layer plane orientation" or " concentric crystallite orientation" .
The most recent studies (Ergun, 1968; Heckmann and Harling, 1966, 1969) have determined that the crystallites are in fact arranged approximately parallel to the particle surface but with a range of possible deviations on either side of the mean. This is known as the " curving statistical crystallite orientation" model.

The observation that pyrolysis temperature determines to a large extent the crystallite dimensions in carbon black particles (Hofmann and Wilm, 1936) led to experiments which showed that heat treatment caused a decrease in the value of inter-layer spacing towards that of natural graphite (Biscoe and Warren, 1942; Bacon, 1951, 1952). Franklin (1950, 1951A,B) proved that the course of this graphitisaton could be followed quantitatively by measuring changes in the observed d_{002} values. She related these values to the p factor (see earlier section) by means of the equation,

$$d_{002} = 3.440-0.086\ (1-p^2).$$

Later, Maire and Mehring (1960) correlated d_{002} values with the degree of graphitisation, g, as defined by,

$$d_{002} = 3.354\ g + 3.440\ (1-g),$$

and Fitzer et al.(1965) used the increase in L_C values as a criterion for graphitisation, rather than d_{002} values. The ultimate perfection which can be achieved by graphitisation was shown to be limited by particle boundaries (Pinnick, 1951) and by internal porosity developed during heat treatment (Imperial and Walker, 1957).

Recent work has been concerned with the catalytic effect of electron bombardment (Mackowsky, 1956) and metals (Schwartz et al., 1967; Weisweiler, 1970; Gillot et al., 1969; Oberlin et al., 1971) on the graphitisation of compact, soft (graphitisable) carbons and porous, hard (non-graphitisable) carbons. A review of the catalytic graphitisation literature is given by Marsh and Warburton (1970).

Table 1.2 summarises the investigations discussed in this section.

1.1.3 Catalysed Carbon Deposition

1.1.3.1 Introduction

Much work has been carried out on the carbon formed by the breakdown of gaseous molecules on metal surfaces. As early as 1871 Bell realised that iron, cobalt and nickel were particularly suitable for this

TABLE 1.2

Investigations of Pyrolytic Carbons

Authors	Year	Results
Debye et al.	1917	X-ray examination of carbon black suggested that it was essentially similar but more finely divided than graphite.
Warren	1934	X-ray results showed that hexagonal crystallites were present among disorganised carbon in carbon black.
Hofmann et al.	1936	Properties of charcoals were discussed. Above 1400°, formation temperature determines L_C and L_A, which increase as the (0002) value decreases.
White et al.	1941	Carbon black formed at 1000°C was shown by electron diffraction to contain crystallites in which carbon atoms are arranged in hexagonal layers. No interlayer order found.
Warren	1941	Theory of X-ray diffraction in random layers as in C black.
Biscoe et al.	1942	Carbon black has a 2 dimensional structure identical to graphite but with a larger turbostratic inter-layer spacing. Heat treatment causes graphitisation around 3000°C.
Gibson et al.	1946	The turbostratic theory of carbon blacks does not apply to carbons formed from oxygen rich chars at 1200°C.
Hall	1948	Dark field electron microscopy showed that some carbon blacks have crystallites whose layers are approximately parallel to their particle's surface.
Bacon	1950, 1951	Graphitisation causes an increase in L_A and L_C and a decrease in interlayer spacing, due to a reduction in non-orientated layers.

TABLE 1.2 (contd.)

Authors	Year	Results
Franklin	1950, 1951A,B	Quantitative study of graphitisation denoted by changes in p, the fraction of non-oriented layers. Graphitisable and non-graphitisable carbons were differentiated.
Pennick	1952	Graphitisation at 300°C led to crystallites of about one-third of the overall particle size; graphitisation is limited by particle boundaries.
Grisdale et al.	1951, 1953	Carbon formed on ceramic sand surfaces has basal planes approx. parallel to the substrate surface. Carbonisation and carbon deposition compared.
Mackowsky et al.	1956	Graphitisation of coal particles by bombardment with an intense electron beam in the electron microscope.
Imperial et al.	1957	Carbons heated at 10 atmospheres to 3600°C contain residual 10% turbostratic character because of porosity.
Mizushima	1959	Discusses the competition between 2- and 3-dimensional growth of crystallites during graphitisation.
Maire et al.	1960	Discusses 2 and 3-dimensional growth in terms of g, the degree of graphitisation.
Fitzer et al.	1965	Use L_C as criterion for graphitisation phenomena rather than the (0002) value.
Heckmann et al.	1966, 1969	Discuss the carbon black "statistical crystallite" model and earlier models.
Notz	1967	Carbon particles separated by thoria treatment and examined by electron microscopy.

TABLE 1.2 (contd.)

Authors	Year	Results
Schwartz et al.	1967	Graphitisation of carbons is catalysed by 5-7% titanium.
Rudee	1967	Domain structure of carbon blacks studied.
Ergun	1968	Carbon black model developed similar to Heckmann.
Maahs	1969	Relationship between L_c and d_{002} obtained for graphite.
Reiger	1970	During graphitisation L_c increases with time, and d_{002} improves with temperature, in general.
Weisweiler	1970	Carbon from polyfurfuryl alcohol graphitised in contact with a Ni/C melt at 1360°.
Roscoe et al.	1970	Carbon stress recrystallised at 3000°C can be grown to 70μ.
Marsh et al.	1970	Review of the catalytic graphitisation literature.
Oberlin et al.	1971	Iron added to hard carbons treated at 1600-1800°C allows graphitisation.

purpose. Later workers (Tropsch et al., 1925; Baukloh et al., 1941; Olmer, 1942; Kehrer et al., 1954; Hughes et al., 1962) have considered the effect on the carbon deposition process of a wide range of metals and have shown that iron, cobalt and nickel give optimum results.

A variety of gases have been used for the studies. Bannerjee et al. (1961) deposited carbon from carbon suboxide, C_3O_2, at 713°C and found that good quality graphite formed on nickel whereas amorphous carbon accumulated on platinum, copper and porcelain substrates. Most earlier experiments used carbon monoxide, as its use in the Fischer/Tropsch synthesis of hydrocarbons had become familiar. Fischer et al. (1926) used iron, cobalt and nickel to catalyse the conversion of hydrogen/carbon monoxide mixtures to hydrocarbons and suggested that the metal carbides were the active species. Further work (Fischer et al., 1928A) indicated an order of activity: Fe > Ni > W > Mo > C. Bahr et al. (1928A) showed that Ni_3C could convert CO/H_2 mixtures to CH_4 at 250°C. However, later work by Weller et al. (1948) and Kimmer et al. (1948A and B) cast doubts on these earlier ideas. The most recent studies have been performed using a variety of hydrocarbon reagents.

1.1.3.2 Carbon Deposition from Carbon Monoxide. Types of Carbon Formed. Essentially three classes of

carbon deposits can be obtained from gaseous pyrolysis: filamentous carbon, single crystal graphite and polycrystalline carbon. There is a continuous gradation between the single crystal and polycrystalline forms of deposit as the temperature of reaction, gas pressure and other variables are gradually altered.

At lower temperatures, usually below 600°C but depending on the conditions, vermicular/filamentary carbon is formed often along with polycrystalline carbons resembling carbon black (Radushkevitch et al., 1952). At 390°C Hofer, Sterling and McCartney (1955) found that Fe, Ni, Co gave vermicular deposits containing metal among the carbon and Davis et al. (1953, 1954, 1957) examined filaments formed in blast furnaces around 450°C.

At temperatures above approximately 600°C single crystal or platelet graphite is formed as well as filamentous carbon. Akamatsu et al. (1954) showed by electron diffraction the existence of three-dimensional order in the carbon. At 550°C on iron Ruston and co-workers (1969) obtained filamentous carbon grown from Fe_7C_3 crystals and lamellar (platelet) graphite formed by the decomposition of Fe_3C. Renshaw et al. (1970, 1971) using iron, nickel and cobalt single crystals also obtained platelet and filamentary carbon, the larger platelets being formed especially at 800°C, the highest temperature used.

Leidheiser and Gwathmey (1948) have shown that carbon is deposited preferentially on the (111) face of nickel from a CO or CO/H_2 atmosphere. Further work by Kehrer and Leidheiser (1954) indicated for iron, cobalt and nickel that minor faces, especially ones around the (111) are the most active.

The Catalyst in the Carbon Formation from Fe/CO.

The most common substrate used in carbon monoxide pyrolyses is iron. Table 1.3 summarises the conditions which have been used to study this system and gives the most important results obtained from them. It can be seen that there is a wide range of suggested catalytic species.

Many workers have shown that free iron is necessary for carbon deposition from CO (Chatterjee et al, 1954; Olmer, 1942; Juliard et al, 1948). Others have suggested that an iron/iron oxide interface is the actual catalyst (Chufarov, 1946; Chufarov et al., 1947; Taylor, 1956).

Akamatsu and Sato (1949) showed that at 500°C iron is first converted to Fe_3C before being coated with carbon. A similar study by Berry and co-workers (1956) on catalysis by iron oxide indicated that the oxide had to be converted to a carbide for the reaction to take place. Between 400°C and 565°C Hagg carbide (Fe_2C) was believed to be the catalyst and between 565°C and 700°C a cementite (Fe_3C) with an abnormally

TABLE I.3

The Decomposition of CO on Iron and Iron Compounds

Authors	year	temperature	material	results
Bell	1871	range	iron oxides	optimum temp. 400-450°C
Boudouard	1899A-F 1900A,B,1901	445-925°	iron oxides	$CO \rightarrow CO_2 + C$ equilibrium studied. A carbonyl suspected
Hilpert et al	1915	below 800° 850° 950°	Fe_2O_3	$CO \rightarrow C$, very fast $CO \rightarrow C + Fe_3C$, fast $CO \rightarrow C$, slowly } Fe_3C is catalyst
O'Hara et al	1923	450-800°	iron and iron oxides	oxide is reduced to iron, which catalyses the reaction.
Fischer et al	1925,1926 1928B	range	iron	Fe_3C is catalyst, carbonyl is not involved.
Waugenheim	1927	below 650°	Fe_2O_3	$Fe_2O_3 \rightarrow Fe$, during deposition
Hofmann et al	1928,1930	400-450° 450-650° 650-700° 275,320°	Fe Fe Fe Fe_2O_3	$C + Fe_3O_4$ formed, little Fe, Fe_3C. $C + FeO$ formed, some Fe, Fe_3C, Fe_3O_4 Fe, C, Fe_3C formed, no oxides Fe_3O_4, Fe_3C, Fe_2C formed also 'X' carbide detected.

Tutiya	1929,1930A,B		Fe Fe_2O_3	Fe is catalyst donor, Fe_3C is catalyst 'X' carbide is iron oxide. $Fe_2O_3 \rightarrow Fe_3C$ during reaction.
Olmer	1942	400-900°	iron, oxide and carbide	only Fe catalyses the CO decomposition.
Chufarov	1946	range	iron ores	optimum temperature is 500°. Fe/Fe_3O_4, Fe_3O_4/Fe_2O_3 interfaces are catalysts.
Chufarov et al	1947	350-750°	iron	optimum temp.= 550°C
Juliard et al	1948	800°	Fe_2O_3	$Fe_2O_3 \rightarrow Fe_3O_4 \rightarrow FeO \rightarrow Fe$. carbon forms only after Fe forms.
Baukloh et al	1936,1940,1941 1942,1950	range	iron and iron oxide	only Fe catalyses carbon formation. inactive carbide forms.
Chatterjee et al	1954	approx.550°	iron and carbide	only Fe catalyses reaction.
Akamatsu et al	1949	500°	iron	$Fe \rightarrow Fe_3C \rightarrow C$, Fe_3C is catalyst carbon gives (hkl) reflections.
Hofer et al	1955	300-800° 390°	iron	iron, carbon, carbide all present carbon filaments formed.
Trillat et al	1950A,B 1951A,B,C	350-800°	iron films	products similar to Hofmann et al (1928,1930).
Fleureau	1953	450-1200°	iron	products similar to Hofmann. maximum rate at 500°. Iron carbonyl→C+Fe_3C.
Raduskovitch et al	1952	600°	iron	single and multiple C threads formed.

Kehrer et al	1954	550°	single crystal iron	rate depends on crystal face. Fe_3C forms before C.
Davis et al	1953,1954 1957	450°	iron and iron oxide	oxide → iron → carbide, which is found in C threads formed.
MacIver et al	1955	400°	iron	element analysis and surface areas of carbons examined.
Taylor	1956	400-1000°	iron, iron oxide	Fe_3O_4/Fe interface is catalyst.
Berry et al	1956	400-565° 565-700°	iron oxide	Hagg carbide is catalyst. abnormal Fe_3C is catalyst.
Walker et al	1959A,B	450-750°	iron	variation of C with conditions. Fe is catalyst, Fe_3C is spent catalyst.
Schenk et al	1960	550°	Fe_2O_3/carbon	rate dependent on temp.
Haas et al	1968	400-1075°	iron pellets	iron is catalyst.
Ruston et al	1969	550°	iron	filamentary C catalysed by Fe_7C_3. lamellar C catalysed by Fe_3C.
Walker et al	1970	800°	several catalysts	activity dependent on oxide film, interface effects etc.
Renshaw et al	1970	550-800°	Fe and Si/Fe single crystals	γFe_2O_3 is catalyst due to its defect structure. αFe_2O_3 is not.

low Curie Point was responsible for the carbon deposition.

Against this evidence for catalysis by iron carbides Walker, Rakszawski and Imperial (1959A and B) showed that loss of catalytic activity by iron was accompanied by a gradual conversion to Fe_3C. Upon addition of hydrogen, which restores the Fe_3C to iron, the activity was regained. This finding is in agreement with earlier conclusions by Baukloh et al. (1936, 1940, 1941, 1942, 1950). These authors used iron and iron oxides and discovered that the oxide was reduced to the free metal which then catalysed the carbon formation until it was gradually carburised. Regeneration occurred, as with Walker et al.(1959A and B) whenever hydrogen was added to the inactive carbide. Other workers, including Trillat and Oketani (1951A) also found that the presence of hydrogen aided the carbon deposition process.

Walker and Thomas (1970) realised that some of the conflicting ideas as to the active species in the Fe/CO reaction were due to the critical dependence of the iron's activity on the thickness of any iron oxide film present and on the exact nature of the iron/iron oxide interface. The observation by Baukloh et al.(1950) that the activity of iron formed by reduction of oxides is dependent on the temperature

at which the reduction is carried out is interesting in this respect. The lower the temperature of formation of the iron the greater the defect concentration in its lattice and the higher the activity found. Recent work by Renshaw, Roscoe and Walker (1970) on Fe and Si Fe single crystals has reasoned that γFe_2O_3 due to its defect structure (see section 1.2.1.) is catalytically active whereas αFe_2O_3, formed in their system above 550°, having a lower defect concentration is less active. In support of this theory they have found that the rate of carbon deposition decreases above 550°C.

Comparison of Iron, Nickel and Cobalt as Catalysts for CO Decomposition.

There is no general agreement in the literature on the relative efficiencies of the three main metals used as catalysts. Boudouard (1899A) said that cobalt and nickel oxides were much superior to iron oxide as catalysts. If the reduction of some metal oxide to metal is necessary for carbon formation to occur, as was suggested by the work of Juliard et al. (1948) for nickel and iron, this would explain the order of catalysis found by Boudouard since iron oxide is the most difficult to reduce. Schenck (1927A) reported that cobalt was better than iron and probably was present during the reaction as mixed crystals of cobalt and cobalt carbide. He found that above 668°C

TABLE 1.4

The Decomposition of CO on Iron, Nickel and Cobalt

Author	year	temperature	material	results
Bell	1871	range	Fe,Co,Ni oxides	oxides are catalysts, different ones work at different optimum temp.'s
Boudouard	1899A-F, 1900A,B,1901	445-925°	Fe,Co,Ni oxides	Co,Ni better catalysts than Fe.
Fischer et al	1925		Fe,Co,Ni oxides	all acted as catalysts.
Fischer et al	1928A		many metals	activity, Fe > Ni > W > Mo > C.
Bahr et al	1928B	range	Ni,NiO	$Ni/NiO \rightarrow Ni_3C \rightarrow Ni+C$.
Olmer	1942		many metals	only Fe,Co,Ni are active catalysts.
Juliard et al	1948	600° 800°	NiO Fe_2O_3	NiO → Ni, after which C forms. $Fe_2O_3 \rightarrow Fe$, after which C forms.
Hofer et al	1955	300-800°	Fe,Ni,Co	vermicular C of several types forms. Metal or carbide in filaments.
Baukloh et al	1950	range	Fe,Ni,Co	Co,Fe activity greater than Ni. each have different optimum temp.'s
Leidheiser et al	1948	550°	single crystal Ni	rate (111) face greater than (110), (100).

Kehrer et al	1954	range	Fe,Co,Ni single crystals	rate dependent on crystallographic face exposed.
Henry	1963		general metal	mathematical model for C formation.
Grenga et al	1966		Ni film [single crystal]	C deposit type dependent on plane exposed.
Walker et al	1970	800°	various Fe,Co, Ni catalysts	activity Fe Co Ni. faceting of catalyst occurs.
Renshaw et al	1970	400-800°	Fe,Fe/Si single crystals	Fe_2O_3 is catalyst.
	1971		Co,Ni single crystals	Ni and Co carbides are catalysts.

the carbide was the catalyst, and even below 668°C it appeared to be involved in the mechanism of carbon deposition. Baukloh and co-workers (1950) found that nickel had lower activity than iron or cobalt and that its optimum efficiency was at a lower temperature than those of the other two metals. Walker and Thomas (1930) used a wide variety of iron, nickel and cobalt catalysts using as an atmosphere a CO/H_2 mixture and found the order of activity to be Fe > Co > Ni.

In summary, the more recent findings appear to indicate that iron is the best catalyst for the conversion of CO to carbon in the conditions normally employed. This is particularly true when hydrogen is added to the CO presumably because this suppresses the formation of more than minute traces of oxide. The major results achieved by workers in the field of carbon monoxide decomposition over metals are listed in Table 1.4.

1.1.3.3 Carbon Deposition from Hydrocarbons

Types of Carbon Formed. In general, similar classes of carbon can be formed from decomposition of hydrocarbon molecules as have been described for CO pyrolysis. Table 1.5 summarises the carbon products obtained by reaction of hydrocarbons over metal substrates.

Several early workers (Robinovich et al, 1959; Nemetschekt, 1959) detected carbon filaments in the

TABLE 1.5

The Decomposition of Hydrocarbons on Iron Nickel and Cobalt

Authors	year	gas	temperature	pressure	solid	results
Robinovich et al	1959	CH_4	925-1000°C	-	Fe,Co,Ni	carbon filaments formed.
		C_6H_6/N_2	830-930	-	Fe,Co,Ni	carbon filaments formed.
		several	800-1250°	-	variety	Fe,Co,Ni are catalysts.
Nemetschekt	1959	several	-	-	Fe oxide	C fibres with 20Å structure.
Shirasaki et al	1965	C_2H_4	400-435°		Ni	mosaic and irregular C film formed.
		iso C_8H_{18}				C formed by a different mechanism from C_2H_4 decomposition mechanism
Karu et al	1966	CH_4	800-1050°	3 -10	Ni foil	single crystal graphite formed.
			800°			single and polycrystalline C formed.
Escombes et al	1967	several	low temp.'s	-	divided Ni	graphite and nickel carbide formed.
Tamai et al	1967	CH_4	900°,1020°	300 torr	several	only metals with unstable carbide are active for C formation.
	1968	several	870-1030°	600 torr	Fe	C and Fe_3C formed } kinetics
					Ni	Ni and C formed } studied.
McCarroll et al	1969	C_2H_4, H_2S		10^{-6} torr	Ni	Ni surface configuration altered.

Presland et al	1969	C_2H_2	1000°C	10^{-2} torr to 100 torr	Ni and Pt	graphite formed, pretreatment affecting its production.
Robertson	1968,1969 1970,1972	CH_4	650,750°	600 torr	Fe,Co,Ni	single crystal,fibrous C formed metal contained in deposit.
Tesner et al	1970	C_2H_2	450-700°	-	nichrome	kinetics of G fibre production studied.
Maire et al	1970	several	20-350°	very low	Ni	ordered C forms below 350°C.
Presland et al	1970	C_2H_2	1000°	0.5 torr	Ni,NiO	NiO inhibits laminar graphite formation.
Blau et al	1970	C_2H_2	800-1200°	0.1-0.5 torr	Ni foil	laminar graphite forms below 0.4 torr, nodular C above 0.4 torr.
Saito et al	1971	several	600°	range	Fe,Ni	C_2H_2 is best for C deposition, amorphous Ni is best catalyst.
Lobo et al	1971A	olefins and C_2H_2	350-800°	100 torr	Ni	rates studied and activation energies found.
	1971B	range		range	several	C formation kinetics and morphology studied.
Haddon	1972	butadiene	200-700°	600 torr	Fe,Ni	carbon filaments examined.

product of hydrocarbon breakdown reactions. Robertson (1968, 1969, 1970, 1972) studied the carbon fibres produced from CH_4 decomposition on Fe, Co, Ni foils at 650°C and 750°C. His work indicated that formation of this material is caused by metallic catalyst particles which are extruded from the metal substrate and maintain a position at the fibre tip as it grows from the deposit surface. Normally an outer coating of crystalline carbon was observed with a hollow inner region containing the catalyst particle. The outer carbon layer was concluded to be non-graphitic (Robertson, 1970) as no general $(h,k,\overline{h+k},l)$ reflections were observed, but it was discovered that the (0002) planes were preferentially orientated parallel to the fibre growth axis [as was found by Davis et al. (1957) for fibres formed by CO/Fe interactions]. An attempt to classify the fibres was made (Robertson, 1968) according to whether metal occurred only at the tip of the fibre or throughout the fibre length.

Karu and Beer (1966) demonstrated that it was feasible to grow single crystals of graphite by passing methane at low pressures over a nickel foil heated to between 800°C and 1050°C. At methane pressures greater than 10^{-2} torr no graphitic film was obtained and at lower temperatures, 700°C to 800°C, polycrystalline and single crystal deposits formed.

Presland and Walker (1969) were able to show that graphite films formed by pyrolysis of acetylene over nickel at 1000°C were oriented with their basal planes parallel to the metal surface. Later work (Presland et al, 1970) proved that a surface oxide coating inhibited the formation of this laminar graphite although a less ordered carbon continued to be deposited. A prior anneal (in vacuo, hydrogen or nitrogen) removed any metal oxide present and prevented impurity affecting the course of the deposition process.

Kinetics of Carbon Deposition from Hydrocarbons.

The work of Cunningham et al. (1957) has suggested that there are major differences between the mechanisms of carbon monoxide and hydrocarbon decomposition over metals. They found that for the formation of carbon by C_2H_2 decomposition over nickel single crystals the (111) planes were least active, in contrast with the results for CO decomposition over nickel mentioned earlier (Leidheiser et al, 1948; Kehrer et al., 1954). This may be due, as Walker and Thomas (1970) have suggested, to the dependence of the CO pyrolysis on the presence of trace amounts of oxide.

The kinetics of the breakdown of hydrocarbon on iron, cobalt and nickel depend on the mode of heating used in the reaction system. Lobo and Trimm (1971), using a furnace which heated the gas, found that

after induction and acceleratory periods the rate of carbon formation from nickel/olefin and nickel/acetylene interactions was constant for long reaction durations. The rate of reaction increased as the temperature was raised until a maximum around 500°C was reached, after which the rate decreased to a miminum about 550° and increased thereafter. The first region (below approximately 500°C) had an activation energy of about 30 Kcals./mole, independent of the hydrocarbon used and was believed to be due to heterogeneous decomposition of the gas on nickel. Above 550°C the activation energy corresponded to that expected for homogeneous pyrolysis and the rate of reaction of acetylene in this temperature region was proportional to the square of its pressure. This is clear evidence for homogeneous decomposition occurring above 550°C on this system. Some work on ethane decomposition on nickel (Lobo, 1971) indicated that the rate rose with temperature between 500°C and 650°C and perhaps increased with reaction duration and hydrogen presence. Haddon (1972) found on heating a tapered nickel foil in a butadiene atmosphere that the areas of thickest carbon deposit occurred at approx. 450°C and at the hottest region of foil which was at 700°C.

Tesner and co-workers (1970) obtained large quantities of carbon fibres by heating nichrome wire

in acetylene at 450-700°C. The rate decreased slowly as the reaction proceeded after a fast initial increase due to the auto-catalytic behaviour of the carbon product, which was also mentioned by Lobo (1971). Gilliland and Horriott (1954) found that the rate of decomposition of CH_4, C_4H_{10} and CO on nickel/silica surfaces at 600-1000°C decreased with time because the exposed nickel was gradually covered by depositing carbon. Tesner et al. (1970) also showed that the rate of reaction, as measured by the increase in weight of carbon, increased if the partial pressure of C_2H_2 was raised or if hydrogen was added rather than nitrogen. They detected a rate maximum about 600°C when a C_2H_2/H_2 mixture was employed. It was observed that the diameter of the fibres increased with temperature as well as with pressure and time.

The decomposition of methane at 900°C and 300 torr was studied by Tamai and co-workers (1967) and the catalysis of the reaction by metals was shown to be dependent on the metal-carbon affinity. The work (Tamai et al., 1968) concerned the effect on the rate of carbon formation on nickel and iron surfaces of altering several parameters. On iron, using methane and ethane, the rate was proportional to pressure at 900°C and at low pressures at 1000°C; using ethylene the rate was independent of pressure

and decreased rapidly with time. Under conditions giving a rate of CH_4 decomposition proportional to pressure the activation energy was 100K cals./mole, equivalent to CH_4 isothermal decomposition, but in the higher temperature and pressure region the activation energy was 53K cals. mole. On nickel for all three gases the rate was independent of pressure in the range studied. This led the authors to conclude that in the presence of nickel surfaces nucleation and growth both occurred in the solid phase whereas with iron nucleation in some cases could take place in the gas phase.

1.2 Materials

1.2.1 Iron

At room temperature iron exists as a body-centred cubic metal, αFe, with unit cell dimension a = 2.8664 Å (A.S.T.M. 6, 696). At 916°C pure iron changes to a face-centred cubic structure, γ Fe, with a = 3.6394 Å, which on further heating returns to the body-centred cubic structure, δ Fe, at 1389°C with a = 2.9256 Å (Basinski et al., 1955). The transition temperatures can be altered by the addition of alloying agents such as sulphur, chromium or phosphorous which cause a contraction of the γ Fe region and an enlargement of the δ Fe region until they are no longer separated by a phase boundary. The presence of carbon reduces the temperature of the $\alpha \rightarrow \gamma$ transition to 723°C (Parkes and Mellor, 1951) and 3.5% silicon completely represses the $\alpha \rightarrow \gamma$ transition (Renshaw et al., 1970).

It is now generally recognised that a metal can recrystallise at a temperature below half that of its melting point in °K. Olmer (1942) observed that iron catalysis of the reaction $CO \longrightarrow C$ was diminished above 580°C due to sintering of the catalyst particles. Work carried out in part 5 of this thesis has indicated that the degree of crystal growth is very much dependent on the gaseous

atmosphere present during heating. Polycrystalline iron surfaces heated to 600°C or above will necessarily experience sintering and the interpretation of any chemical reaction of them will be further complicated. To minimise this effect the metal foils employed in these studies were normally pre-annealed.

Chemical reactions carried out in a conventionally clean apparatus contain appreciable amounts of impurities. Iron is particularly susceptible to oxidation by traces of oxygen, partial pressures of approximately 10^{-12} torr being enough to convert $Fe \longrightarrow Fe_2O_3$ at 700°C (Richardson and Jeffes, 1949). Iron has three non-hydrated stoichiometric oxides: FeO, Fe_3O_4 and Fe_2O_3. FeO at room temperature and above has a face--centred cubic (NaCl type) structure but below 200°K its lattice becomes rhombohedral due to Jahn-Teller distortion (A.S.T.M. 6, 711). Its molecular formula is more accurately represented by $Fe_{0.953}O$ (Chemical Rubber Co., 1969-70) and it therefore has an associated defect structure. Fe_3O_4 has a spinel lattice, the oxygen ions being arranged in close-packed cubic structure. Two iron atoms are contained in octahedrally coordinated sites in the lattice and the third is in

a tetrahedrally coordinated site. The crystal geometry is described by the molecular form, $Fe^{III}(Fe^{II}Fe^{III})O_4$, the Fe^{II} ion preferring to exist in the octahedral site because of the increase in crystal field stabilisation energy. Fe_2O_3 can occur in two crystallographic forms: αFe_2O_3 is thermodynamically more stable and has a rhombohedral, ilmenite-type structure. The oxygen ions are hexagonally close-packed with Fe^{3+} ions present in the octahedral sites in the lattice.

γ Fe_2O_3 has a tetragonal structure which is best regarded as an Fe_3O_4 spinel lattice with a fraction of the Fe^{II} sites vacant. This gives the crystal a large number of defects with renders it metastable with respect to αFe_2O_3.

The reduction of iron oxides by carbon and carbon monoxide has been extensively studied (Tutiya, 1930A; Juliard et al., 1948; Berry et al., 1956; McRae, 1965) and it has been shown to proceed by a gradual decrease in the oxidation state of the iron:

$$Fe_2O_3 \longrightarrow Fe_3O_4 \longrightarrow FeO \longrightarrow Fe$$

Colombo and co-workers (1967) followed the reduction of several oxides below 400°C and determined that the reaction pathway was,

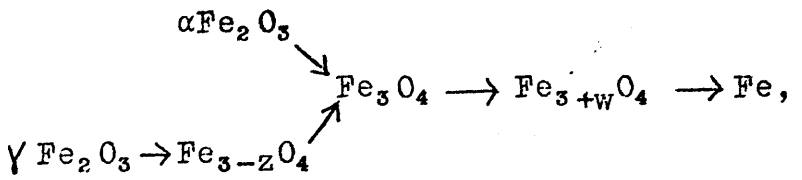

where $z \leqslant \frac{1}{3}$, $w < 1$. They deduced that the kinetic behaviour during reduction of oxides was caused by differences in the degree of crystal order and grain boundary area of the oxides. The range of compositions for which a spinel structure is possible is $Fe_{3-\frac{1}{3}}O_4$ to $Fe_{3+w}O_4$.

The ability of iron oxides to exist in compositions which vary from the stoichiometric formulae has been put forward by a number of people as an explanation for the catalytic behaviour of the substances (Renshaw et al., 1970). In particular, the interfaces between lattices in which iron has a different oxidation state are regarded as active sites (Chufarov, 1946; Taylor, 1956; Venkatachalam et al., 1971).

The solubility of hydrogen in iron is 10^{-4}% at 600°C and 4×10^{-4}% at 1000°C (Sidgwick, 1962). Carbon solubility in αFe is very low, 0.003% by weight at 20°C rising to a maximum of 0.036% at 723°C (Parkes and Mellor, 1951). The solid solution formed, with a heat of solution of 21.3K cals./mole (McLellan et al., 1970), is known as ferrite. Calculations indicate that the interstitial carbon is

present in octahedral holes in the αFe lattice (Flocken, 1971). In γ Fe the carbon solubility is 0.87% at 723°C, the A_1 transition point, and increases to a maximum of 1.7% at 1130°C, the resulting solid solution being austenite. The higher solubility is due to the larger volume available for interstitial atoms in the octahedral sites in the γ Fe lattice.

A wide range of iron carbides and solid solutions of carbon in iron are known. Many, however, only form under unusual conditions. The carbides $Fe_{23}C_6$, Fe_6C and Fe_7C_3 occur in special steels (Taylor, 1961). The formation of Fe_8C and $Fe_{16}C_2$ (Kuo, 1959) and probably the carbide "FeC" reported by Eckstrom and Adcock (1950) have been carried out only in the presence of nitrogen. The compound Fe_4C was prepared at 400-480°C from CO/Fe interactions and decomposes to Fe_3C (Pinsker et al., 1957) but neither Fe_4C nor the carbide, $Fe_{12}C_5$ have been detected in carbon deposition studies (Allen, 1966).

Several phases, mixtures of Fe and Fe_3C are known to separate in the manufacture of steels under a variety of conditions (Barrett, 1943). Figure 1.1 represents part of the phase diagram for the iron--carbon system (from Parkes and Mellor, 1951). The equilibrium form below 723°C is pearlite and other forms such as martensite, a body-centred

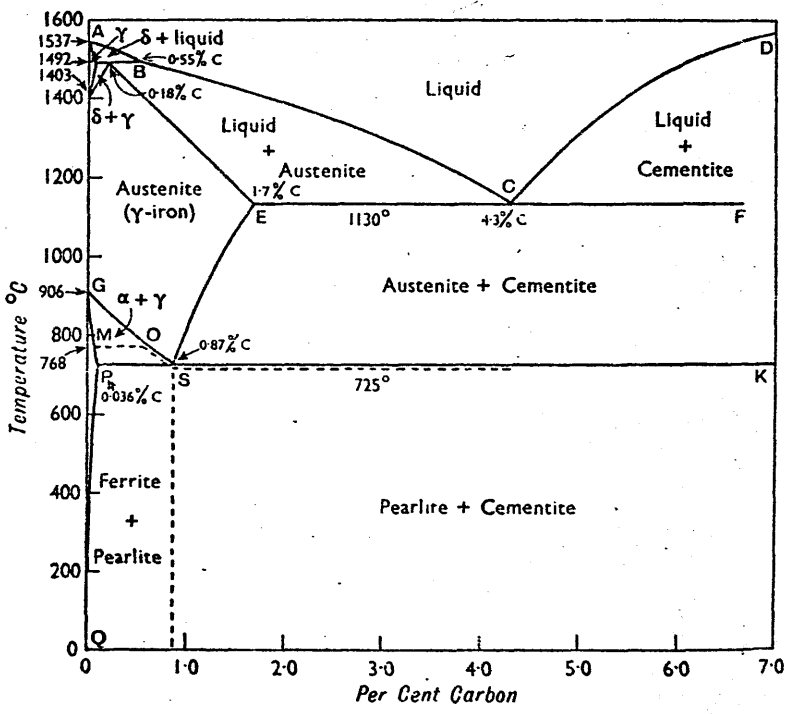

FIGURE 1.1 The Iron-Carbon System

tetragonal iron lattice containing interstitial carbon atoms (Hagg 1934A, Ron et al., 1968) can be converted to pearlite by tempering. The intermediates sorbite and troostite form and decompose during this process. Other phases such as bainite, a lower temperature form, are produced by the conversion of retained austenite to cementite and ferrite (Kuteliya et al., 1969A,B,C).

The carbides most frequently encountered during carbon deposition experiments on iron surfaces are cementite-θ Fe_3C, Hagg carbide -$\chi Fe_{20}C_9$ and ϵ Fe_2C. Of these carbides Fe_3C is the longest known and the best established. Schenk et al. (1903, 1926, 1927A and B) have studied the production and decomposition of Fe_3C in several different systems and the Fe-O-C equilibrium at various temperatures. Lipson and Petch (1940) proved that the Fe_3C lattice was orthorhombic with unit cell dimensions a = 4.5234 Å, b = 5.0883 Å, c = 6.7426 Å. Fruchart et al. (1963) discussed the Fe_3C lattice in terms of the radius ratio of the C and Fe species and explained the structure as consisting of prisms of Fe atoms, each alternate prism having a central C atom. Cementite is thought to decompose to graphite and iron via an unstable carbide and Shalashov et al. (1966) have obtained evidence that at 700°C in vacuo Fe_3C forms ferrite by going through a meta-stable austenitic phase.

Both Hofmann et al. (1930) and Tutiya (1930B) obtained a second carbide during the decomposition of CO over Fe and Gluud and co-workers (1929) showed that at 275°C Fe_3O_4 was reduced by CO giving rise to a phase of constant composition equivalent to approximately Fe_2C. Hagg (1934B) obtained an X-ray powder photograph of this compound and was able to show that it was unstable above 225°, completely

decomposing to Fe_3C at 500°C. Later work (Jack, 1946, 1948) determined that this material, now known as Hagg carbide, contained 30.5-32.1 atoms %C and crystallised in the orthorhombic system with a = 9.04, b = $a\sqrt{3}$ = 15.66 Å, c = 7.92 Å. Trillat and Oketani (1951 A, C) suggested that experimental observations could equally well be explained by a primitive hexagonal lattice with a' = 2a, c' = c or by monoclinic or triclinic systems.

Pichler and Merkel (see Hofer et al., 1949) reported the existence of two carbides of general formula Fe_2C having different Curie Points and Halle and Herbst (see Hofer et al., 1949) claimed to have detected a hexagonal carbide of iron. Hofer and co-workers (1949) established that one of these reported carbides with a Curie Point of 247°C ($\pm$3°C) was Hagg carbide and the other with a Curie Point of 380°C was a hexagonal carbide now known as ϵ Fe_2C having unit cell dimensions, a = 2.754 Å, c = 4.349 Å (A.S.T.M. 6, 670). This compound was prepared by treating powdered Fe at 240°C with CO for more than 500 hours and decomposes above 300°C to give Hagg carbide. Nagakura (1959) has obtained ϵ Fe_2C from polycrystalline αFe films but not from single crystal films, the ϵ Fe_2C having a similar crystal size to that of the original αFe. This supports his mechanism that ϵ Fe_2C forms by diffusion of C atoms into the αFe lattice via dislocations without any recrystallisation.

Allen (1966) discussed the structure of iron carbides in terms of defect models based on the relatively stable Fe_3C lattice. Compounds of composition Fe_xC, with $x < 3$, could form either by replacing Fe with C in the Fe_3C lattice or by placing excess C atoms in interstitial positions in the lattice. The latter would explain why graphite is formed during Fe_3C decomposition but not by $XFe_{20}C_9$ decomposition as too little energy is released by the removal of an interstitial C atom from $XFe_{20}C_9$ to form a graphite lattice.

The catalytic intervention of iron carbides in the Fischer-Tropsch synthesis of hydrocarbons was ruled out according to thermodynamic and C^{14} tracer evidence from Kimmer et al. (1948A, B), Kryukov et al. (1970) found that Fe_2C formed by the action of CO/H_2 on Fe diffused into the Fe granules taking no further part in the reaction sequence. Podgurski, Kimmer and co-workers (1950) have studied the interconversion of iron carbides and supplied information on their adsorptive properties. Hydrogen and carbon monoxide are not chemisorbed by $XFe_{20}C_9$ at low temperatures and at 100° and 200°C. However, CO chemisorbs on partly carbided Fe at -40°C to -195°C, indicating that carbide formation proceeds by the nucleation and growth of individual carbide crystals and not by the gradual thickening of a uniform layer of carbide on the Fe surface. They assumed that, since X, Θ and ϵ carbides have similar ferromagnetic moments, ϵ and Θ carbides

would have adsorptive properties similar to those of $XFe_{20}C_9$.

Chufarov and Antonova (1947) have studied the effect of various substances on the catalysis of the Bell reaction ($2CO \rightleftharpoons C + CO_2$) by iron. The presence of the relatively unstable sulphates of Cu, Al and Mn in 5% concentrations stopped the reaction completely at 450°C and retarded it by factors of 12 to 40 at 650°C-750°C. The more stable sulphates of Na and Mg had less effect. Inhibition of the catalysis occurred upon addition of sulphur-containing decomposition products, especially SO_2. Berry and co-workers (1956) also found that sulphur in the gas or solid phase prevented catalysis of the reaction, as did small doses of NH_3. However, these effects could be offset by adding zinc or alkaline compounds, and the presence of H_2 or H_2O accelerated the reaction. Both Schenk et al.(1960) and Karcher et al.(1971) divided iron and steel poisons into ones which led to irreversible inhibition such as SO_2, H_2S, silanes and ones which were effective only if continuously added such as Cl_2, nitrogen compounds. The adsorption of sulphur on the (100) face of Fe was investigated by L.E.E.D. by Margot et al.(1970). At 20°C and 5×10^{-9} torr H_2S, a C(2 x 2) structure forms on the Fe surface due to S^{2-} ions. The intensity of this adsorption increases with temperature and pressure until 500°C and 3×10^{-2} torr

when a disordered structure results. At this point the addition of H_2 and H_2S leads to completely saturated adsorption.

1.2.2. Nickel

Nickel at 20°C has a face-centred cubic structure with a = 3.5238 (A.S.T.M. 4, 850). Early preparations of nickel films produced a hexagonal close-packed lattice (Mellor, 1922) and this modification, though not normally encountered, is known as αNi. The face-centred cubic structure is βNi. (Von Nostrand Ltd., 1964).

Several investigations (Bollmann, 1958-1959; Bartuska, 1970) have shown that polygonisation of nickel foils starts around 150°C and recrystallisation nuclei appear at 200-250°C in pure nickel. In lower purity nickel (Larikov et al., 1965; Bartuska, 1970) polygonisation and recrystallisation occur at about 150°C higher. Fuks and co-workers (1970) found that in very strained nickel lattices such as thin films deposited at low temperatures recrystallisation can take place below 175°C by a stress relaxation process requiring a lower activation energy than normal coarse grain formation. The presence of even trace amounts (10^{-7} torr) of adsorbed gas at 20°C helps to release the compressive stresses in the nickel films (Janssen, 1969). Small deformations in nickel can lead to recrystallisation by grain boundary migration

(Bailey et al., 1962; Dubovitskaya et al., 1970).

Many nickel oxides were reported in the early literature including Ni_2O, Ni_2O_3, Ni_3O_4, NiO_2 as well as the fully characterised NiO. Nickel is more resistant to oxidation than iron but will form NiO fairly readily above room temperature. The oxide NiO has the same face-centred cubic structure as nickel itself. The temperature of formation affects its lattice parameters (Chambard et al., 1971) but the unit cell dimension is usually taken as 4.1769 Å (A.S.T.M. 4, 835). Nickel hydroxide, $Ni(OH)_2$, has a well established hexagonal structure with a = 3.126 Å c = 4.605 Å (A.S.T.M. 14, 117). Apart from NiO the only anhydrous oxide of nickel whose existence is likely is Ni_2O_3, nickel sesquioxide. Nickel oxide prepared by heating Ni in oxygen at 400-480°C is said to contain up to 3% Ni_2O_3 (Sidgwick, 1962) and Aggarwal and Goswani (1961) have detected a phase which they identify as Ni_2O_3 formed in an evaporated film of Ni and NiO on rocksalt at 400°C. They suggest a hexagonal lattice with unit cell dimensions a = 4.61 Å, c = 5.61 Å. Hydrated nickel oxides are fairly common. Glamser and Einerhand (1950 A and B) reported a number of higher hydroxides, of which the best defined is βNiOOH (A.S.T.M. 6, 141) which can be considered as a hydrate of Ni_2O_3: $Ni_2O_3 + H_2O \longrightarrow 2\beta NiOOH$

The solubility of hydrogen in Ni is relatively high. At 25°C Ni absorbs 4.15 times its own volume of H_2 (calculated at N.T.P.). At 600°C 5.4×10^{-4}% and at 1400°C 1.54×10^{-3}% H_2 dissolve in Ni (Sidgwick, 1962). Nickel dissolves 0.23%C at 1000°C but no carbide is stable at such a high temperature (Hansen, 1958). In fact only one carbide (hexagonal) Ni_3C has a completely established structure. Bahr et al. (1928B, 1930, 1933) formed Ni_3C below 270°C by the action of Ni or NiO on CO. The Ni_3C decomposed to Ni between 380°C and 420°C and it was suggested that this occurred via a second carbide Ni_3C_2. Tutiya (1931) claimed the formation of a percarbide at 270°C which rapidly decomposed at 284°C to give Ni_3C. Jacobson and Westgren (1933) carried out an X-ray analysis of Ni_3C and proved its hexagonal structure. Their unit cell dimensions, a = 2.646 Å, c = 4.329 Å are similar to those accepted at present (A.S.T.M. 6, 697). It was suggested by Bromley et al. (1960) that Ni_3C can be formed at relatively low temperatures because it is an interstitial carbide, the C atoms preferring to enter a partially constructed lattice rather than nucleate a graphite lattice even though Ni_3C is unstable with respect to graphite and Ni. In 1938 Kohlhaas and Meyer proposed the existence of an orthorhombic Ni_3C isomorphous with Co_3C and Fe_3C, but this has not been substantiated.

Several other caribdes are known to exist; $Ni_{23}C_6$, NiC and Ni_6C are found in alloys, especially steels, and Tebboth (1948) has proposed that Ni_6C is an intermediate in the decomposition of Ni_3C. Hofer and co-workers (1950) have rejected this suggestion because of the observed kinetics in their Ni_3C decomposition experiments. Nickel acetylide, NiC_2, has been prepared (Durand, 1923) and Pugh et al. (1961), during the synthesis of diamond at high temperatures and pressures between Ni and graphite blocks identified a percarbide, Ni_xC ($x > 4$) by X-ray analysis (A.S.T. 14, 20). Recently, Renshaw et al. (1971) have observed a lattice based on the normal hexagonal Ni_3C structure but with the C atoms regularly arranged in the lattice instead of occurring randomly in interstitial positions. The unit cell dimensions of the carbide superlattice were given by Nagakura (1957, 1958) and are related to those of the normal Ni_3C unit cell according to $a' = a\ 3\ Ni_3C$, $c' = 3c\ Ni_3C$.

The addition of H_2S or C_2H_4 to a Ni(111) face was studied using L.E.E.D. by McCarroll, Edmonds and Pitkethly (1969) and it was determined that the S or C atoms formed, respectively, altered the orientation of the top Ni layer to a (100) configuration. Riwan (1971) found by Auger spectrometry that trace amounts of S contained in nominally pure Ni segrated to the (110) Ni face during thermal conditioning.

The addition of $(NH_4)_2S$ to a Ni catalyst being used for C deposition from C_2H_4 was found (Shirasaki et al., 1965) to selectively poison the metal grain boundaries. Richardson (1971) investigated the poisoning of Ni catalysts by H_2S, CS_2 and $(C_2H_5)_2S$ and described the features of the nickel-sulphur interactions. The regeneration of S-poisoned Ni catalysts by oxidation above 600°C was recommended by Rostrup-Nielsen (1971).

1.2.3 Catalyst Discussion

The importance of carbidic phases lies in the fact that they are inevitably formed in low temperature (below approximately 600°C) carbon deposition reactions. Even at higher temperatures their transient existence has been postulated to explain carbon formation and it is widely recognised that the success of iron, cobalt and nickel as carbon deposition catalysts is because their carbon affinity is intermediate between that of titanium and tungsten which form very stable carbides and that of silver and gold which form no carbides (Tamai et al., 1967).

Matsumoto et al. (1970) have shown that nickel degrades hydrocarbons by α scission producing C_1 species, whereas platinum acts by a β carbonium ion mechanism and this may explain why nickel can cause the build up of highly ordered carbon at much lower temperatures; the C_1 species would be expected to easily slot into

position in the growing graphite lattice because of their high mobility (see section 4.1) in contrast to the larger hydrocarbon fragments from platinum. The I.R. spectra of CO chemisorbed on Fe, Co and Ni at 113°K under ultra high vacuum have been shown to be similar (Bradshaw et al., 1970). Only some of the adsorbed gas is responsible for the spectra indicating the presence of at least two types of adsorbed molecules. Bearing in mind the behaviour found by Maire et al. (1970) and Edmonds, McCarroll and Pitkethly (1969 A and B, 1971) by L.E.E.D. for CO and hydrocarbon adsorption at comparatively low temperatures, the complexity of the interactions with Fe, Co and Ni becomes apparent. With Cu, Ag and Au Bradshaw and Pritchard (1970) found much simpler and totally reversible adsorption. These L.E.E.D. studies have also shown that the presence of even trace amounts of impurities such as sulphur, hydrogen, carbon and oxygen (Portele, 1969) has a definite bearing on the type of reaction which the metal surface will undergo. It is becoming more evident that totally reproducible results will only be achieved with a complex system such as is used in carbon deposition studies under ultra-pure conditions.

The correlation between the catalytic activity of Fe and Ni with high energy centres such as dislocation cores is uncertain. Miyazaki et al. (1971)

and Grenga and Lawless (1966) found no preferred deposition at activated points on the nickel surfaces and Renshaw et al.(1970) using Fe/Si single crystals with dislocation arrays detected no improved catalysis. However, Walker and Thomas (1970) stated that dislocation cores in Fe did function as active centres and Schrader et al.(1971) successfully employed mechanically activated Ni catalysts.

1.2.4 Hydrocarbons

The thermodynamic stability of paraffins decreases with increasing chain length, all being unstable with respect to carbon and hydrogen above room temperature except CH_4, C_2H_6, C_3H_8 (Parks and Huffmann, 1932). Relevant thermodynamic data is given in Table 1.6, (from Kearby, 1955).

Table 1.6

Hydrocarbon Stability Data

Hydrocarbon	Inversion temp.	Temp at which compound becomes stable with respect to equivalent paraffin.	Heat of formation of C in K cals./ g.atom of C at 700°C
CH_4	570°C	-	-4
C_2H_6	200°C	730°C	-
C_3H_8	100°C		-14
C_3H_6	below 20°C	600°C	-14
C_4H_6	below 20°	660°C	-14

It can be seen from the table given that while CH_4 has a higher stability at 700°C the other hydrocarbons employed in the present studies, C_3H_8, C_3H_6 and C_4H_4 (butadiene) are remarkably similar in this respect.

The breakdown of hydrocarbons to give carbon is known to be a complex process. Frey and Hepp (1933) have listed the decomposition products at 400-575°C and in section 1.1.2 the various possible hydrocarbon intermediates were mentioned and their role in determining the final carbon product discussed. Acetylene is the intermediate most frequently encountered and it is practically unique in becoming less unstable with respect to carbon and hydrogen with increasing temperature. Above 1200°C it is thermodynamically even more stable than CH_4. However, because of the kinetically active triple bond it will still break down rapidly to carbon at elevated temperatures.

In the presence of a catalyst the breakdown patterns of the gases will be altered because the catalyst increases the rate of formation and decomposition of various intermediates to different extents. For example, Frey (1934) has described the pyrolysis of paraffins on catalyst surfaces. As has been mentioned, nickel especially tends to form surface C_1 species and it is likely that acetylenic species are less important. The metal catalyst may also form secondary products such as carbides or oxides (with

acetone, or if oxygen impurities are present) and these may well interfere with the other chemical reactions occurring. A further feature of solid/gas interactions is the possible effect of physical processes such as diffusion, solution on the course of the carbon deposition. The overall rate of production of carbon will depend in a complicated manner on all of these features and to understand the kinetics required a knowledge of the relative importances of the individual processes which can only be obtained by morphological and analytical studies.

1.3 Transmission Electron Microscopy (T.E.M.)

1.3.1. Introduction

The use of electron microscopes to obtain enlarged images of specimens dates from Knoll and Ruska (1932). Early microscopes (between 1932 and 1950) have been described by various authors (Zworykin et al, 1945; Cosslett, 1951; Hall, 1953) and the theories of electron optics (Heidenreich, 1964; Hirsch et al., 1965) and practical techniques used in microscopy (Kay, 1965) have been much discussed. More recent reviews of the state of development have been given by Fisher et al. (1970) and Cosslett (1970).

The microscope used for most of this work, the Siemens Elmiskop I, has been described in some detail by Hirsch et al. (1965). The beam of electrons accelerated from a tungsten filament by a potential of 40kV, 60kV , 80kV or 100kV is focussed on the specimen, using a single or double condenser system, as a spot whose diameter can be adjusted from 60 μ to 2 μ, according to the degree of demagnification produced by the first condenser lens. The image of the specimen is magnified by three magnetic lenses, the objective, intermediate and projector lenses, and a final magnification of up to 160,000X can be attained. The ray diagram showing the formation of the magnificent image using one condenser lens is given in Figure 1.2 The magnification achieved by the objective lens was

Figure 1.2

Ray Diagrams for (a) Transmission Microscopy and

(b) Selected Area Diffraction.

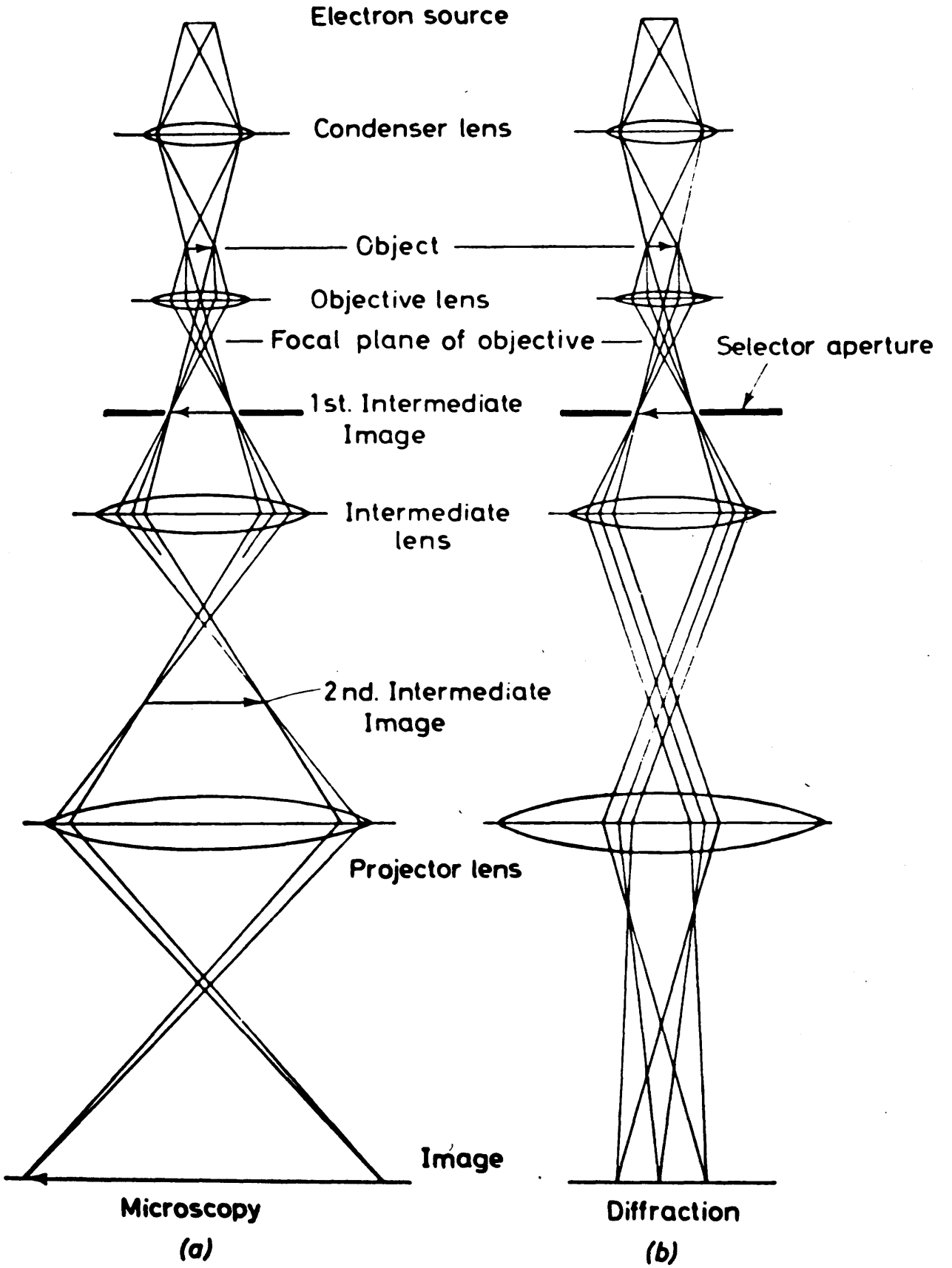

Ray Diagrams for (a) Transmission Microscopy and (b) Selected Area Diffraction. (From Hirsch, Howie, Nicholson, Pashley and Whelan, 1965).

increased by the use of an objective pole-piece of focal length 2.1 mm. instead of the normal 2.8 mm. (at 80kV) giving an overall magnification increase of approx. 30% and an improved resolution.

1.3.2. Diffraction: The second major use of electron microscopy, as an analytical tool, is dependent on the ability of crystalline specimens to diffract beams of electrons. On going through a suitable object electrons are diffracted at angles determined by the lattice parameters of the specimen. The beams are focussed normally at the second focal plane of the objective lens as indicated by Figure 1.2. An image of the pattern at this plane is then obtained by use of the intermediate and projector lenses.

Selected Area Diffraction. The technique of selected area electron diffraction, introduced by Le Poole (1947), was employed frequently during the course of this work. A diffraction aperture is placed in the path of the beam at the first intermediate image plane and the strength of the intermediate lens is reduced until an image of the second focal plane of the objective lens is projected on to the final screen.

From the resulting diffraction pattern the particular lattice spacing, d, corresponding to a reflection of radius R can be calculated from the equation,

$$d.R = K ,$$

where K is the camera constant and is given by the product of the electronic wavelength, λ, and the effective camera length, L. The camera constant is an experimentally determined quantity, its value being found by measuring the R values of a known specimen, usually an evaporated film of thallium chloride. Inaccuracies in selected area work have been discussed by Phillips (1960), Agar (1960), Rieko (1961), Alderson and Halliday (1965), Hirsch et al. (1965) and Andrews et al. (1967) and are due mainly to spherical aberration and variations in the value of K.
The selected area technique is extensively used to identify the chemical nature of materials and to supply crystallographic information about individual crystals.

Dark Field Microscopy. With a crystalline specimen a selected area diffraction pattern can be obtained, as previously described. If the objective aperture is placed over a particular Bragg reflection and the diffraction aperture and specimen image are focussed at the first intermediate image plane then a dark field image of the sample will be obtained. Areas of specimen responsible for the given reflection will appear bright against a dark background.
Spherical aberration errors are introduced by the use of electrons removed from the optical axis to image the specimen. To reduce this effect and improve

image quality the illumination system can be tilted about the object until the desired reflection lies along the new optical axis. Dark field microscopy is important in specimen orientation studies where determination of the region of specimens contributing to particular diffracted beams is required.

1.3.3. Contrast

Contrast in electron microscope images arises from interactions between the electron beam and the atoms of the specimen.

1.3.3.1 Elastic Scattering

When electrons interact with the nuclei of the specimen they do so elastically, without any loss of energy. The resulting diffracted beams of electrons are coherent with respect to the transmitted beam and, in crystals, diverge from it at angles determined by the lattice parameters of the specimen (see previous section). The overall elastic scattering cross-section, Qel, was given by Hirsch et al. (1965) as:

$$Q_{el} = \int_{\alpha = 0}^{\alpha = 2\pi} \int_{\beta = 0}^{\beta = \pi} |\psi g|^2 \sin\beta d\beta d\alpha,$$

where, α is the angle variable about the optic axis,

β is the scattering angle,

ψg is the amplitude of the scattered wave.

The use of an aperture (the objective aperture) near the second focal plane of the objective lens

(Hiedenreich, 1964) makes it possible to separate the contrast due to elastic scattering into contributions from two distinct mechanisms, namely, phase contrast and diffraction contrast. In the equation,

$$Q_{el} = \int_{\alpha=0}^{\alpha=2\pi}\int_{\beta=0}^{\beta=\beta_{obj}} \left|\psi g(\alpha,\beta)\right|^2 \sin\beta d\beta d\alpha \quad +$$

$$\int_{\alpha=0}^{\alpha=2\pi}\int_{\beta=\beta_{obj}}^{\beta=\pi} \left|\psi g(\alpha,\beta)\right|^2 \sin\beta d\beta d\alpha,$$

the first expression describes the scattering cross section for phase contrast and is due to that fraction of the diffracted electrons which pass through the objective aperture; the second expression computes the cross-section for diffraction contrast and is due to diffracted electrons which do not pass through the aperture and do not therefore contribute to the final image.

Diffraction Contrast arises because of variations in the orientation of crystalline specimens. The electron beam will be strongly diffracted by an array of lattice planes at a particular orientation and if the diffracted beam is removed by the objective aperture this area of the crystal will show up in the final image as a dark spot. Darker areas will also result from thicker

parts of the specimen due to their increased diffracting ability (thickness contrast) and from regions of specimen containing atoms of higher atomic number (mass-thickness contrast).

The mathematical theory which attempts to explain the electron scattering phenomenon and to calculate the intensities of diffracted beams is known as the Kinematical Theory (Heidenreich, 1964 and Hirsch et al., 1965). It assumes that the diffracted intensity is low and therefore neglects any further interactions of the diffracted electrons. This assumption is valid, in general, for thin specimens and the theory accounts for variations in contrast due to dislocations, buckling contours and other features. The Kinematical Theory in its original form does not explain the formation of moire fringes and, for thicker specimens where its main assumption becomes invalid, the Dynamical Theory was introduced. This theory takes into account the secondary effects produced by interactions of the diffracted electrons within the crystal.

Phase Contrast is the dominant mechanism for the production of contrast in electron images of specimens less than 100 Å thick when detail less than 10 Å in size is required (Heidenreich, 1967). Transmitted electrons, of amplitude T, and diffracted electrons, of amplitude D and phase ($\frac{\pi}{2}$ + X) relative to T pass through the objective aperture and by/

interference a combined electronic wave function,

$$\psi = T + iDe^{iX} ,$$

with intensity,

$$|\psi|^2 = 1 - 2TD \sin X,$$

is formed. The maximum contrast is,

$$G_{max} = 4TD, \text{ when } \sin X = 1 \text{ and } X = \frac{\pi}{2}(4I + 1),$$

where I is an integer.

The contrast produced here is phase contrast as it depends on the phase difference, X, introduced into the diffracted electron wave by the scattering process. Most micrographs contain a phase contrast contribution except at exact focus when phase contrast becomes zero. The exact degree of defocussing, ΔL_0, necessary to produce maximum contrast in a given set of conditions can be calculated. (Thon, 1966A). A knowledge of the value of ΔL_0 is useful when imaging features less than 10 Å in size.

A series of intensity maxima are formed in the second focal plane of the objective lens by interference phenomena, according to the equation,

$$P = \pm I \frac{\lambda}{a} L_0 ,$$

where, P denotes the position of the maximum from the optic axis,

a is the unit cell dimension,

L_0 is the object distance and

I is the spectral order describing the phase change on diffraction, X(I).

(i) For I = 1, the phase change on scattering = $\frac{\pi}{2}$ giving rise to a half period image.

(ii) For I = 0 and I = 1, the phase change, $\pm \pi$, gives the true lattice periodicity.

(iii) For I = 0, a uniform intensity image is formed.

In general the greater the number of spectral orders allowed to contribute to the final image the better is the phase contrast. Recent workers (Thon, 1966B; Mollenstedt et al., 1968; Heppe et al., 1969) have acted on a suggestion by Hoppe (1961 and 1963) that "zonal correction apertures" would increase phase contrast in the image and facilitate interpretation of high resolution micrographs. Alternatively, the same results can be obtained by using an optical diffractometer to filter and reconstitute the image of an electron micrograph (Thon and Siegel, 1970).

1.3.3.2. Inelastic Scattering

When the electron beam interacts with orbital electrons from the specimen inelastic scattering occurs and the specimen gains energy, causing an increase in temperature and often resulting in damage to the specimen. If the inelastic scattering cross-section is calculated it is found that most scattering occurs within an angle, $\beta < \beta_{obj}$, but no improvement in

phase contrast results due to the incoherence of inelastically scattered electrons. Normally, specimens of low atomic number, e.g. carbon, are unsuitable for phase contrast because of the high proportion of electrons which are inelastically scattered (Crewe, 1970).

1.3.4. Resolution:

Resolving power has been defined by Cosslett (1951) as the closest distance of approach of two point objects at which they can still be distinguished as separate entities. However, a generally agreed standard test of resolving power in electron microscopy is difficult to achieve. Hillier (1945) suggested as a criterion the highest useful magnification of which a micrograph is capable. Alternatively, the minimum separation between points in a micrograph can be used or the measurement of the smallest detectable opaque particle on a thin support film can give estimates of ultimate resolution. A further criterion due to Haine (1949, 1950, 1961) concerns the width of Fresnel fringes at the edges of specimens.

The factor limiting the resolving power of an optical microscope is the diffraction effect occurring at the aperture of the lenses. This limits the resolution to the order of the wavelength of the light used (approximately 0.5 μ). If the ultimate resolution in images formed by high energy electrons was determined

by this same limitation then the observation of atomic detail down to about 0.05 Å in separation would be possible. Unfortunately, imperfections in the electron optics, in the high voltage supply, and in the specimen stability make this standard of resolution impossible to attain. Some of the more important factors controlling the amount of information which can be retrieved from the diffracted electron beams will now be considered.

1. Spherical aberration of the objective lens is generally the largest single factor determining the resolution limit in the electron microscope. It arises because the power of an electromagnetic lens is greater for rays further from the optic axis, with the result that the image of any point in the object is a disc of finite radius, Δr_S. To reduce this aberration a limiting aperture is placed in the second focal plane of the objective lens. This aperture removes the most widely diffracted rays but results in a reduction of the information content of the final image. This aperture diffraction aberration, Δr_D, is given by Jenkins and White (1951) as:

$$\Delta r_D = \frac{0.61 \lambda}{\alpha} , \qquad (1.1)$$

where α is the angle subtended at the specimen by the objective aperture and λ is the electronic wavelength. The radius, Δr_S, of the disc of confusion produced by

spherical aberration is given by,

$$\Delta r_S = C_S \alpha^3, \qquad \ldots\ldots\ldots \quad (1.2)$$

where C_S is the spherical aberrations coefficient of the objective lens. Thus, combining equations (1.1) and (1.2), the optimum semi-aperture angle, α_{opt}, is given by:

$$\alpha_{opt} = A \lambda^{\frac{1}{4}} C_S^{-\frac{1}{4}}$$

and the minimum aberrations, $\Delta r_{min.}$ is,

$$\Delta r_{min.} = B \lambda^{\frac{3}{4}} C_S^{\frac{1}{4}},$$

where A and B are constants, approximately unity. Normally the objective aperture diameter lies between 30 μ and 50 μ, for work where diffraction contrast is beneficial. However, if an increase in phase contrast is desirable the objective aperture can be removed completely. Because the spherical aberration constant is proportional to the focal length of the objective lens removal of the aperture can be justified in microscopes having an objective pole-piece of very short focal length. In the present case, as previously mentioned, the focal length was 2.1 mm.

2. Chromatic aberration arises if there is an energy spread of the imaging electrons, producing alterations in the effective focal length of the objective lens. Electrons which have lost energy are bent more by the objective field and lead to a disc of confusion in the image plane. The chromatic aberration constant, C_C,

like C_S, usually have a value similar to the focal length of the objective lens.

3. Coherence of a beam of electrons in the electron microscope is essential for the observation of interference effects such as Fresnel fringes. If two incoherent sources are observed in a microscope the intensity at the image plane is the sum of the intensities of each one taken individually (Hall, 1953); if the two sources are coherent then the intensity is an interference pattern for which the two parts must be added with due regard to relative phase. Coherence is improved by use of a condenser aperture, usually of diameter 100μ or 200μ but 50μ apertures can be employed for high resolution studies.

4. Astigmatism in a lens causes a point object to be imaged as two mutually perpendicular lines at different levels in image space. Hillier and Ramberg (1947) produced the first " stigmator" - an elliptical field which can be adjusted in magnitude and direction to compensate for the inhomogeneity of the lens. In the Elmiskop I there are stigmators in the illuminating system and in the objective lens.

5. Specimen Instabilities of several types can affect the resolution attainable even under optimum instrumental conditions. Chemical instability in the form of beam damage can be reduced by means of image intensifier systems; physical instability in the form

of specimen drift can be avoided by using correctly supported objects. The prevention of contamination build up on specimens is now routinely performed by the use of liquid nitrogen-cooled jackets which surround the specimen and attract the hydrocarbon vapours which cause the contamination.

1.3.5. High Voltage Electron Microscopy:

Conventional electron microscopes use electrons accelerated through potentials of 30kV to 100kV. For certain types of work, however, electrons of much greater energy (around 1 Mv) are preferable, the advantages being two-fold:

1. A greater transmission of electrons through thick specimens at small angles of scattering is obtained, enabling specimens of considerable thickness to be examined. The information available from the study of metal films in the electron microscope is of limited help in extending our knowledge of bulk metal properties because of the special effects encountered in films thin enough to be examined in a conventional microscope. Much thicker metal specimens can be looked at using a 1 MeV microscope.

2. A smaller absorption of energy from the electron beam of the specimen takes place. This effect is advantageous in the examination of biological materials and other potentially unstable substances.

In the present work a thick sample was examined using the A.E.I. 1MeV microscope at A.E.R.E. Harwell

1.4. Other Physical Techniques

1.4.1. Scanning Electron Microscopy (S.E.M.)

Scanning microscopy is a technique for observing the surface of samples too thick for examination by transmission microscopy (T.E.M.). Its resolution, while not as good as a T.E.M. is appreciably better than that of an optical light microscope (O.L.M.) and its depth of field is at least 300 x that of an O.L.M. (15 μ at 10,000 x). Recent reviews of S.E.M. include those of Cosslett (1970), Fisher et al.(1970) and Kammlett (1971).

Figure 1.3 illustrates the components of a scanning microscope. A heated tungsten filament emits electrons which are accelerated under a positive potential of 1 to 50 kV and are passed through a series of two or three condenser lenses. Thus, a demagnified image of the source is achieved at the specimen surface. The electrons interact with the solid specimen and generate a variety of signals which can be collected, amplified and used to control the brightness on a cathode ray tube (C.R.T.). To obtain the signals the electron beam is scanned in a raster fashion over a chosen area of sample by two pairs of electromagnetic deflection coils. Because the C.R.T. scan is synchronised with the beam scan the signals are transferred with a one-to-one correspondence as an image display of the scanned region. Changes in

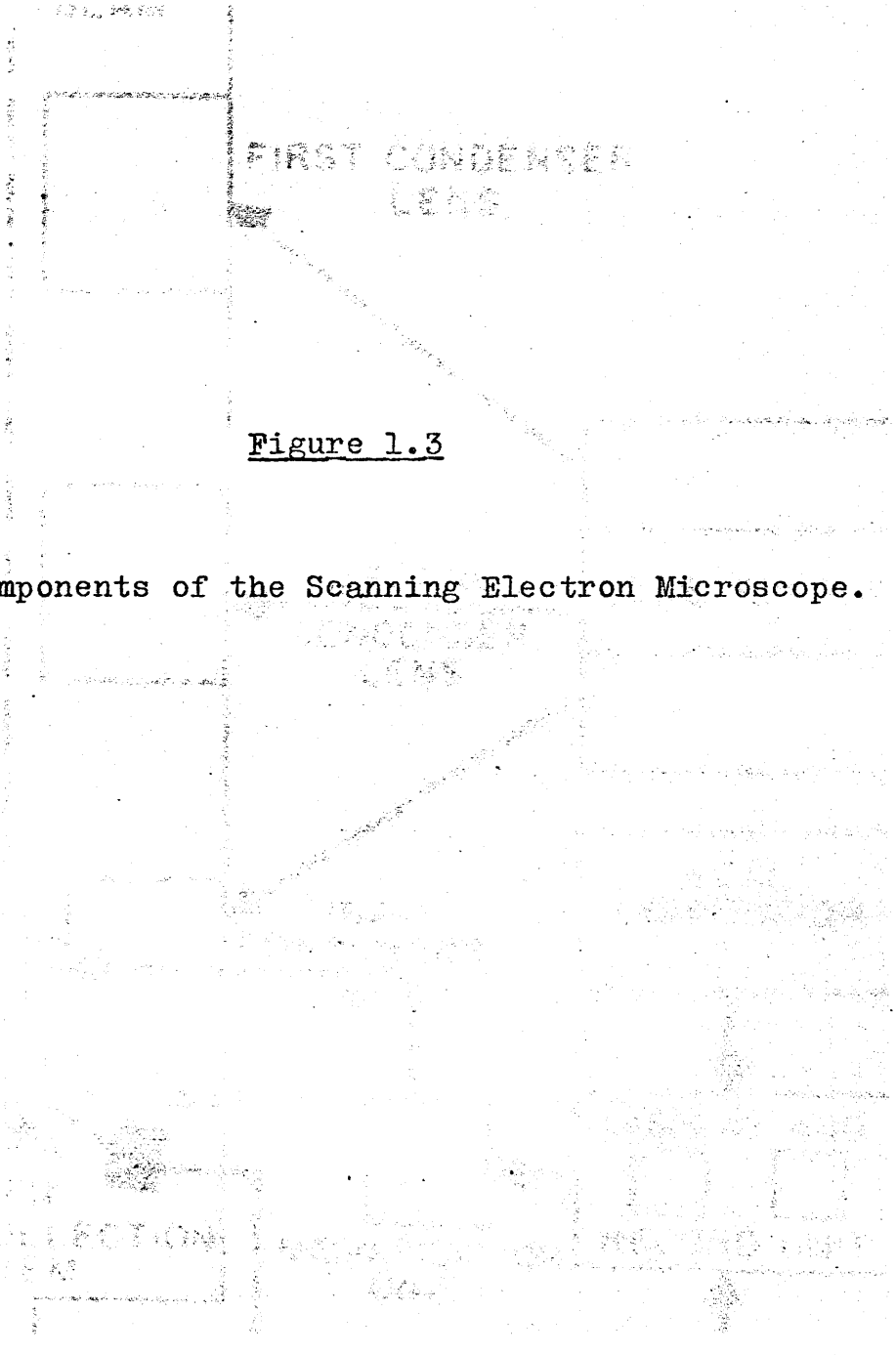

Figure 1.3

Components of the Scanning Electron Microscope.

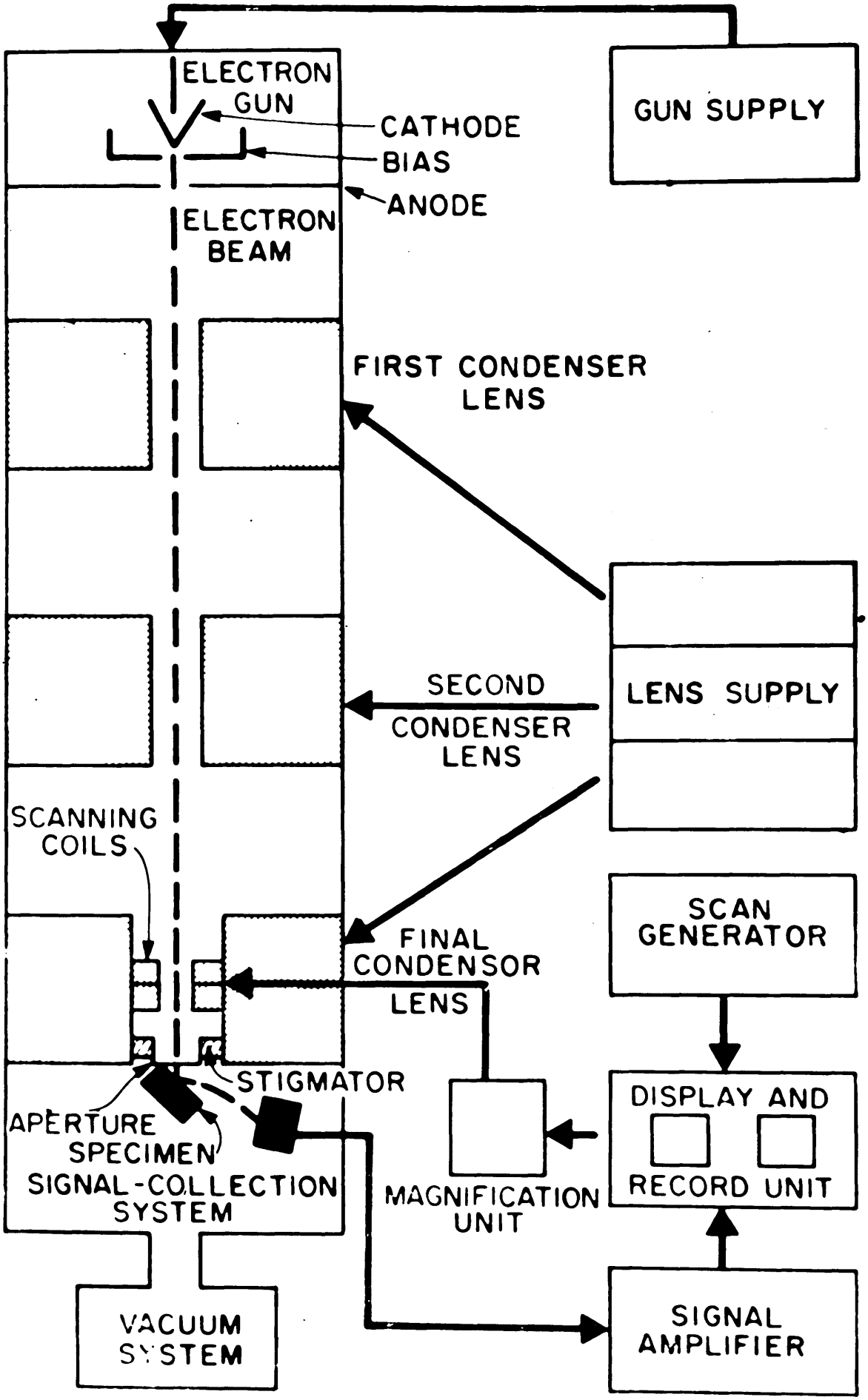

Instrument component of the SEM.

brightness represent changes in particular properties of the specimen.

Normally the instrument is used in the emissive mode, the secondary electrons emitted from the specimen being collected and utilised in the formation of a specimen image. The reflected primary electrons can be made use of but give less detail about surface features (Everhart et al., 1959).

It is found that elevated regions of the specimen will act as enhanced sources of secondary electrons due to their greater irradiation and will appear bright, whereas depressions will come up dark, in the final image. Similarly, high atomic weight elements will interact more with the primary electrons and will appear as bright spots in the image. However, their electron scattering will be mainly elastic and if inelastically scattered electrons are used to image the sample these spots will not show up (Crewe et al., 1970).

Microprobe: The X-rays formed by electrons dropping into lower energy orbitals during these interactions are characteristic of the element involved. Hence, if the X-rays are collected, an analysis of the elements present in the specimens can be obtained. The collection is performed by use of various analyser crystals which diffract the X-rays at angles dependent on their wavelength and therefore separate the X-rays according to their source elements.

1.4.2. Mass Spectrometry

The gaseous products of many of the carbon deposition experiments were analysed using an A.E.I. M.S.12 mass spectrometer, a diagram of which is shown in Figure 1.4. The sample gas is ionised by electron bombardment in the ion chamber, the resulting ions being separated according to mass to charge ratios by means of the magnetic analyser. The strength of the magnetic field is kept constant while the potential through which the ions are accelerated is continuously varied. The mass range of interest is then scanned using the adjustable slit in the collector assembly. Each focussed beam on passing through the slit strikes the collector plate where it acquires an electron to neutralise each positive ion it contains. This produces a flow of current in the collector circuit which is amplified and recorded as a peak on a moving chart, the magnitude of the peak being proportional to the relative abundance of each ionic species (Hill, 1966).

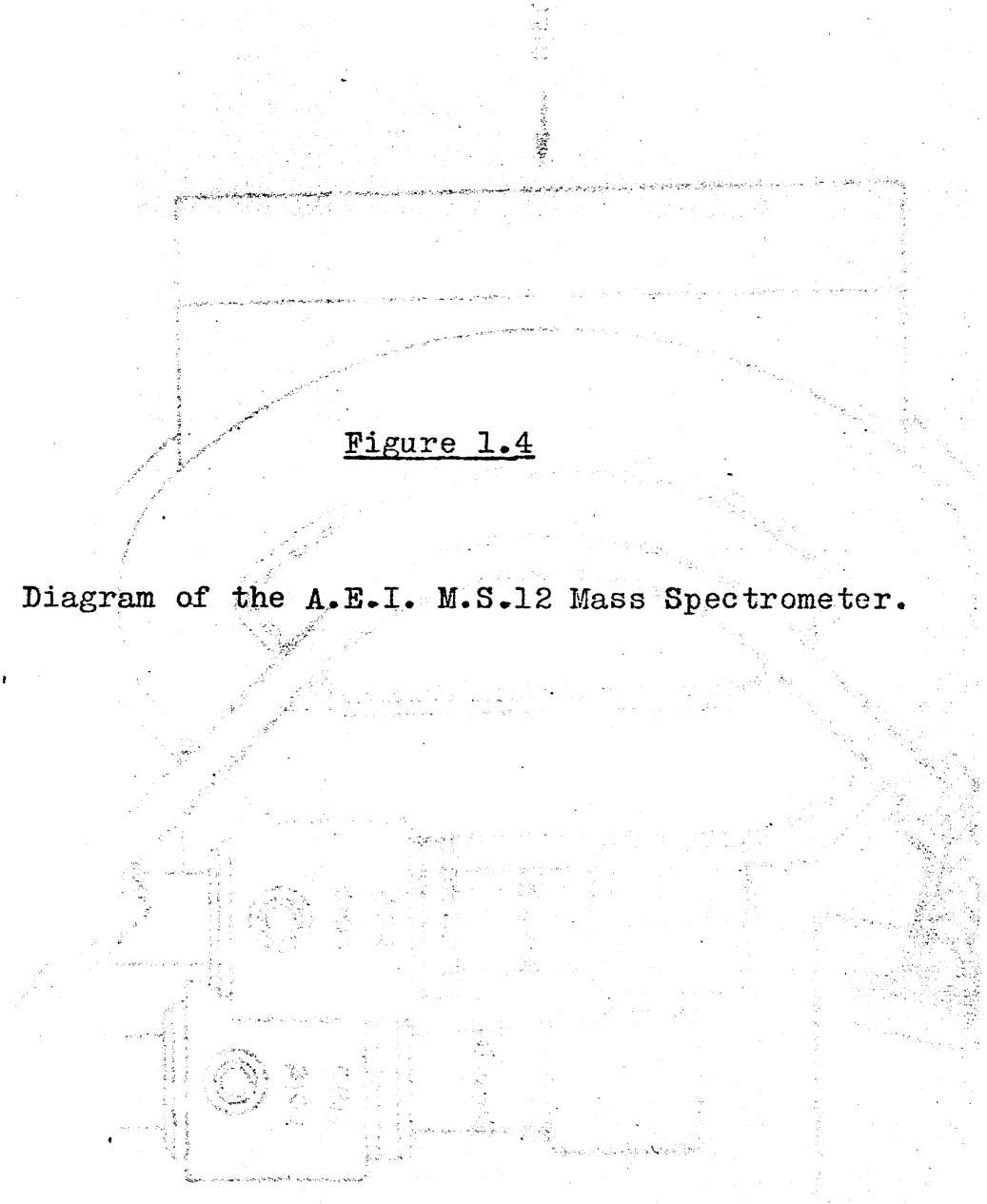

Figure 1.4

Diagram of the A.E.I. M.S.12 Mass Spectrometer.

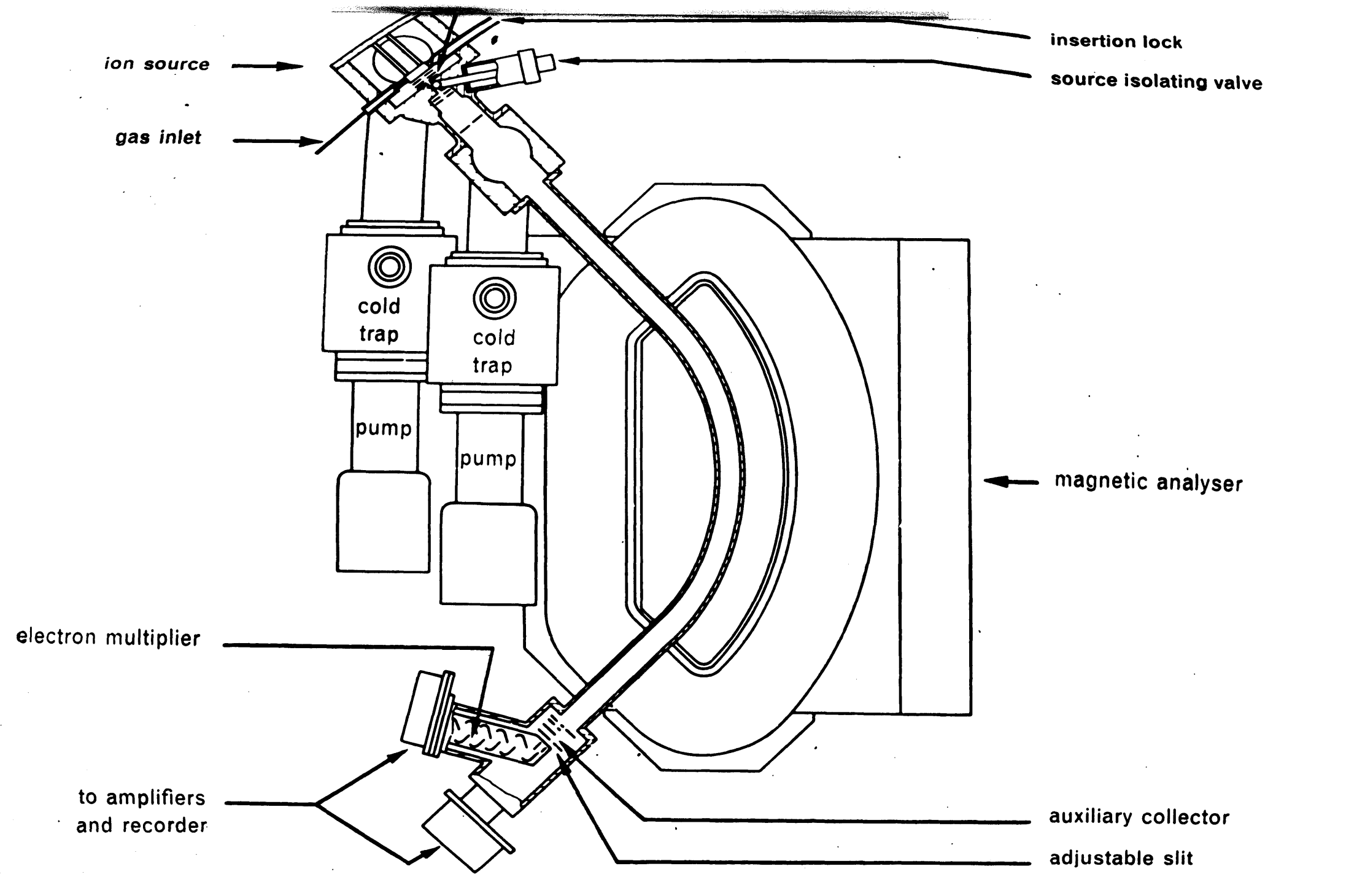
ion source
gas inlet
insertion lock
source isolating valve
cold trap
cold trap
pump
pump
magnetic analyser
electron multiplier
to amplifiers and recorder
auxiliary collector
adjustable slit

CHAPTER 2

EXPERIMENTAL

2. EXPERIMENTAL

Contents

2. EXPERIMENTAL

2.1. Apparatus

2.1.1. Reaction Vessel

The carbon deposition experiments were carried out in the apparatus shown in Figure 2.1. It consists essentially of a commercial coating unit incorporating a bell-jar which encloses a reaction volume of approximately 20 litres. The base-plate of the bell-jar contains numerous portals for the entry of electrodes, vacuum gauges, gas sampling bottles and temperature monitoring units. Reagent gases were passed into the bell-jar via $\frac{1}{2}$" bore copper tubing from their respective cylinders or containers. This design permitted interactions with more than one gas concurrently without exposing the materials to the atmosphere and also allowed an improved pumping speed and better final vacuum in the apparatus. To obtain a vacuum of better than 10^{-6} torr the oil diffusion pump was equipped with a liquid nitrogen cold trap, the vacuum being measured using Pirani, Penning and Ionisation Gauges. The amount of reagent gas in the system was monitored by a Capsule Dial Gauge in the pressure range 5 torr to 600 torr and by a Pirani Guage below 5 torr.

Also attached to the bell-jar base-plate are gas sampling bottles for examination of reagent and

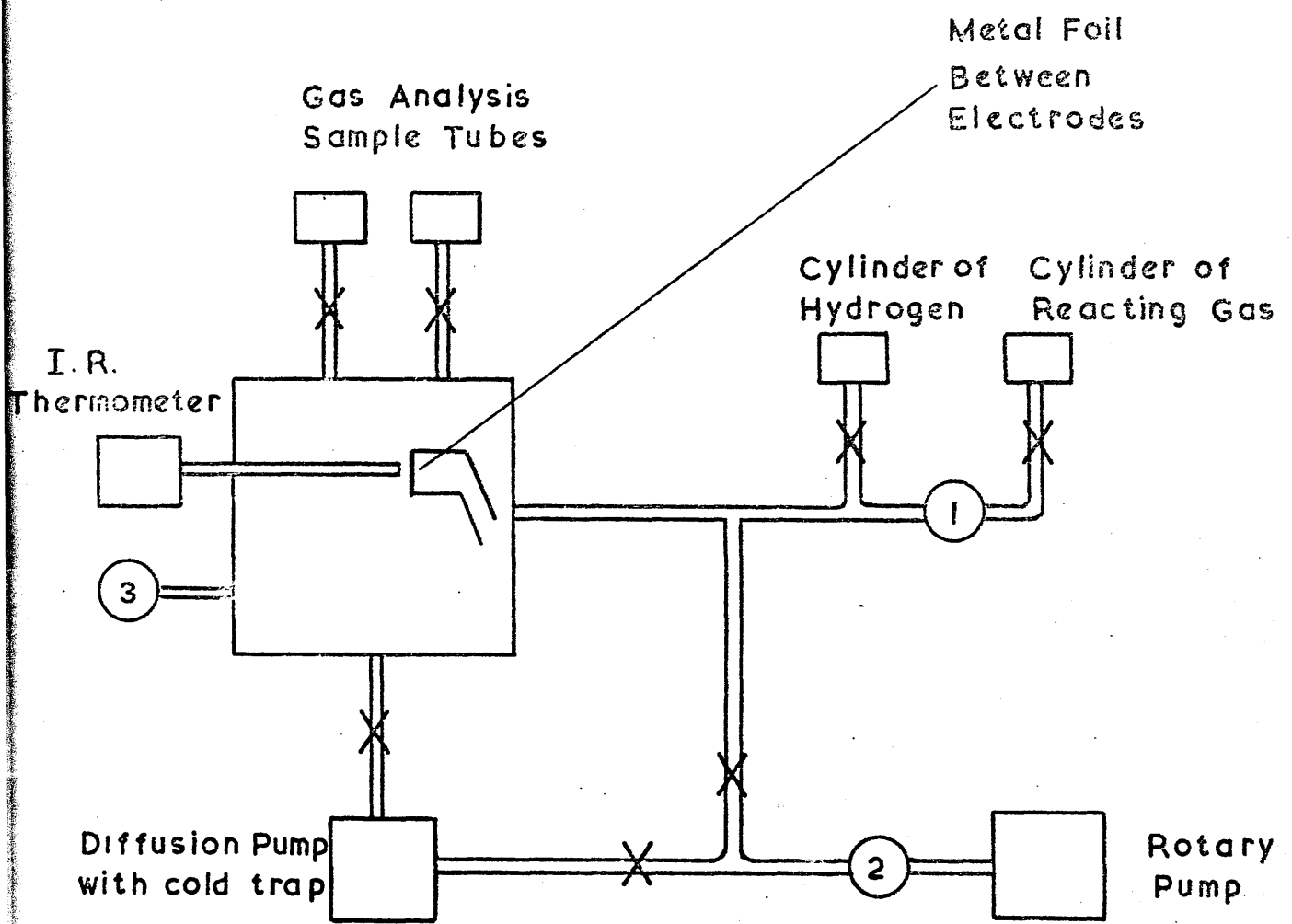

X — Valve

O — Pressure Gauge

1 — 0 - 760 Torr Gauge

2 — Pirani Gauge

3 — Penning and Ionisation Gauges.

FIGURE 2.1

product gases by mass spectrometry. These attachments to the bell-jar are shown schematically in Figure 2.2.

2.1.2. Heating Units

The metal used in the deposition experiments was raised to the reaction temperature by resistance heating, the passage of an electrical current through the foil. A voltage stabiliser was used during the heating processes to improve the temperature measurement and control. The stabiliser, from Servomex Controls Ltd., type A.C.2 Mark IIB, maintained a constant voltage supply to an accuracy of 0.25%, equivalent to $\pm$ 0.6 volts at 240 volts mains.

A diagram of the electrical circuitry contained in the apparatus is given in Figure 2.3. Three sets of electrodes are available for use in the bell-jar, the power being taken from two 8 amp/240 volt variac units. Each output is converted by a step-down transformer of voltage ratio 20:1, to give a final power supply in the form of 12 volts/60 amps., suitable for heating metal foils whose resistance is of the order of 0.1Ω.

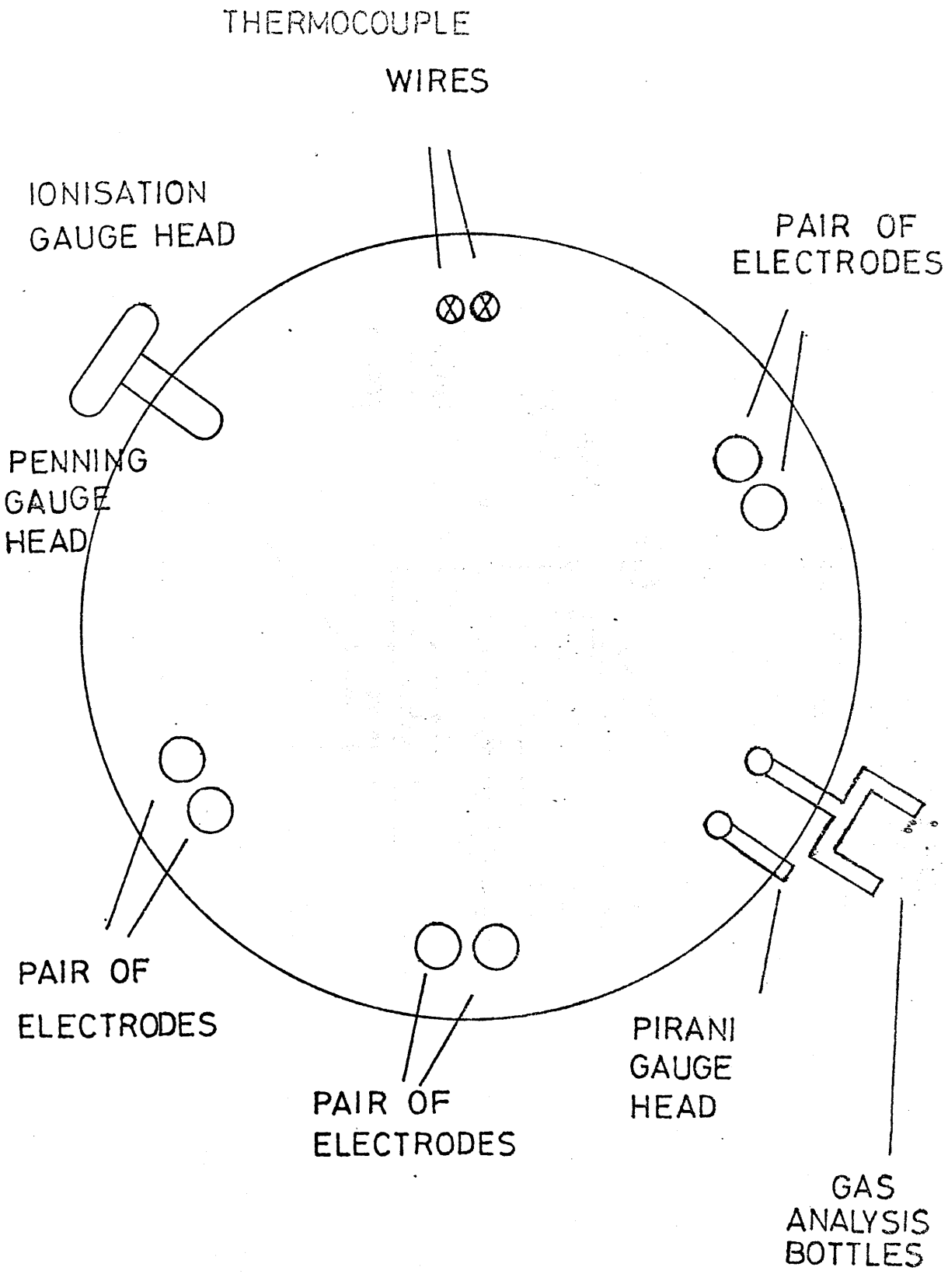
THERMOCOUPLE
WIRES
IONISATION
GAUGE HEAD
PAIR OF
ELECTRODES
PENNING
GAUGE
HEAD
PAIR OF
ELECTRODES
PAIR OF
ELECTRODES
PIRANI
GAUGE
HEAD
GAS
ANALYSIS
BOTTLES

FIGURE 2.2

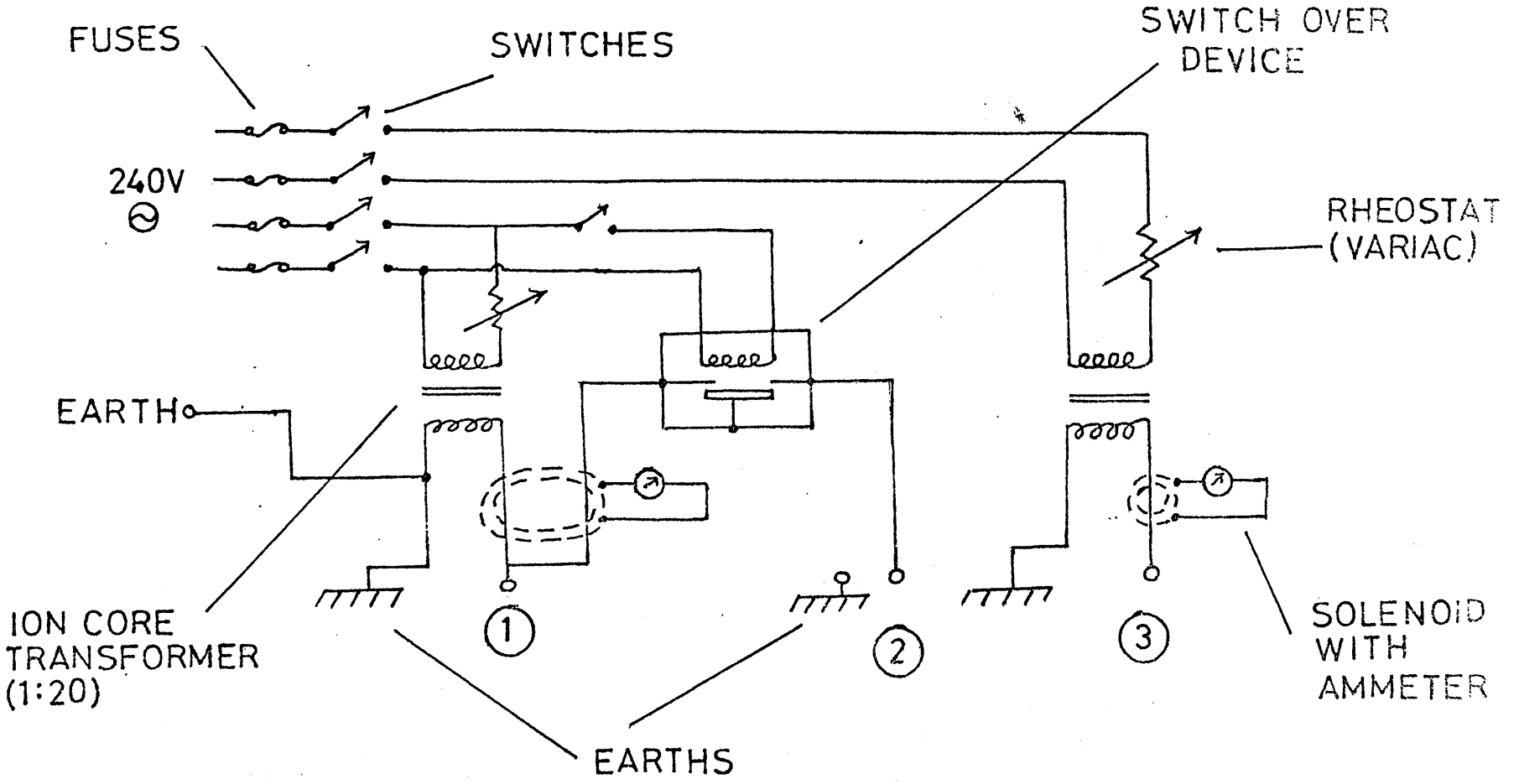

FUSES 4A ANTI-SURGE

FIGURE 2.3

The method of resistance heating had the advantage that very rapid temperature changes could be induced, because of the low heat capacity of the thin foil, less than 0.1 joules per°C being required. The disadvantage of the technique was that a temperature gradient between the centre and the edge of the foil inevitably occurred. Shaping the foil to reduce this effect was not undertaken because of the difficulty of achieving reproducible results. Instead, it was intended that selected experiments in which there was a need for a constant temperature along the foil would be carried out in a furnace designed and constructed for this purpose.

The furnace consists of a cylindrical block of stainless steel of height 5 cm. and diameter 7.5 cm. giving a heat capacity of approximately 900 joules per °C. The block can be separated into two equal parts, each of height 2.5 cm. to allow the insertion of a piece of nickel foil. A central, cylindrically-shaped hole in the block of diameter 2 cm. permits gas access to the foil and exposes an area of foil approximately equal to that used in the resistance heating method. The two halves of the block are clamped together using three stainless steel screws ensuring that the metal foil is held steady and that there is good thermal contact between the two parts of the block. The symmetry of the heating block is desirable to maintain

as evenly as possible the temperature around the foil.

The heating coil was obtained from Heatrod Elements Ltd. and has an output of up to two kilowatts. A stainless steel shield containing an inner film of asbestos was placed round the furnace to reduce heat transfer to the rest of the apparatus.

2.1.3. Temperature Measurement

In most of the experiments performed by resistance heating the temperature of the foil centre was monitored by a Pt/Pt 13% Rh thermocouple inserted into a hole in the centre of the foil. Due to the variable contact between foil and thermocouple the inaccuracy was of the order of 5% or 35°C at 200°C. Some later work employed an infra-red detector to measure and control the temperature of the foil. Its intrinsic accuracy was much higher (± 5°C) but the need for frequent recalibration of the control unit, necessitated by a gradual accumulation of evaporated metal from the hot foil on to the light pipe, limited the usefulness of this method. A diagram of the control system for the infra-red thermometer is given in Figure 2.4.

The temperature of the steel furnace is measured by means of a Pt/Pt 13%Rh thermocouple tightly fastened to the base of the block. The output from the thermocouple in the form of an E.M.F. is fed into a unit which controls the temperature of the block via

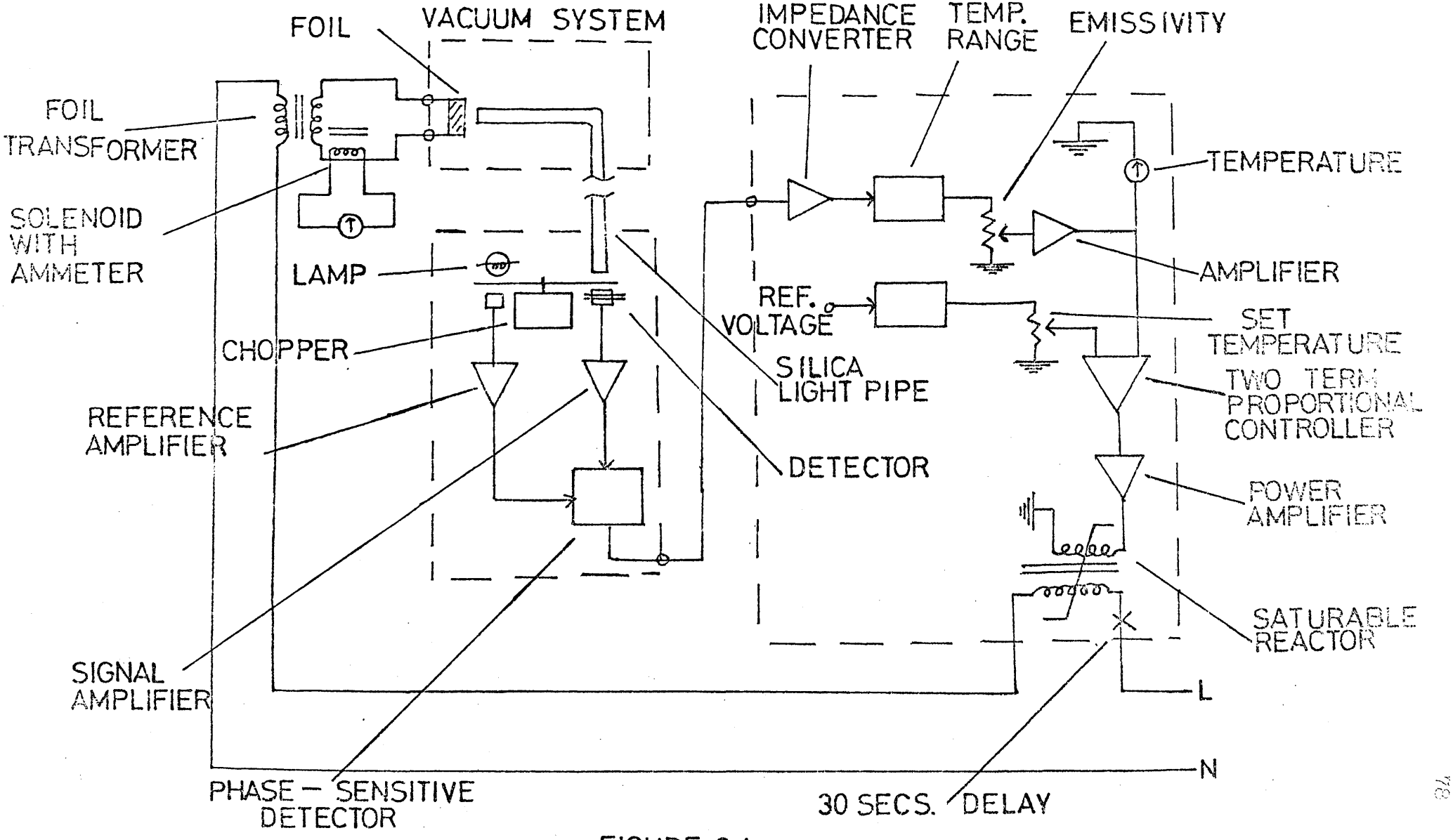
FOIL
VACUUM SYSTEM
IMPEDANCE CONVERTER
TEMP. RANGE
EMISSIVITY
FOIL TRANSFORMER
SOLENOID WITH AMMETER
LAMP
CHOPPER
REFERENCE AMPLIFIER
SIGNAL AMPLIFIER
PHASE – SENSITIVE DETECTOR
SILICA LIGHT PIPE
DETECTOR
REF. VOLTAGE
TEMPERATURE
AMPLIFIER
SET TEMPERATURE
TWO TERM PROPORTIONAL CONTROLLER
POWER AMPLIFIER
SATURABLE REACTOR
30 SECS. DELAY
L
N

FIGURE 2.4

proportional, integral and differential monitors. The accuracy of the temperature control is better than 5°C at 700°C. A diagram of the control system is shown in Figure 2.5.

2.2. Materials

2.2.1. Foils.

The metals used in these studies were iron and nickel, the majority of the experiments being performed with nickel. Both were in the form of thin polycrystalline rolled sheets. In the case of nickel this meant that the (123) crystallographic plane was preferentially exposed, whereas with iron the (100) plane was the one most commonly found at the surface (Taylor, 1961). The foils during reaction had two exposed faces with dimensions 7 mm. x 40 mm, giving a nominal surface area of $(5.6 \pm 0.4)\text{cm}^2$.

The purity of the foils is indicated below:

1. Nickel: two grades were employed, both 0.1 mm. thick.

(a) 99.9% pure, from Metals Research Ltd.

(b) 99.9% pure, from Johnson, Matthey and Co. Ltd.

Impurities:	Cu	< 50	V	< 50
(ppm)	W	< 20	B	< 50
(Robertson, 1968)	Co	< 50	Pb	< 20
	Sn	< 20	Al	< 50
	Si	< 100	Mn	< 40
	P	< 20	C	< 90

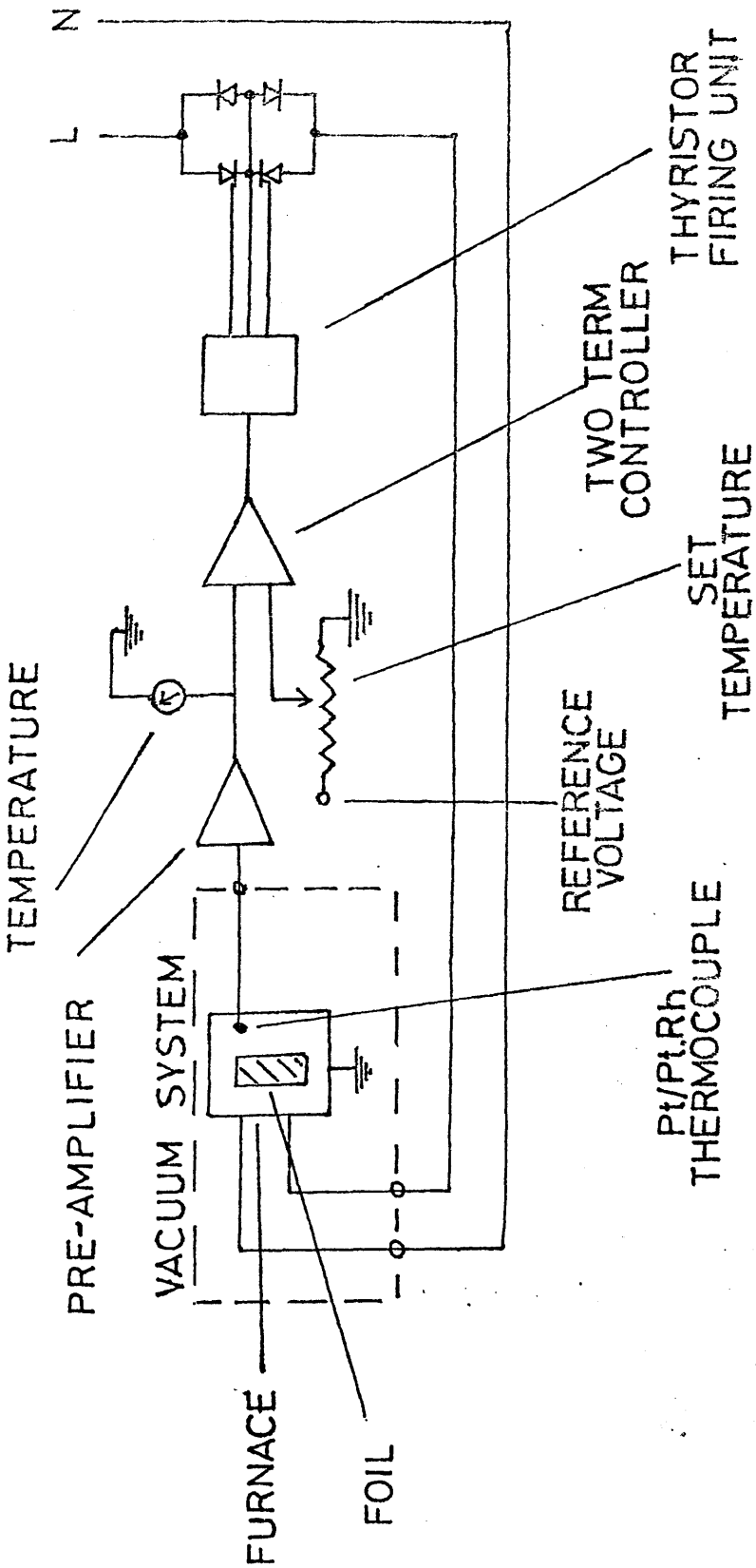
N
L
THYRISTOR FIRING UNIT
TWO TERM CONTROLLER
SET TEMPERATURE
REFERENCE VOLTAGE
Pt/Pt.Rh THERMOCOUPLE
TEMPERATURE
PRE-AMPLIFIER
VACUUM SYSTEM
FURNACE
FOIL

FIGURE 2.5

2. Iron: 99.95% pure, from Metals Research Ltd., 0.075 mm. thick.

Impurities: (ppm)					
	Ag	< 1	Si	< 2
	Mn	= 3	Ni	< 2
	Mg	< 1	Cu	< 1

2.2.2. Gases (or Vapours).

The following gas-phase materials were used in this work:

Hydrogen (Air Products Ltd.) 99% pure, and further purified by the addition of an Engelhard catalytic purifier which is specified as reducing the oxygen content to below one part per million.

Methane: two grades were employed

(a) Air Products - 99% pure

impurities: (ppm) (Robertson, 1968)
- ethane 6000
- propane 500
- n-butane 100
- i-butane 100

(b) B.O.C. research grade X - 99.99% pure.

3. Propane: two grades were employed

(1) Matheson Co., 99.9% pure

(2) Matheson Co. research grade, 99.99% pure

impurities: (ppm)				
isobutane	= 65	ethane	< 15
nitrogen	< 5	methane	< 5
oxygen	< 5	butane	< 1

4. Propylene: two grades were employed

(1) Matheson Co., 99.9% pure.

(2) Matheson Co. research grade, 99.99% pure.

The largest impurity is propane.

5. Acetone: Analar grade.

impurities: (ppm)	acetic acid	20	formaldehyde	20
	water	2000	methanol	500
	alkalinity	12	reducing agents	2
	non-volatile matter	5		

The acetone before use was frozen in liquid nitrogen and heated to room temperature several times while the system was being continuously evacuated to remove oxygen and other dissolved gases from the liquid.

6. Butadiene: B.O.C., 99.9% pure

2.3 Procedure

2.3.1. Deposition Procedure:

The metal foil to be heated was cut to size and cleaned by ultrasonics in distilled water, ethanol and acetone before being weighed. It was then placed in position between a pair of electrodes in the apparatus previously described. The system was evacuated, flushed several times with hydrogen and left evacuating overnight. The foil was heated at 700°C in 600 torr H_2 for 2 hours. After the foil had cooled the reaction chamber was again pumped out,

flushed several times with the reagent gas and the evacuation procedure continued overnight. The reagent gas was passed into the bell-jar until the desired pressure was attained and left in contact with the heated foil for the required length of time. In experiments designed to study the effect of the foil pretreatment on the final product one or more of the stages just described were omitted. After reaction the apparatus was allowed to cool to room temperature and the foil with deposit was removed and weighed.

2.3.2. Specimen Preparation for Transmission Microscopy

The deposit was prepared for examination by transmission electron microscopy in one of two ways:

1. Some foil plus deposit was immersed in concentrated analar hydrochloric acid and left overnight, at the end of which period part of the foil had dissolved leaving a film of carbon floating on the surface of the liquid. After washing in distilled water the film was broken up into pieces suitable for placing unsupported on a copper grid specimen holder. Because no underlayer of supporting medium was necessary specimens prepared in this manner were ideally suited for high resolution microscopy. The acid treatment ensured that the topography of the deposit remained intact and could be examined but no reliable

information concerning the metal contained among the carbon could be obtained.

2. Alternatively, a piece of foil with deposit was placed in a test-tube in distilled water or cyclohexane and subjected to ultrasonic disintegration. One drop of the resulting suspension dried onto a silica support film held on a copper grid or a platinum/iridium mount gave a convenient specimen for examination by transmission microscopy. This method was particularly suitable for examining the thicker products of longer duration experiments and was used to complement the first technique in the study of deposits.

2.4. Product Examination

2.4.1. Transmission Microscopy Techniques

Several techniques connected with the examination of particular features of the reaction products in the transmission electron microscope are now discussed.

1. Shadowing. To obtain information on deposit morphology specimens were shadowed by coating at an angle of 15° with an evaporated film made from two parts nickel and one part palladium.

2. In Situ Oxidation. The Siemens Elmiskop I microscope was used to study the behaviour of the carbonaceous products of several reactions towards oxidative attack. A special gas inlet attachment

(Fryer, 1968) constructed from the objective aperture drive allows the complete oxidation process to be observed and recorded. The specimen was maintained at the desired temperature while the gas, normally oxygen, was passed into the microscope column at a rate controlled by a needle-valve. The gas pressure at the Penning gauge head is kept at about 10^{-3} torr, low enough for the high voltage supply to function, but because of the design of the gas inlet device this corresponds to a much higher pressure (possibly 1 torr) at the specimen.

2.4.2. X-Ray Powder Analysis

A Phillips X-ray powder camera was used to give information on the layer-spacings of the pyrolytic graphite. Approximately 1 mg. of deposit was mixed with an equal quantity of " Durafix" adhesive and rolled into the form of a thin film. It was left to dry for four hours, positioned in the camera and exposed to Co Kα radiation (protected from Co Kβ rays by an Fe filter) for a suitable period, normally about 6 hours.

2.4.3. Mass Spectrometry

The mass spectra obtained from the M.S.12 spectrometer were interpreted by comparison with the breakdown patterns of the possible products (Dow, Cornu and Massot). In general a number of gases were

identified in each spectrum and it was found necessary to make a correction for the varying sensitivity of the instrument towards different molecular ion fragments (Otvos et al., 1956). This procedure made available quantitative data on the product gas compositions of desired experiments.

2.4.4. Scanning Electron Microscopy

Specimens to be examined by scanning electron microscopy were prepared by attaching pieces of metal foil containing deposit to specimen blocks using "Durafix" adhesive. Electrical contact between the block and the foil was ensured by smearing the edge of the foil with colloidal silver in acetone.

CHAPTER 3

RESULTS

3. RESULTS

Contents

3. RESULTS

3.1. Transmission Electron Microscopy

3.1.1. General Deposition Morphology

Most of the carbon deposition studies were carried out at 700°C. The overall appearance of the deposit at this temperature depended on the rate and duration of the reaction as well as on the particular metal grains on which the carbon was formed. The interactions utilised to deposit carbon are indicated in Table 3.1, the most frequently used one being the Ni/CH_4 system.

Table 3.1

Reagents used for Carbon Deposition Experiments.

	Methane	Propane	Propylene	Butadiene	Acetone
Nickel	✓	✓	✓	✓	✓
Iron	✓				

In sections 3.1.1 to 3.1.7 the deposits formed at the foil centre are discussed. The deposits from the cooler edge regions are considered separately in section 3.1.8. The conditions under which the most important experiments were performed are listed in Table 3.2.

In all cases carbon was preferentially formed at the sites of the metal grain boundaries giving rise to a series of thicker bands in the deposit film delineating the shapes and extents of the metal grains.

Table 3.2

Experimental Conditions for Carbon Deposition Studies

Experiment	Pressure (torr)	Time (hrs.)	Comments
1A	600	2	
1D	"	20	
1E	"	4	
1F	"	"	Foil and powder used
1G,1H	"	2	
1I	"	0.5	
1J	"	22	
1K	20	7.5	
1L	100	2	
1M	300	"	
1N	540	"	60 torr H_2 also present
1O	1	"	
1P	600	"	
1Q,1R	60	"	
1S,1T	20	"	
1V,1W	1	30	
1X	600	4	H_2 pretreatment at room temp. only.
1Y	600	6	No pretreatment.
1Z	"	4	" "
1AA	"	6	Pretreatment in vacuo.
1AB	"	4	" " "
1AC	"	"	Normal pretreatment
1AD	"	"	" "
1AE	"	"	Foil etched in HCl

Table 3.2 (contd.)

Experiment	Pressure (torr)	Time (hrs.)	Comments
1AF	600	33.5	Foil cooled after reaction by instantaneous removal of heating current.
1AG	"	"	Foil cooled slowly over 6 minutes.
1AH	"	0.25	Conditions as for 1AF.
1AI	"	"	Conditions as for 1AG.
1AJ	"	0.5	
1AK	"	0.088	
5D	600	1	
5E	"	4	
5F	100	2	
5G	300	"	
5H	540	"	
5I	1	"	60 torr H_2 also present.
7A	600	2	Temperature = 600°C
7C	"	4	
7D,7E	10	"	
7F,7G	4	30	
7H	5	0.5	NiO coated
7I	"	0.3	" "
7J,7K	0.02	4	
7L	0.06	0.25	O_2 present
12A	600	5.5	Temperature = 600°C
12B	"	0.5	" "
12C	20	7	" "

Table 3.2 (contd.)

Experiment	Pressure (torr)	Time (hrs.)	Comments
12D	20	0.5	
12E	"	1.5	
16A	40	3.5	
16B	20	0.83	
16C	"	0.5	
23A,23B	20	2	
23C,23D	1	2	
23E,23F	1	0.5	
23G,23H	600	0.5	
23I,23J	20	28	
23L	0.024	0.5	
23M	"	2	
23N	0.02	8.25	
23O	"	0.5	
23P	"	2	

In Table 3.2:

1. all temperatures are 700°C unless otherwise stated.
2. Experiment 1 refers to Ni/CH_4.
   " 2 " " Fe/CH_4.
   " 7 " " Ni/C_3H_8.
   " 12 " " Ni/propylene.
   " 16 " " Ni/acetone
   " 23 " " Ni/butadiene.
3. Experiments grouped together were performed simultaneously.

Plate 3.1 from experiment 12C contains shadowed deposit from several grains, the thicker boundary material being apparent. Variations in the appearance of the deposit were also dependent on the particular grain examined. Often, regular features such as are visible in Plate 3.2, from experiment 1AH, were observed within individual grains. They are termed " growth fronts" in this work and are perhaps suggestive of an epitaxial relationship, though this was never proved.

Experiments were carried out to determine to what extent the foil pretreatment affected the morphology of the product of Ni/CH_4 interactions. It was concluded that annealing in vacuo was as efficient as the normal pre-anneal in hydrogen for preparing the nickel for carbon deposition catalysis. When no pre-anneal was employed carbon was deposited but at a reduced rate and the resulting crystals were smaller and had a lesser degree of orientation than those found in normal deposits.

The addition of 10% H_2 to CH_4 for carbon deposition on Fe and Ni did not significantly improve either the rate of deposition or the quality of the product contrary to the results of several other workers. It is possible that H_2 helped the initial breakdown of the hydrocarbon species until more H_2 is formed by the hydrocarbon-to-carbon conversion. If this is true then the H_2 which will undoubtedly have been adsorbed on the

Plate 3.1

Shadowed deposit from experiment 12C showing the thicker material formed on metal grain boundaries. [1A 70 824].

magnification = 17,200X.

Plate 3.2

Regular features present among the carbon deposit from experiment 1AH. [NS 72 400].

magnification = 25,800X.

metal foil by the H_2 anneal may have been sufficient to accelerate the commencement of the reaction, rendering any further H_2 addition unnecessary.

The addition of O_2 to C_3H_8 employed for carbon deposition on Ni caused the formation of NiO and other Ni compounds and partially inhibited carbon formation.

3.1.2. Flake Graphite

In all reactions at 700°C the first deposit was a layer of flake graphite on the metal surface. The crystal size of this material was controlled by the rate of reaction, being largest for slow interactions. For this reason it was easier to obtain large platelets, with L_A up to 10μ, at low pressures and with saturated gases. An example of this single crystal graphite from experiment 5F is given in Plate 3.3. The selected area diffraction (S.A.D.) pattern from an individual crystal had the appearance of Plate 3.4 in which only lattice planes perpendicular to the basal (0002) planes are visible, indicating that the platelet graphite has deposited with its basal planes parallel to the metal substrate. This was true of all of the reactions studied at 600°C and 700°C. Because of this no direct measurement of the crystal L_C dimension was possible but from the thickness of the specimens L_C values over 1000 Å were estimated. Due to the variation in orientation of the crystals certain planes not quite

Plate 3.3

Single crystals of graphite from experiment 5F. [1A 71 540].

magnification = 90,000X

Plate 3.4 (inset)

Selected area diffraction pattern from an individual graphite crystal. [1A 72 91].

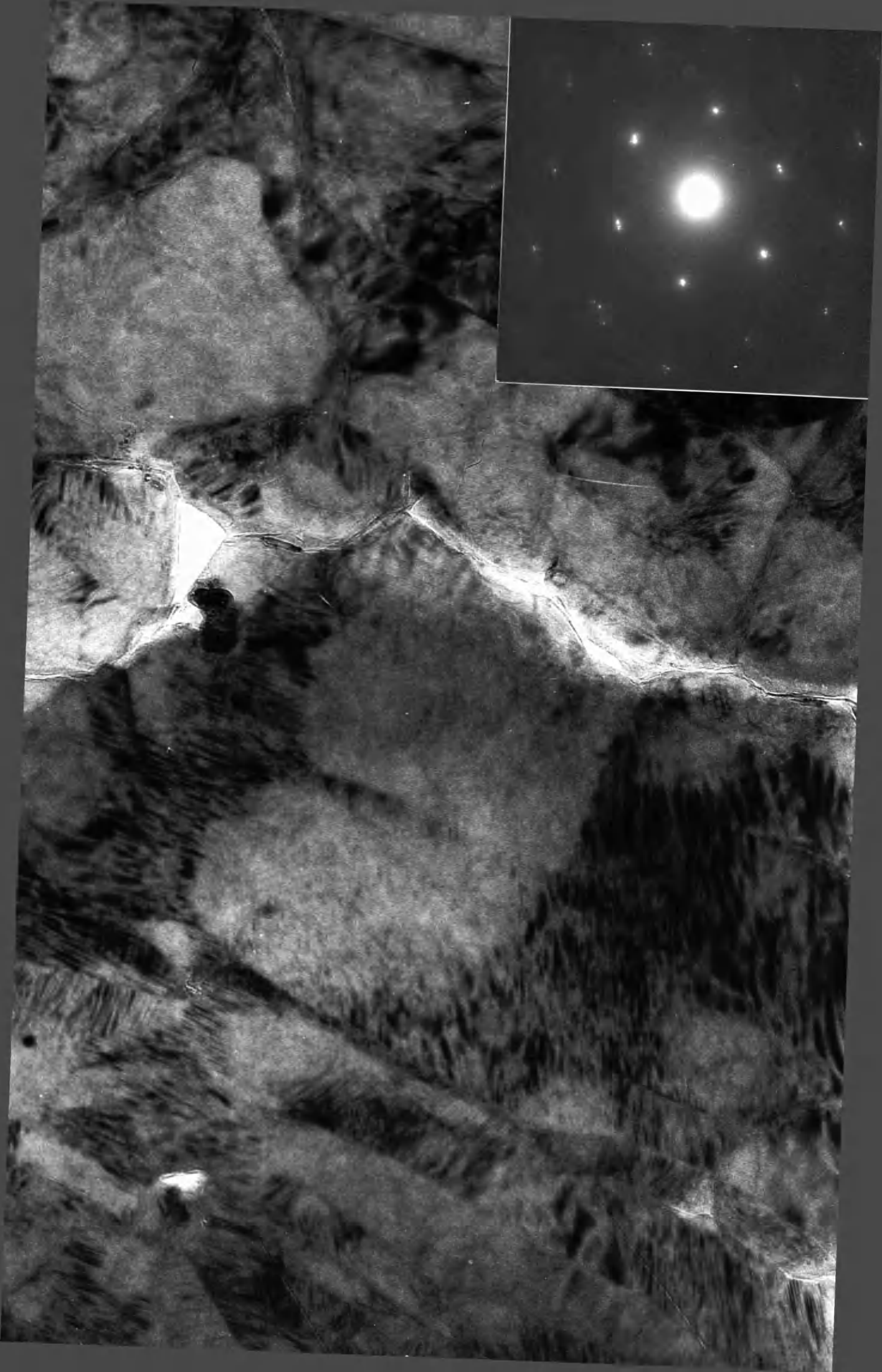

perpendicular to the (0002) planes often gave rise to reflections in the diffraction patterns of graphite flakes. Such an S.A.D. pattern is given in Plate 3.5. The lattice spacings obtained from this pattern confirm by the presence of the general (hkl) reflections that the product had three-dimensional order. Table 3.3 lists the spacings from Plate 3.5.

Table 3.3

d spacings of graphite platelet deposit (in Å).

Plate 3.5	SP1 graphite	Index	Difference
3.383	3.355	0002	0.028
2.117	2.128	$10\bar{1}0$	0.011
2.045	2.032	$10\bar{1}1$	0.013
1.688	1.678	0004	0.010
1.229	1.229	$11\bar{2}0$	0.000
1.160	1.153	$11\bar{2}2$	0.007
1.055	1.064	$20\bar{2}0$	0.009
0.997	0.990	$10\bar{1}6$	0.007

A common feature of the platelet graphite was the presence of large arrays of moire fringes. An example in Plate 3.6 was taken from experiment 1L. The moire fringes are known to represent minor imperfections in highly crystalline materials and ones in graphite have been interpreted as twist boundaries between overlapping crystals (Presland et al., 1969). The planes responsible for the moire patterns can be identified by

Plate 3.5

Selected area diffraction pattern showing the (hkl) reflections of three-dimensionally ordered graphite. [1A 70 1090].

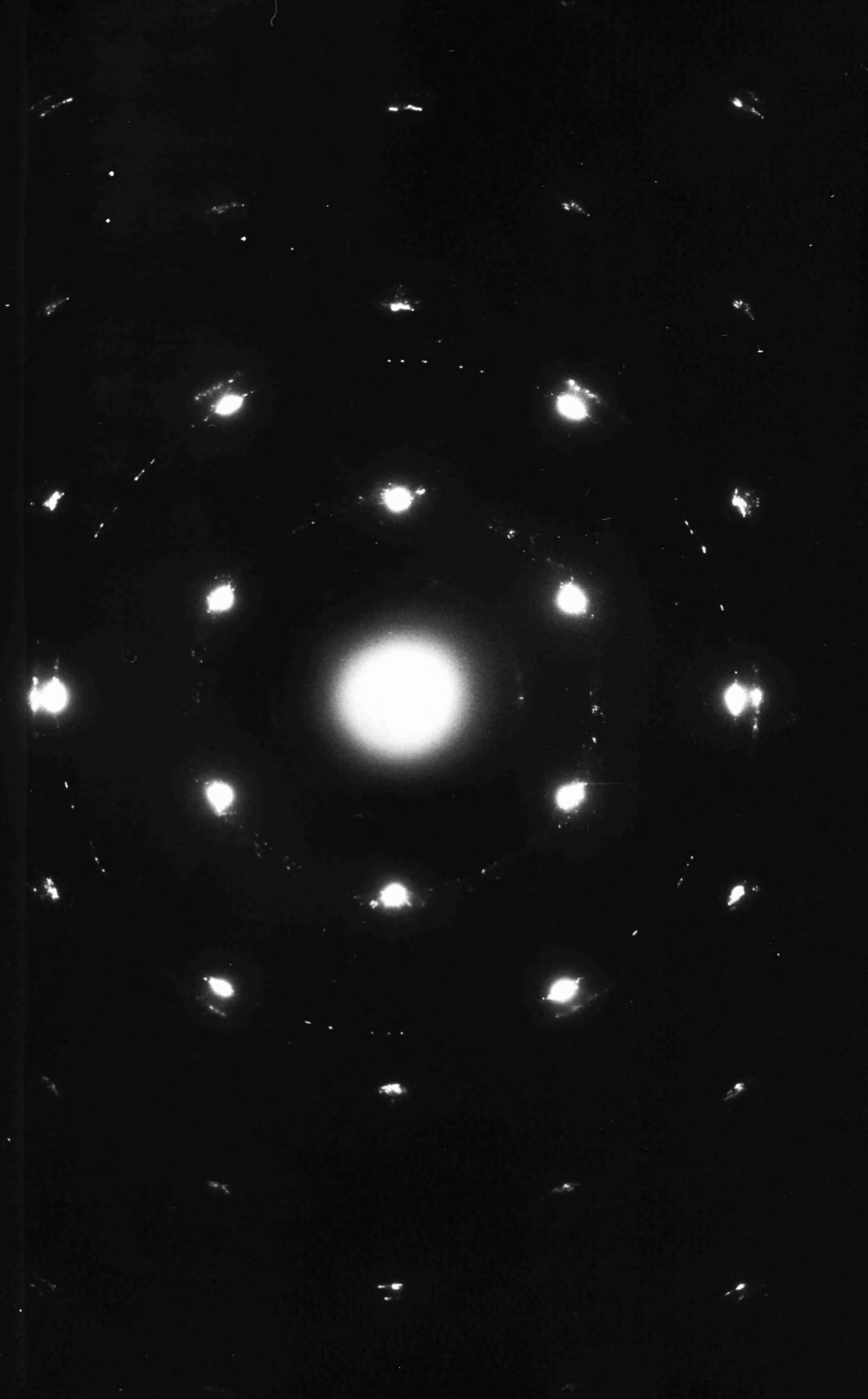

Plate 3.6

Platelet graphite from experiment 1L containing large areas of moire fringes. [1A 71 514].

Magnification = 84,00X.

Plate 3.7

Dark field $(10\bar{1}0)$ micrograph of moire fringes from a region of experiment 12C deposit. [1A 70 838].

magnification = 100,000X.

Plate 3.8

Dark field $(11\bar{2}0)$ micrograph of moire fringes from the same region of experiment 12C deposit as Plate 3.7. [1A 70 839].

magnification = 100,000X.

Plate 3.9

Shadowed deposit from experiment 12C containing a network of graphite tilt boundaries. [1A 70 826].

magnification = 16,400X.

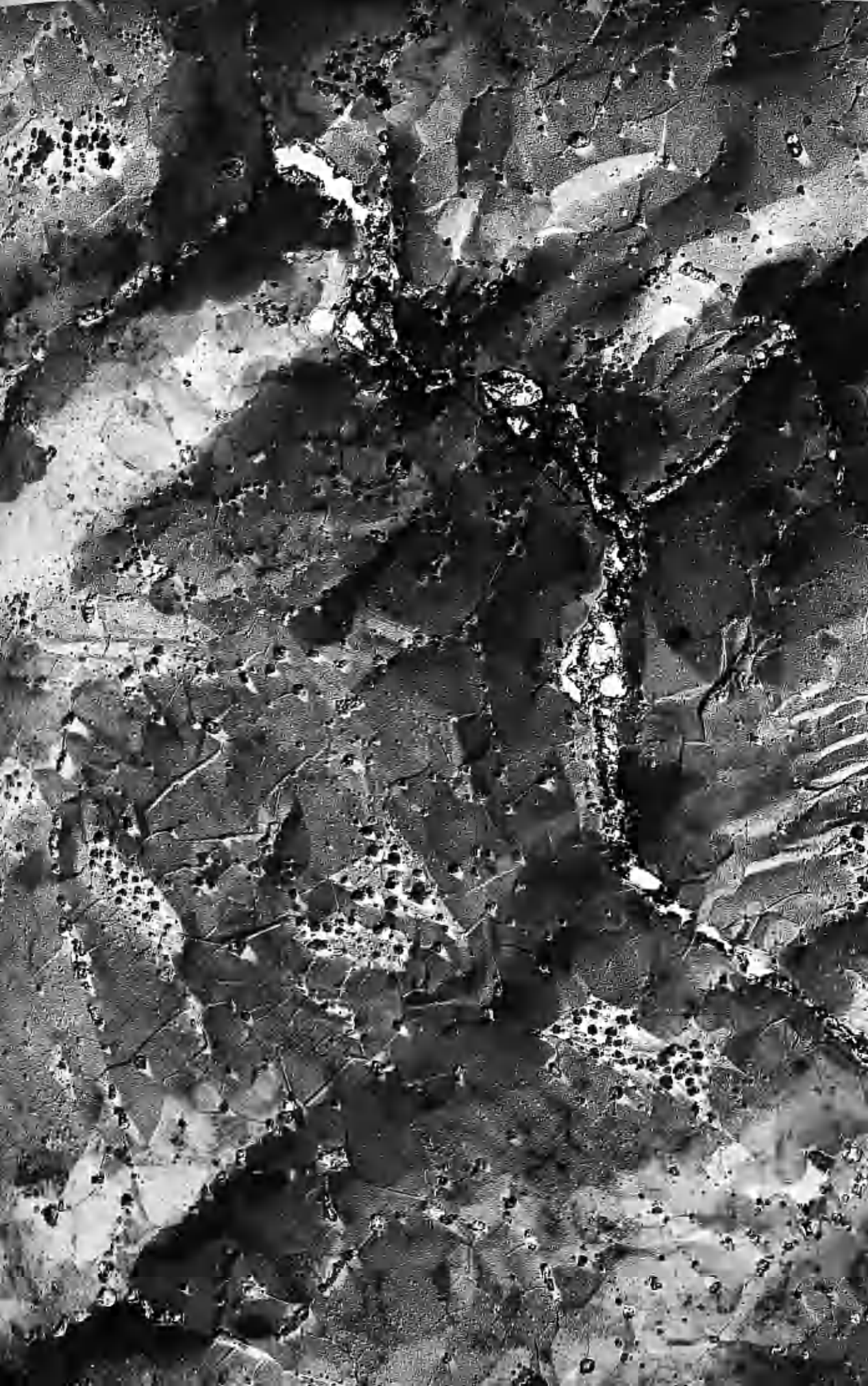

Plate 3.10

Graphite crystals of varying thicknesses from experiment 1AD. [NS 72 72].

magnification = 33,800X.

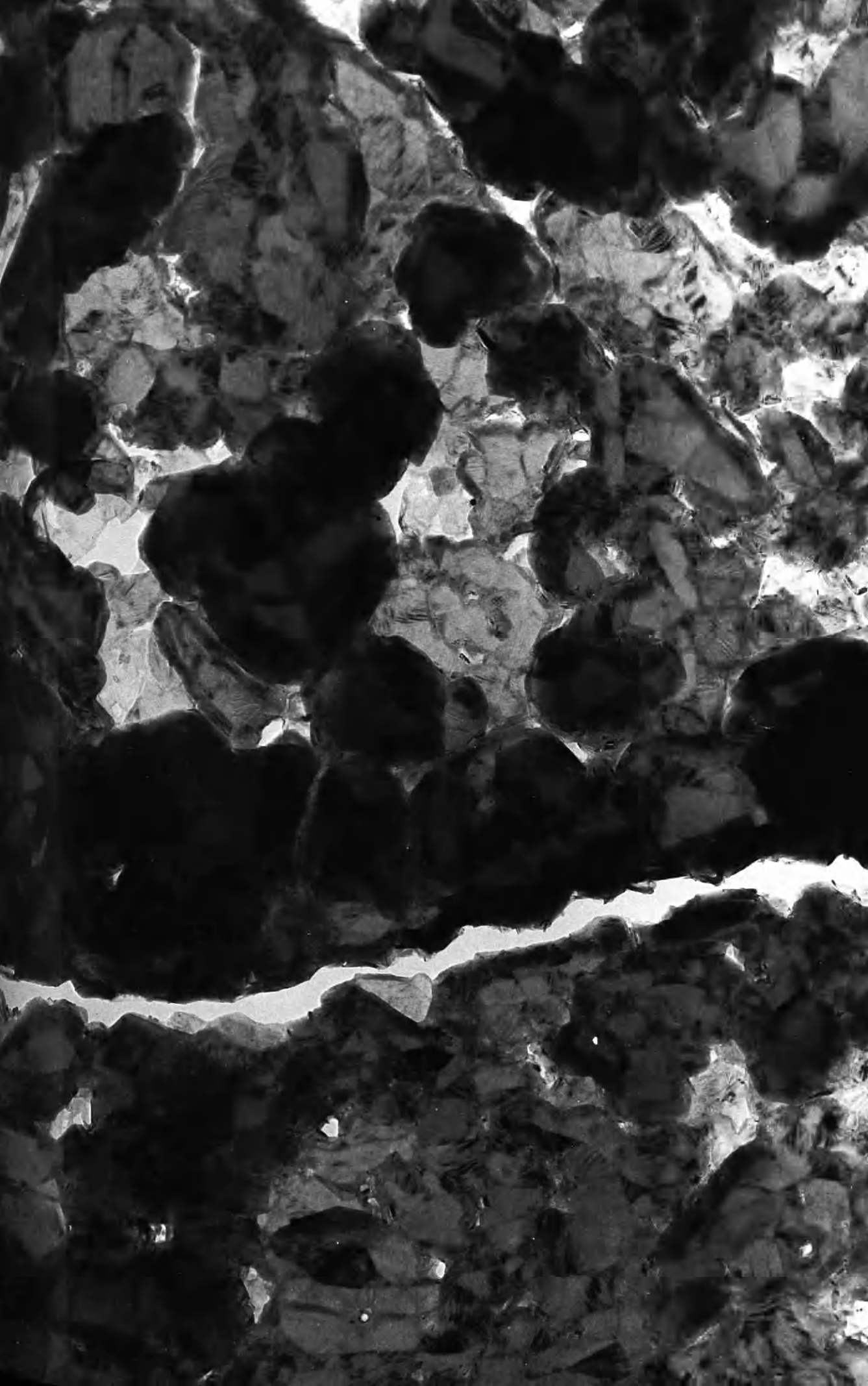

dark field studies and from measurements of the moire spacing, D, the angle of mismatch, α, can be determined according to,

$$D = \frac{d_{hkl}}{\alpha} ,$$

where d_{hkl} is the spacing of the relevant lattice plane. In Plates 3.7 and 3.8, taken from the same area of experiment 12C product, dark field $(10\bar{1}0)$ and $(11\bar{2}0)$ images respectively of moire fringes are shown. The values of D are 66.4 Å and 34.4 Å and the calculated values of α are 1°55' and 1°51' respectively. The angle of twist in this case is therefore 1°53' $\pm$ 3'. Tilt boundaries in synthetic graphite have also been reported. The shadowed area in Plate 3.9 from experiment 12C resembles the tilt boundary networks described by Presland and Walker (1969). Hence the existence of overlapping sub-grains of pyrolytic graphite is well established.

In this work there was some evidence that more than one layer of platelet graphite could form and observations showed that variations in the thickness of individual crystals could be very marked. Plate 3.10 exhibits numerous crystals of widely differing thicknesses. In several short duration experiments a very thin film ($<$ 100 Å) of polycrystalline carbon was observed, along with the flake graphite, which was thought to have formed by the carbon dissolved in nickel at 700°C coming out of

solution on cooling to room temperature (Derbyshire et al, 1972). Accordingly, experiments were performed to determine whether the rate of cooling of the metal foil after reaction had any bearing on the morphology of this carbon film. An area of film from experiment 1AH is shown in Plate 3.11 and its polycrystalline nature is revealed. The crystallinity of these films were not significantly improved by cooling over a period of six minutes.

A further feature of the platelet deposit was the bending often observed at the edge of crystals. Whereas normally the basal graphite planes lay horizontally on the metal surface, dark field and S.A.D. studies indicated that planes turned up at the edges of crystals under certain conditions. It has been suggested (Presland et al, 1969) that this effect is due to differential contraction of the metal and graphite lattices between 700°C and 20°C. On cooling from 700°C nickel contracts in length by approximately 1% (Hampel, 1968) while the graphite dimension change is negligible in comparison ($< 10^{-3}\%$). This explanation is certainly adequate for the amount of lattice distortion found with thinner deposits but in longer duration experiments individual crystals curled up beyond the 1% which can be accounted for by contraction effects. This phenomenon will be discussed in section 3.1.3.

Plate 3.11

An area of thin, polycrystalline film from experiment 1AH with its diffraction pattern. [NS 72 393].

magnification = 84,000X.

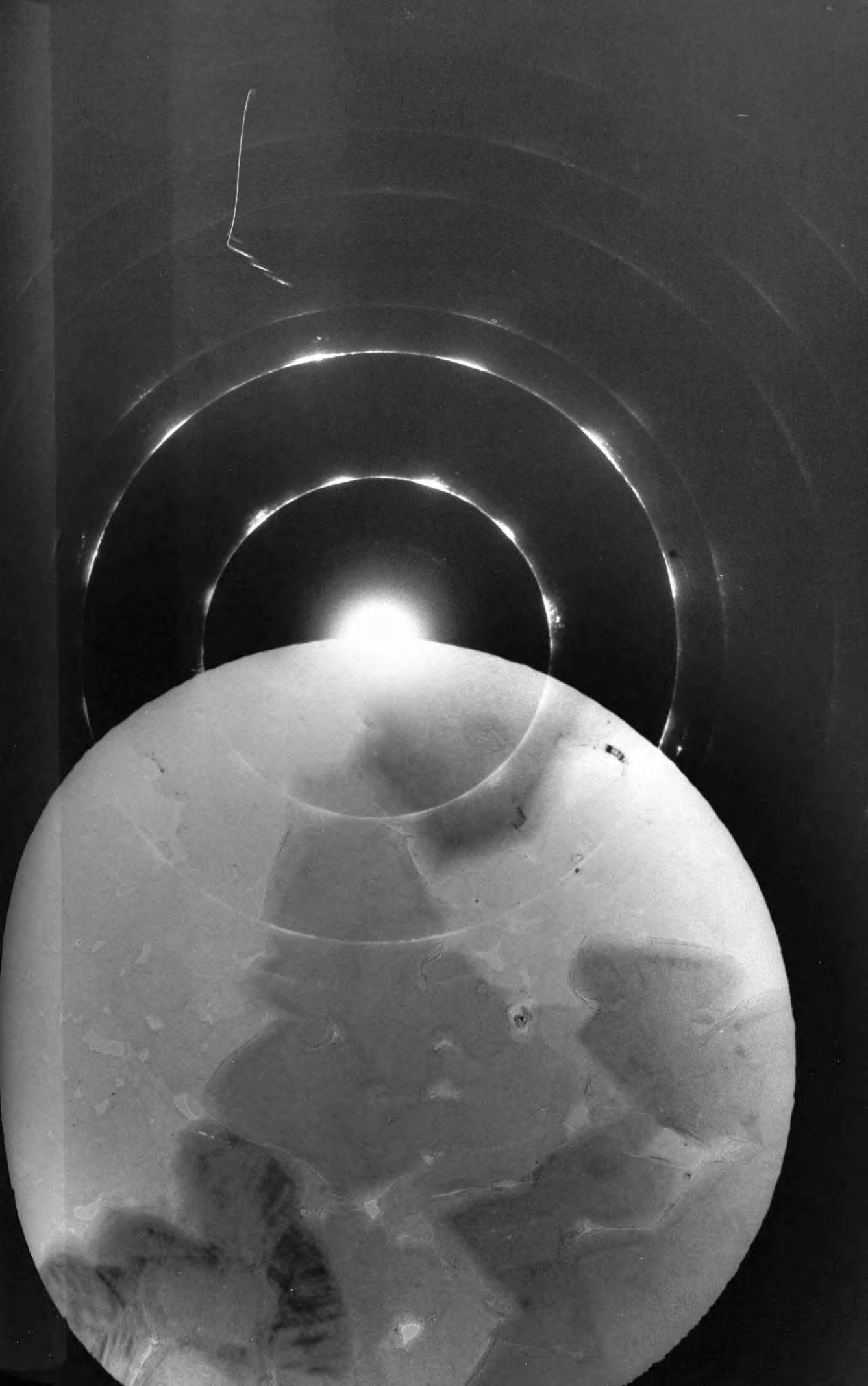

As well as the folding which occurred along the graphite crystal boundaries and sub-boundaries an additional distortion of the lattice was often observed at the intersection point of several crystals. A number of these features termed " diffracting edges" are shown in Plate 3.12 from experiment I 0. The diffraction pattern of the region around one of these gaps in the graphite matrix is contained in Plate 3.13. Bordering the gap there is a region of altered contrast denoting a bending of the (0002) planes, accompanied by diffraction effects proved by dark field studies to be caused by vertically oriented (0002) planes. The presence of the (0002) ring in Plate 3.13 verifies that the graphite around this hole has been forced into adopting a vertical configuration. The reason for this effect is discussed in Section 3.1.4.

3.1.3. Non-oriented Carbon

As has already been mentioned, the first type of deposit from the gas/metal interactions being studied was platelet graphite. When this material had covered the whole of the metal surface the L_A dimension could only be increased by distortion of the lattice at the crystal edges so that the graphite planes could extend in a non-horizontal direction. After this stage has been reached the carbon material can no longer be

Plate 3.12

A number of diffracting edges formed in experiment 1 0 at the intersection of platelet graphite crystals. [1A 71 674].

magnification = 16,800X.

Plate 3.13

An individual diffracting edge with its diffraction pattern which contains strong (0002) reflections. [1A 71 662].

magnification = 110,000X.

considered platelet graphite. The crystal size has decreased and S.A.D. patterns have gradually become polycrystalline, showing no preferred orientation and for this reason the material has been called here "non-oriented carbon". Non-oriented carbon of this type was formed from all of the interactions listed in Table 3.1 when sufficiently long reactions were carried out. An example from experiment 1AF is given in Plate 3.14 and its diffraction pattern is shown in Plate 3.15.

Because of the faster deposition from unsaturated gases (see section 3.6) it was easier to obtain non-oriented carbon from propylene and butadiene. An extreme instance of its formation on top of a layer of flake material, from experiment 12B at 600°C, is shown in Plate 3.16. This latter example of non-oriented material was fundamentally different from the former one and appeared to be a non-catalysed solid-phase carbon. The non-catalysed carbon only formed at higher pressures (600 torr) and with the unsaturated gases.

3.1.4. Filamentary Carbon

Filamentary carbons were observed in all of the systems studied though their exact morphology depended on the individual reaction conditions. The features common to all types were: an outer covering of carbon enclosing a region which was either hollow or contained

Plate 3.14

Non-oriented carbon from experiment 1AF.
[NS 72 343].

magnification = 84,000X.

Plate 3.15

Selected area diffraction pattern of the material in Plate 3.14. [NS 72 344].

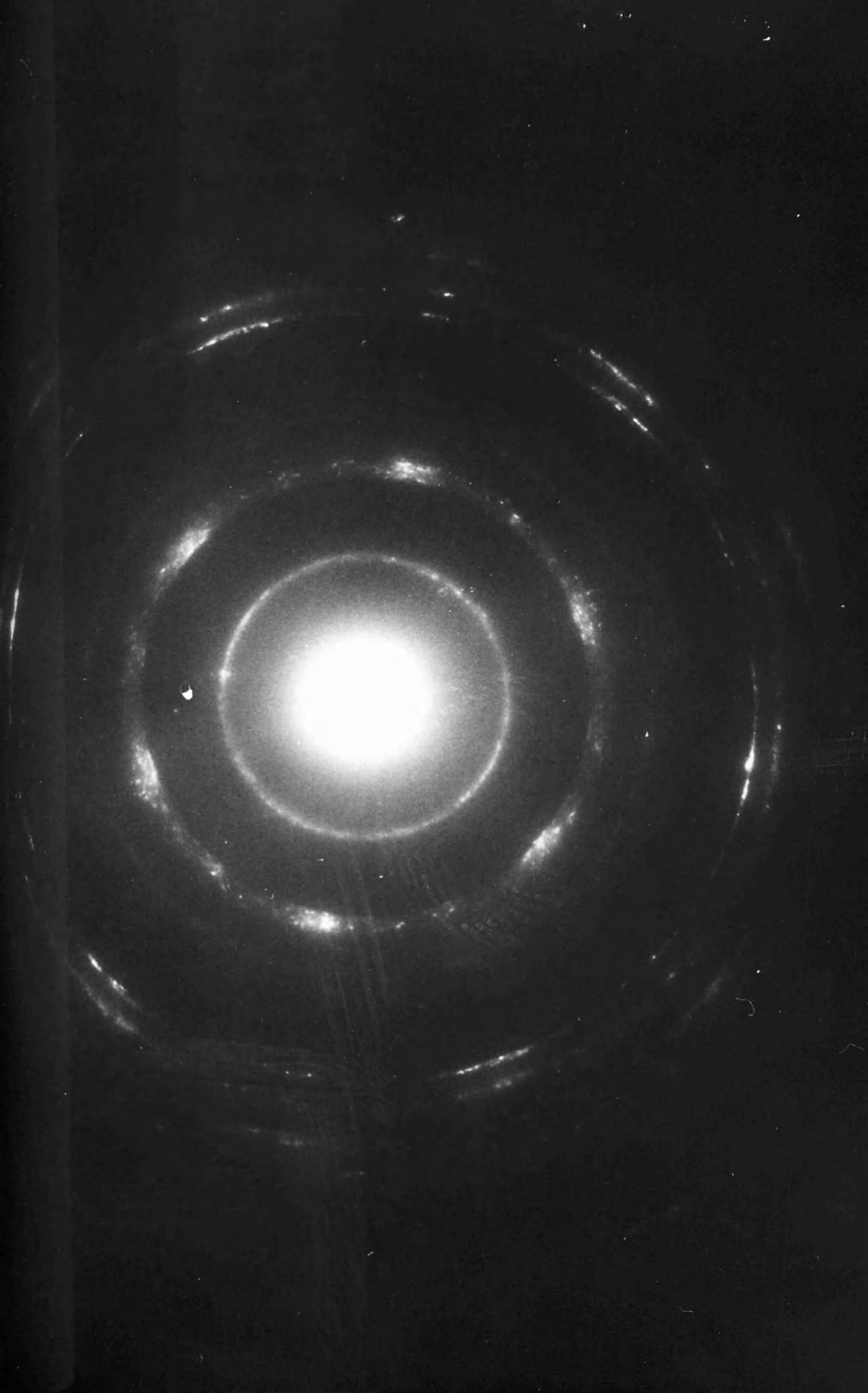

Plate 3.16

Solid-phase carbon formed during experiment 12B. [NS 70 949].

magnification = 148,000X.

small amounts of less crystalline carbon; a metal particle responsible for the filament's growth present at its tip and often along part of the enclosed region. The filaments formed in fast reactions were rather featureless. One from experiment 23B is shown in Plate 3.17. Slower reactions led to the production of a more highly structured type of filament whose crystallinity and degree of preferred orientation justify their being called graphite fibres. One particular class of fibre could be formed under suitable conditions from all of the interactions listed in Table 3.1 and several other classes were found under more restricted conditions.

The features of this major class of fibre are typified by the cluster of fibres in Plate 3.18 from experiment 1D. The fibres occurred frequently in complex branching and clustering arrangements, each branch having diffraction effects prominent along its edges. The (0002) dark field micrograph of Plate 3.18 shown in Plate 3.19 indicates that the (0002) planes were responsible for these diffraction effects and that the planes were wound cylindrically around the main axis of each branch. Selected area electron diffraction evidence verified that the fibres comprised three--dimensionally ordered graphite as shown by the presence of general ($hk\bar{h}+\bar{k}l$) reflections and the arced nature of the (0002) reflection in the diffraction patterns

Plate 3.17

Non-graphitic filament formed from experiment 23B. [NS 71 770].

magnification = 88,000X.

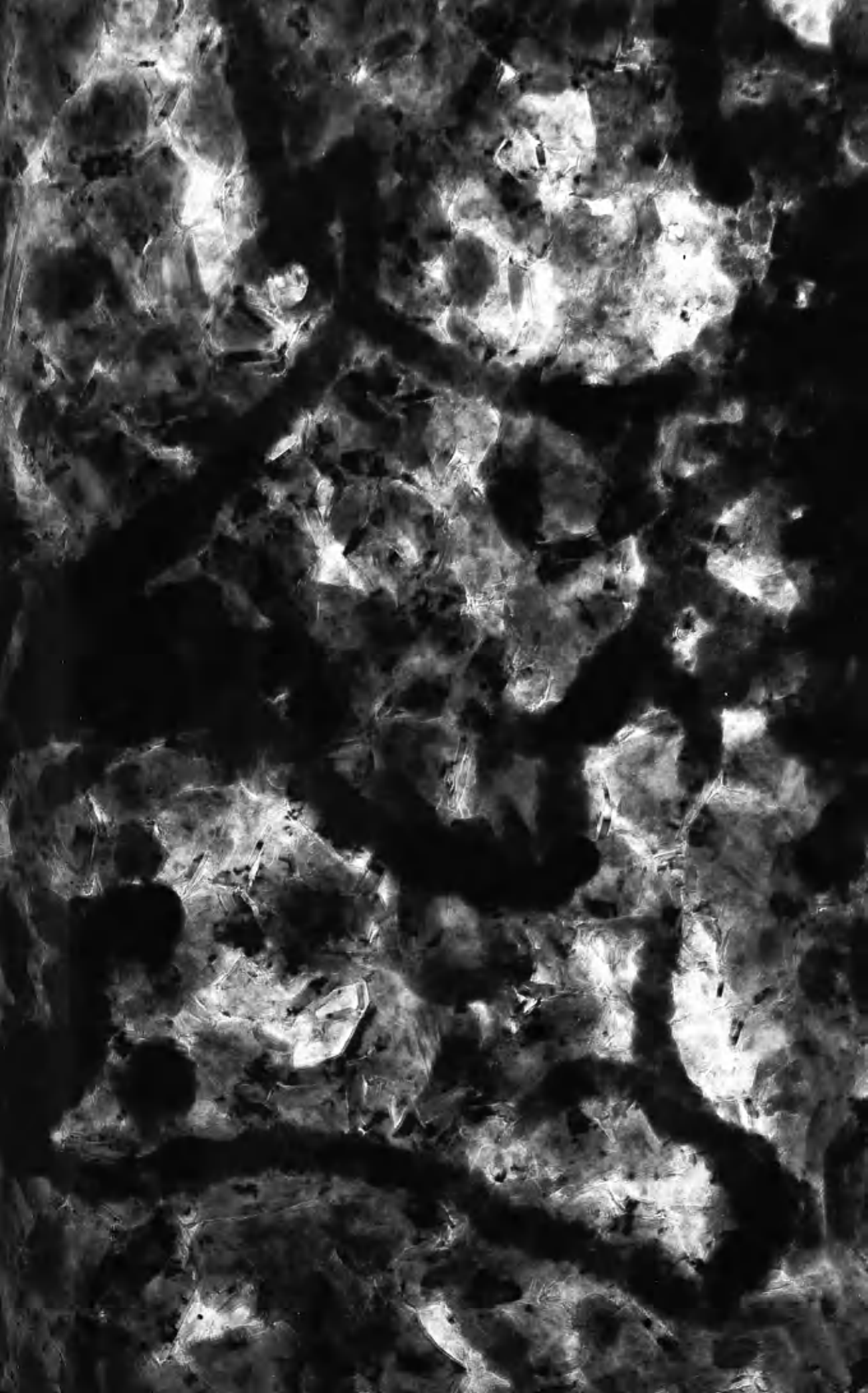

Plate 3.18

Cluster of graphitic fibres from experiment 1D. [1A 70 1764].

magnification = 80,000X.

Plate 3.19

An (0002) dark field micrograph of the same area of experiment 1D deposit as Plate 3.18. [1A 70 1765].

magnification = 120,000X.

confirmed that the basal planes were preferentially oriented parallel to the fibre growth axis. Measurements on a large number of these fibres established that the clusters grew to dimensions of more than 10μ x 10μ .

The simplest fibres in this category consisted of individual hemispherical mounds containing a central metal particle surrounded by carbon deposit whose (0002) layer planes remain parallel to the fibre surface. More extensive growth led to fibres with the appearance of those in Plate 3.20 from experiment 1Q and further development produced the type of clustering already shown in Plate 3.18. The acid treatment used to prepare specimens for transmission microscopy examination frequently removed metal from the fibres but in every case where fibrous samples were prepared without recourse to acid treatment it was found that all separate branches contained metal at their tips and often distributed throughout their central regions.

Attempts to positively identify by electron diffraction the metallic particles contained in the fibres have met with some success. Plate 3.21 shows the diffraction pattern obtained from the tip of a fibre. The measured spacings are those of graphite and a compound of nickel, Ni_2O_3. These extra lattice spacings were also detected in a less complete form in several other diffraction patterns of these fibres.

Plate 3.20

Fibres from experiment 1Q showing an earlier stage in the clustering process. [1A 71 784].

magnification = 152,000X.

Plate 3.21

Metal-containing fibre tip with its selected area diffraction pattern, from experiment 1D. [1A 71 63].

magnification = 100,000X.

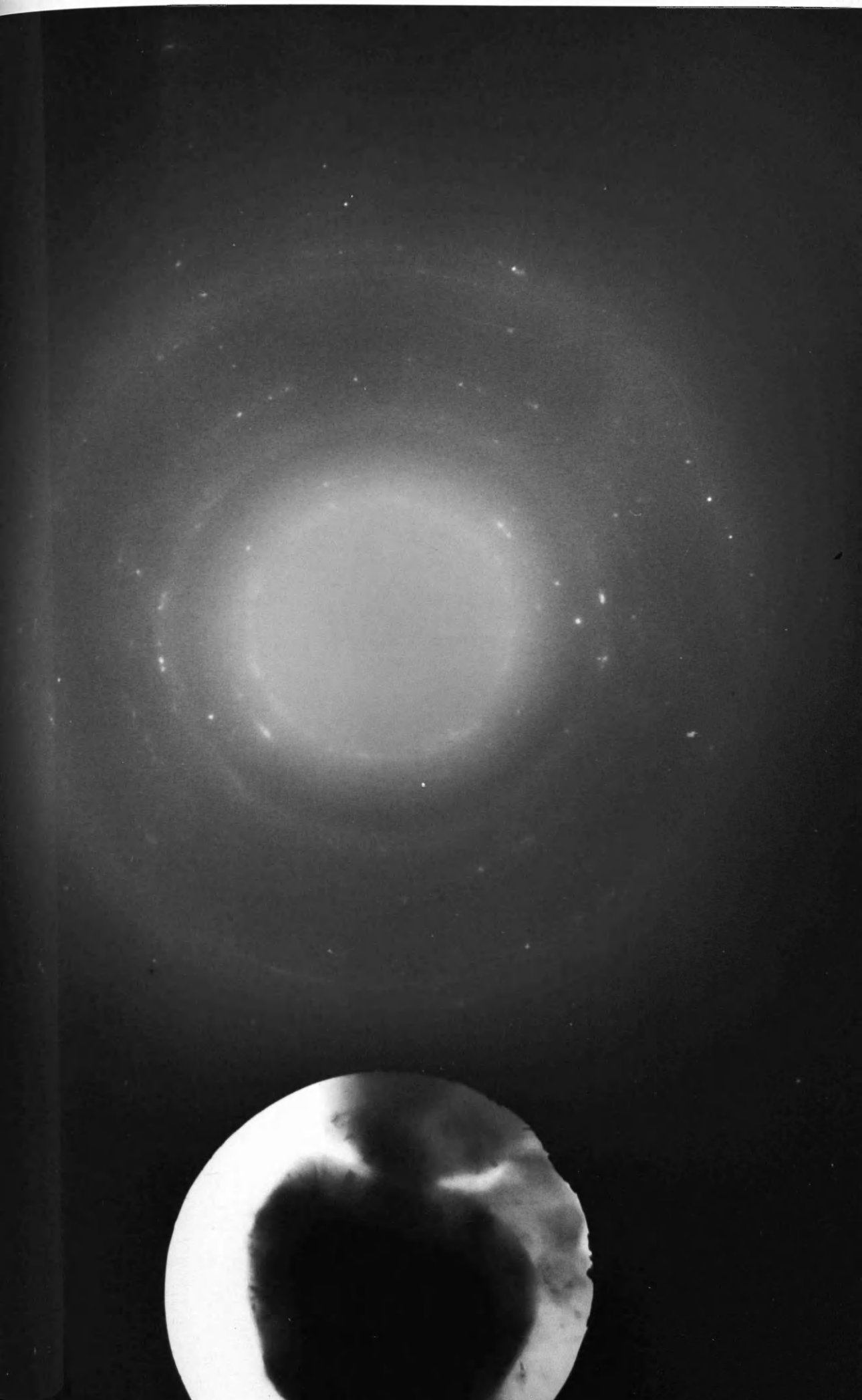

The full list is included in Table 3.4.

Table 3.4

d Spacings from two metal-containing graphite fibres (in Å).

SP1 graphite	Plate 3.21	Second graphite fibre	Ni_2O_3
3.355	3.33	3.34	3.23
	2.83	2.86	2.80
	2.264		2.30
2.128	2.120	2.137	
2.032	2.001	2.018	2.02
	1.765	1.707	
	1.60		1.62
	1.42		1.40
1.229	1.238		
1.153	1.159		
1.064	1.060		1.11

Plate 3.22 shows a typical member of a class of fibres found only in C_3H_8/Ni interactions. The most notable features were the amorphous or hollow central region and surrounding this a band of crystalline carbon of constant thickness exhibiting Bragg diffraction contrast effects. It should be pointed out that the metallic particle found at the tip of the fibres has been removed in this case by acid. The periodic arcing effects across the central region in Plate 3.22

Plate 3.22

Typical fibre formed from experiment 7C.
[1A 70 820].

magnification = 900,000X.

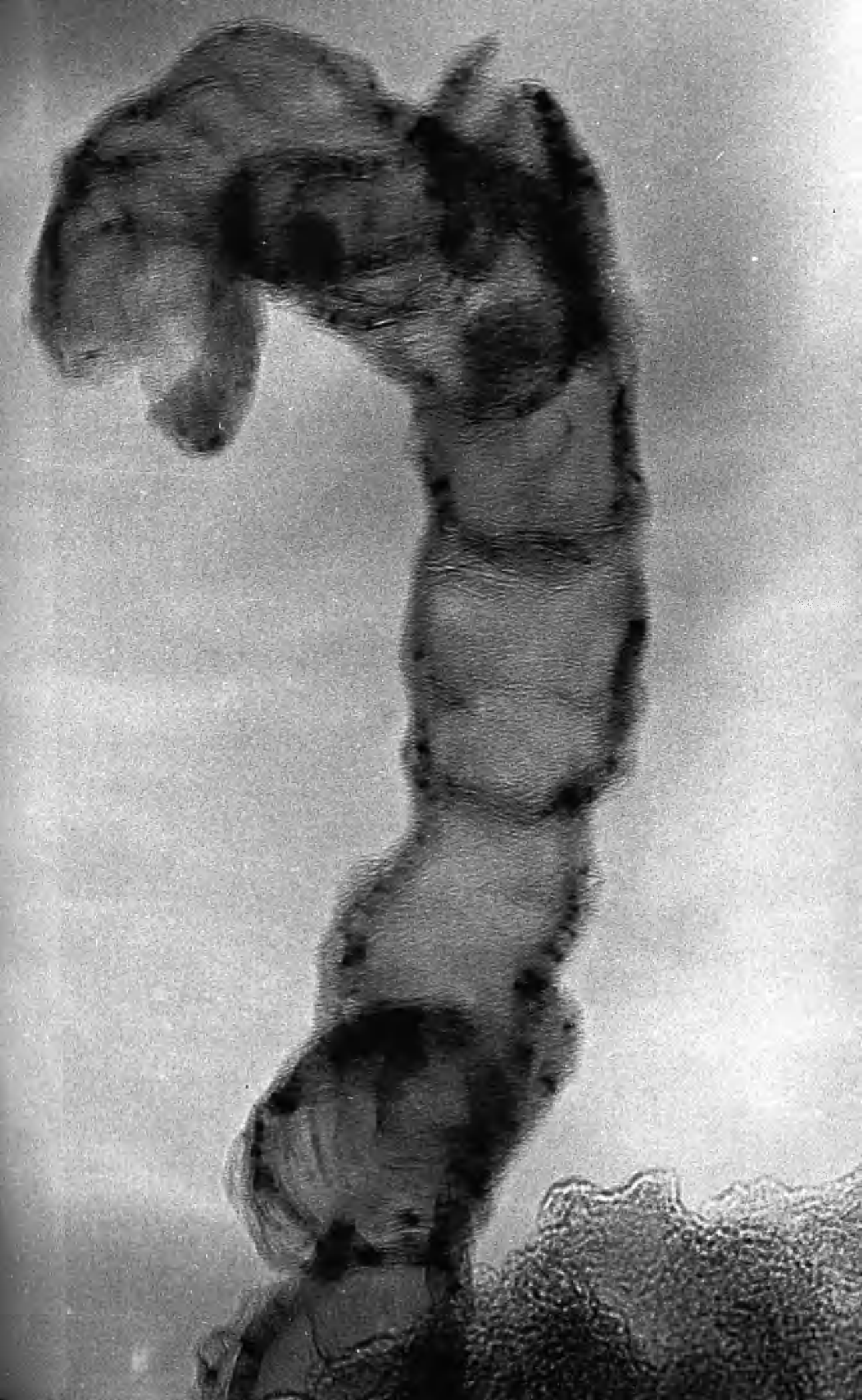

represent positions of enhanced diffraction contrast due to the bending of the fibre. This type of fibre was normally small ($< 0.5\mu$), comparatively straight and contained a metallic particle only at the fibre tip. The metal had a regular, geometric outline in contrast to the liquid appearance of the metal in the previously described fibres.

Arced carbon diffraction patterns from these fibres, such as the one in Plate 3.23, indicated the alignment between the (0002) lattice planes and the main fibre axis. The deviation from the ideal orientation in this plate is $\pm$ 30° but this is due partly at least to variations in the fibre growth direction. Confirmation that the basal planes were parallel to the major axis was given by the perpendicular orientation of the (0002) domains and also by high resolution electron microscopy discussed in section 3.1.5.

Branching of these fibres was limited but did occur in one or two instances. Plate 3.24 from experiment 7C contains at the junction of the two fibres a small area of resolved planes of separation 4.8 Å, which corresponds to moire fringes, probably due to a misalignment of the (0002) planes of the two fibres. The presence of moire fringes over an area of 10,000 $Å^2$ means that the degree of lattice perfection in the fibres is much higher than anticipated

Plate 3.23 (inset)

Arced diffraction pattern from a single fibre showing the alignment of the (0002) planes with the main fibre axis. The apparent misorientation of 25° is due to rotation of the magnetic lenses within the microscope. [1A 70 1345].

magnification = 35,000X.

Plate 3.24

Branched fibre from experiment 7C containing an area of moire fringes. [1A 70 809A].

magnification = 1,120,000X.

This conclusion was verified by later studies. The fibres in Plate 3.24 do not portray the same featureless central region apparent in Plate 3.22. It is possible that the difference is due to a slower growth in the former fibres allowing a degree of infilling of the central region by growth on the underside of the metal particle via a bulk diffusion mechanism. Some fibres contained both kinds of central zones indicating a variation in growth rate within the one fibre. This latter conclusion was also implied by the frequent changes in the direction of the fibre's growth denoted by the arcing effects mentioned before.

A type of fibre found only in Fe/CH_4 interactions is shown in Plate 3.25 from experiment 5E. In spite of the high fibre density in this region no branching has occurred and the fibres were much thinner and less complex than the more general fibre type. In these fibres, as in previous ones, there was a variation in appearance of the central zone. Note also the narrowing of the carbon wall at the tip of the largest fibre in this micrograph. Branching has occurred in the fibre in Plate 3.26, from experiment 5E, shown with its S.A.D. pattern which contains polycrystalline carbon and a spot pattern from the metal present. It can be seen that the spots from the iron compound superimpose exactly on the (0002) and (0004) carbon rings. The composition of the catalyst particle has

Plate 3.25

An example of fibres formed from experiment 5E. [NS 71 257].

magnification = 140,000X.

Plate 3.26

A metal-containing fibre from experiment 5E with its diffraction pattern. [NS 71 260].

magnification = 96,000X.

not been unambiguously ascertained but it is known that several iron carbides have the 3.4 Å and 1.7 Å spacings found here.

The diffracting edges mentioned in section 3.1.2 consisted of a region of graphite around central gaps with the graphite basal planes gradually changing from the horizontal to the vertical orientation. It is thought that these features were formed when the laterally expanding flake graphite caused the formation of nodules in the metal foil. These blocked any further horizontal growth and led to the lattice bending in order to continue growth over the uneven surface. If the bending proceeded to the extent that the basal planes became vertical, as frequently occurred, then a situation tailor-made for the extrusion of a graphite fibre has developed; a metal nodule only partly attached to the remainder of the foil has become available and has been surrounded by a circle of graphite whose (0002) planes have oriented parallel to the potential fibre axis. Experiments 1AD and 1AE were performed to determine whether the fibres formed from loose metal particles on the foil surface or whether it was the growth of the platelet graphite which actually caused nodules to form. Fibres formed equally well on an etched foil as on an unetched one, implying that loose particles were not necessary for fibre nucleation.

After the pre-fibre stage discussed above the metal could either have detached from the foil surface and catalysed the outward growth of a fibre or remained connected to the foil to form a coating of carbon around its surface. The latter case corresponds to the formation of a hemispherical fibre. If the metal mound under consideration lost immediate contact with the foil then a longer fibre resulted. However, if the metal moving outward from the deposit surface was replenished from the surface metal pool then a situation like that of the fibre in Plate 3.27 occurred and continuing growth led to a fibre containing metal at the tip and along the body of the fibre. An abundance of metal could then allow fibre branching, as frequently found.

3.1.5. High Resolution Microscopy

Plate 3.28 from experiment 1D contains a hemispherical fibre whose basal planes have been resolved in the electron microscope. While the layer planes are initially parallel to the fibre axis they bend at its tip in order to remain parallel to the fibre surface. This observation indicates that the significant features common to all fibres encountered was the parallelism between the graphite basal planes and the metal surface at the point in time when the metal catalysed the deposition of that part of each plane. Part of a fibre from experiment 5E is shown in Plate 3.29. It contains

Plate 3.27

A fibre whose metallic particle is attached to the surface metal which acts as a pool for further metal extrusion. [UBG 9].

magnification = 1,400,000.

Plate 3.28

A hemispherical fibre from experiment 1D showing the resolved basal graphite planes. [UBG 12].

magnification = 1,400,000.

Plate 3.29

Part of a fibre from experiment 5E establishing the highly ordered arrangement of the graphite layer planes parallel to the fibre growth axis. [JLH 0218].

magnification = 1,520,000X.

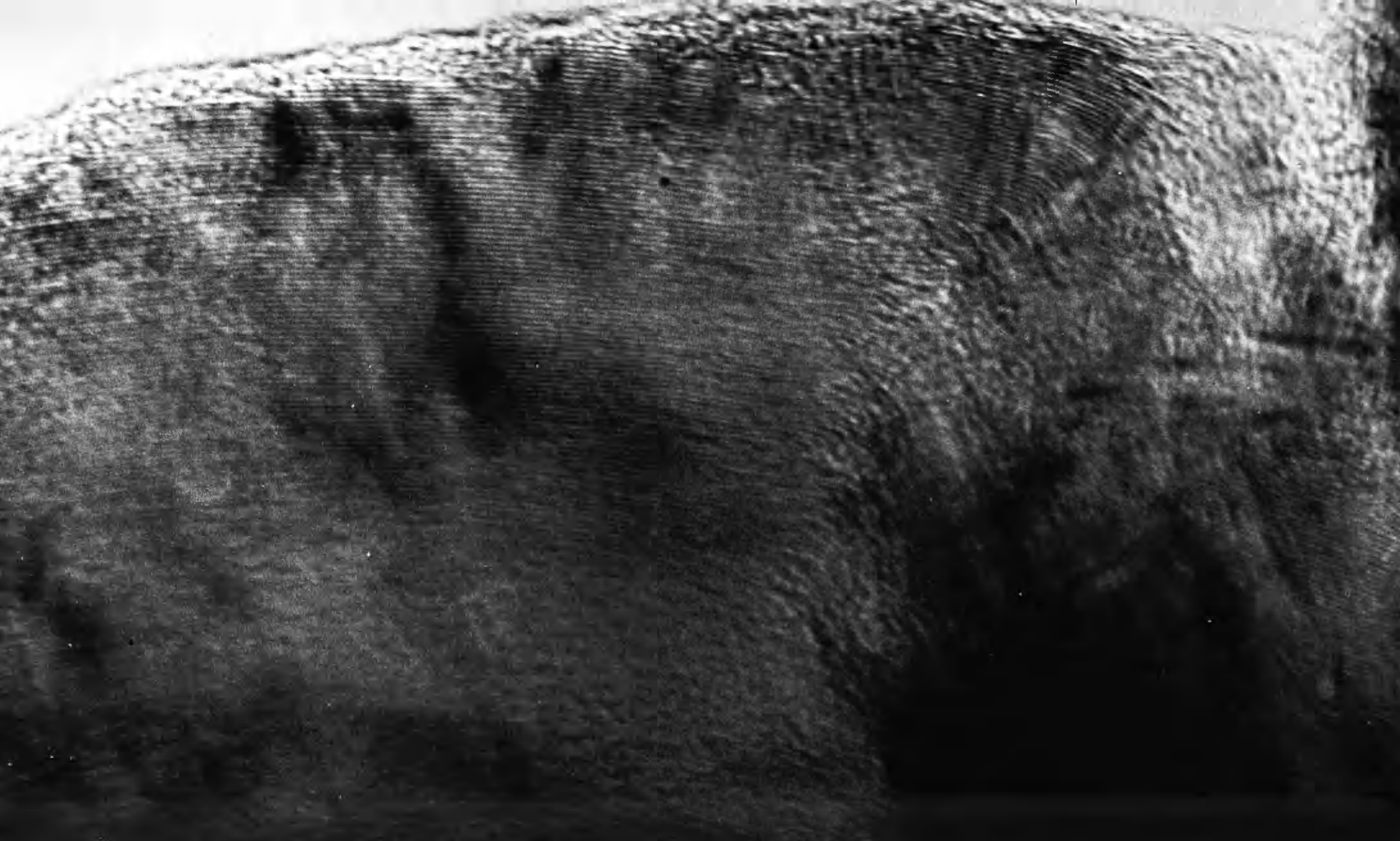

large areas of resolved (0002) planes and establishes that the 150 layer planes in the carbon wall are all arranged in a highly ordered manner parallel to the fibre growth axis.

It has been mentioned previously that the diameter of the carbon wall, which was constant along each fibre, narrowed appreciably at the region containing the catalyst particle. Plate 3.30 contains resolved planes from the tip of a fibre whose metal has been removed by acid.
The gradual narrowing of the edge region is interpreted as meaning that the carbon layers are still growing and have not yet attained the uniform thickness of the remainder of the fibre, as they have not been in contact with the metal for a sufficient period of time. Measurements on a number of fibres showed that on average each (0002) plane in the growth region extended beyond its outer neighbour for a distance of approx. 20 Å.

High resolution studies on the "propane" type of fibres produced results similar to those just discussed. The fibre in Plate 3.31 contains resolved planes even at its base where the fibre has grown from the carbon matrix. The basal planes are everywhere oriented parallel to the growth axis of the fibre.

Plate 3.30

Resolved layer planes from the tip of a graphitic fibre showing the narrowing of the carbon wall in the growth region. [JLH 0209].

magnification = 2,220,000X.

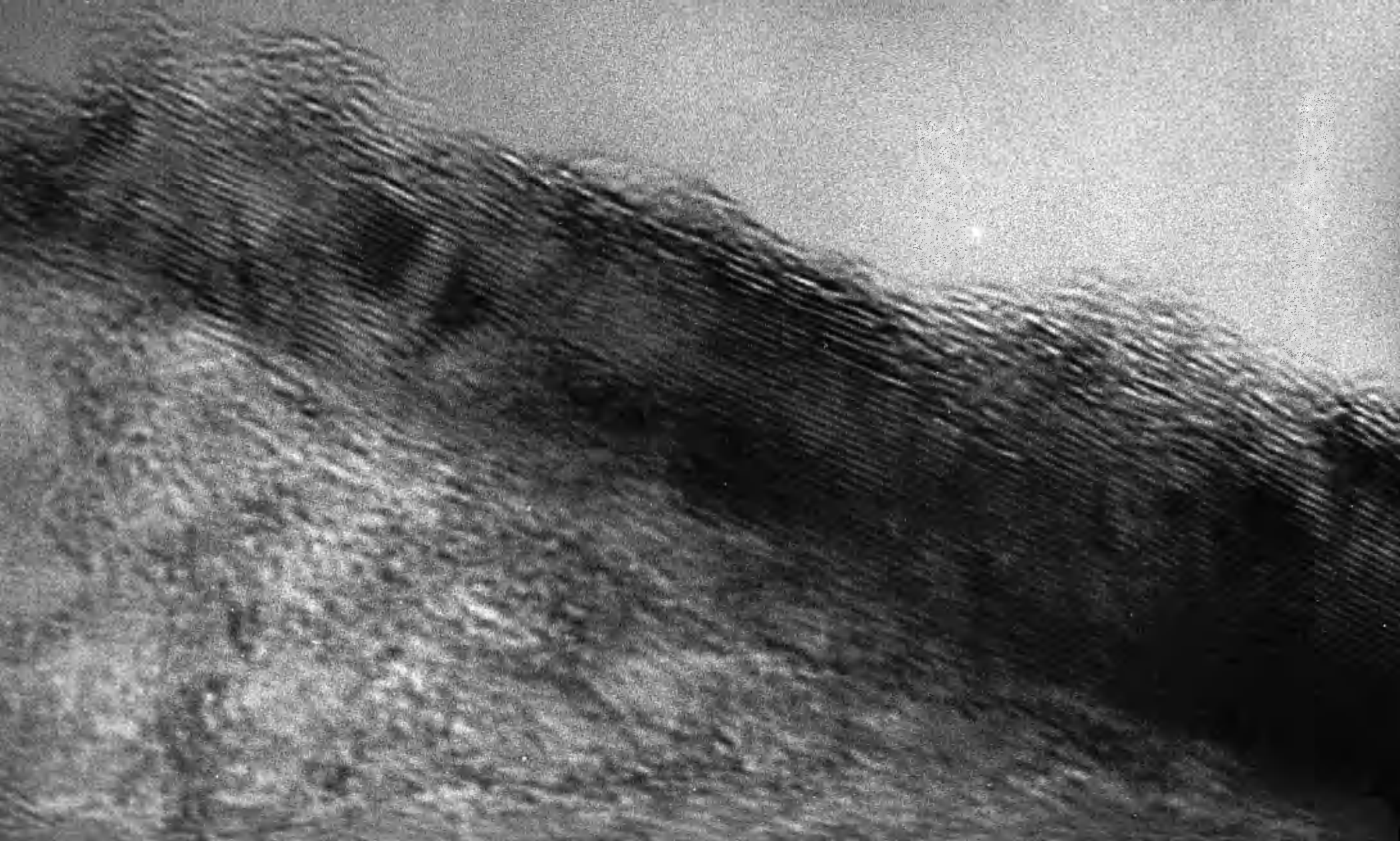

Plate 3.31

Oriented basal planes visible throughout a graphitic fibre formed in experiment 7C. [UBF 8].

magnification = 960,000.

3.1.6. High Voltage Electron Microscopy

Studies using a 1 Me.V. microscope on deposits from experiment 1E which were too thick for conventional microscopy have supplied further evidence for the increasing complexity of the deposit morphology when the reaction has continued beyond the stage of platelet graphite formation. The absence of some of the metal due to acid treatment made interpretation of the deposit's appearance uncertain. The chief problem was in determining how much of the later carbon deposit could be classified as fibrous and how much as non-oriented. A high proportion of the carbon in Plate 3.32 has vertically oriented basal planes as shown by the bands of carbon possessing diffracting regions, in contrast with the situation when platelet graphite was being deposited. This feature is typical of both fibrous and non-oriented deposits. One area of opaque material between walls of carbon is probably metal and the resulting feature can be described as fibrous graphite. However, it remains a matter of conjecture how many of the remaining diffracting bands are due to fibres and how many to non-oriented carbon.

A further advantage of the increased extinction distance using a 1 Me.V. microscope was that it enabled grain boundary deposit to be examined. Plate 3.33 reveals that the carbon forms with its (0002) planes approximately parallel to the line of the metal grain

Plate 3.32

Complex morphology of deposit from experiment 1E. [34 FR].

magnification = 216,000X.

Plate 3.33

Metal grain boundary deposit from experiment 1E showing the alignment of the carbon basal planes parallel to the line of the boundary. [31 FR].

magnification = 240,000X.

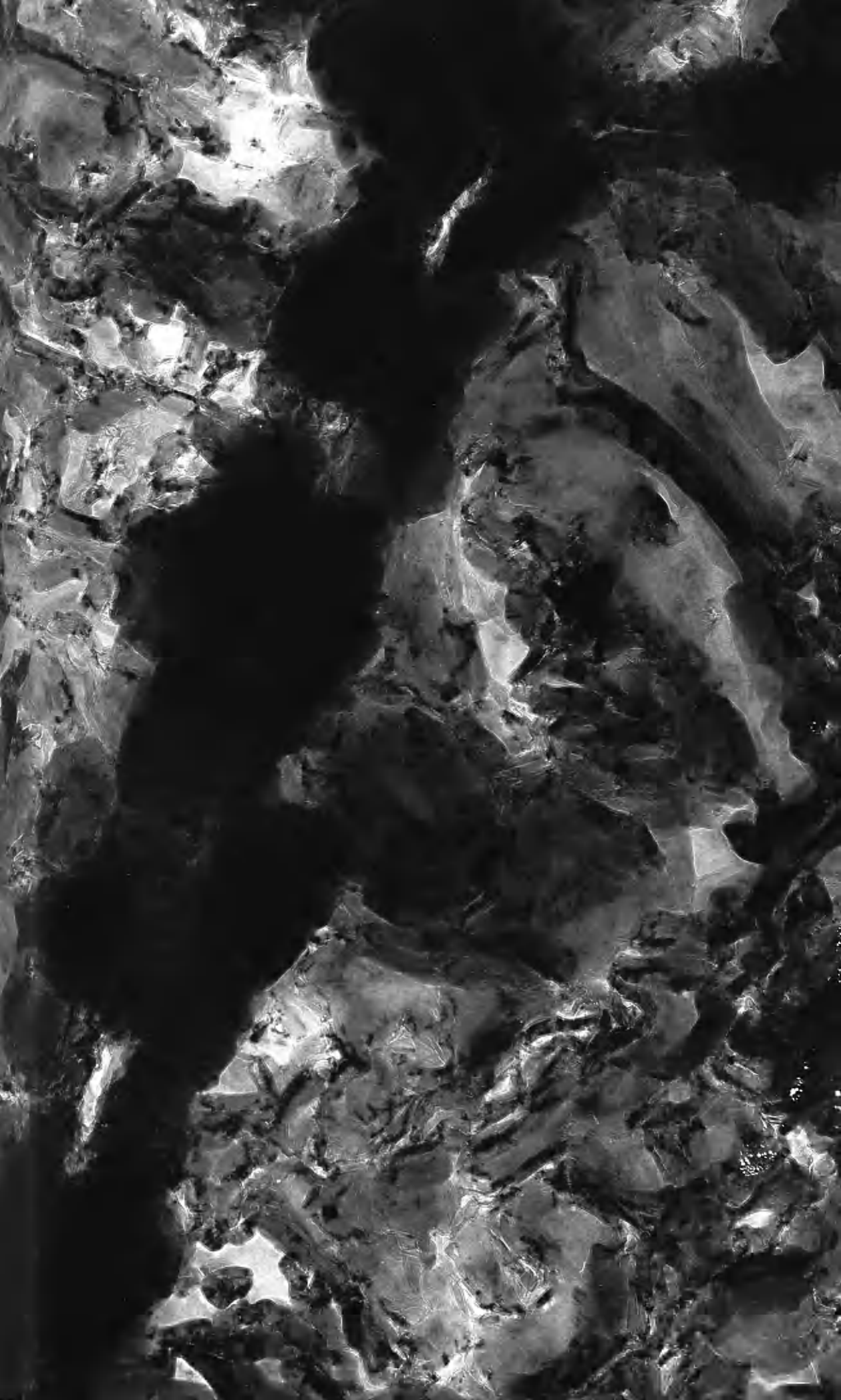

boundary. This can be deduced from the fact that the (0002) domains are aligned perpendicular to this direction and indicates that the carbon is not a randomly oriented polycrystalline material.

3.1.7. Metal Compounds Formed during Carbon Deposition

Preliminary deposition experiments were performed in an apparatus whose working vacuum was worse than 10^{-5} torr. Various metal compounds were encountered regularly among the carbon deposits. Nickel oxide, NiO, and βNiOOH were identified and several iron oxides were detected by electron diffraction. Apart from their production during oxidation studies these compounds have not been formed in the more controlled conditions of later experiments.

On several occasions additional nickel compounds were detected but have not been identified. The lattice spacings of the most common ones are listed in Table 3.5.

Table 3.5

d spacings, in Å, of unidentified nickel compounds.

Compound I	Compound II
4.54	5.92
3.38	4.96
2.86	3.16
2.43	3.00
1.95	2.84
1.85	1.94
1.66	1.60
1.55	1.50
1.42	1.37
1.37	1.20
	1.07

Both of these materials were formed in larger quantities in experiments 7H and 7I in which oxygen was introduced into the system and it is likely that they too were impurity products rather than catalytic intermediates.

The evidence for catalysis by metal compounds rather than by the free metal was inconclusive. The absence of any particular metal compound among most of the deposits suggested that no definite route such as $M \rightarrow MX \rightarrow C$ existed, where MX is the possible catalyst, and therefore that the free metal was likely to be the catalyst by default. However, a firm conclusion as to the nature of the catalyst would require more positive evidence.

3.1.8. Edge Deposits

Because of the temperature gradient along the metal foils during carbon deposition the regions away from the foil centre were much cooler than the nominal foil temperature. The deposits on these edge regions, formed at approximately 450°C, were examined separately and found to have a completely different morphology. The nature of the carbon formed was again determined primarily by the rate and extent of deposition rather than by the particular gas or metal employed. Metal grain boundaries were sites of preferred deposition, as at the foil centre, but due to the incomplete annealing at the lower temperature smaller grains were frequently encountered. Plate 3.34 from experiment 7K contains partially formed boundary deposits made up of continuous rows of individual clumps or nodules of material.

Plate 3.34

Typical appearance of carbon deposited at the cooler parts of metal foils. [NS 72 743].

magnification = 88,000X.

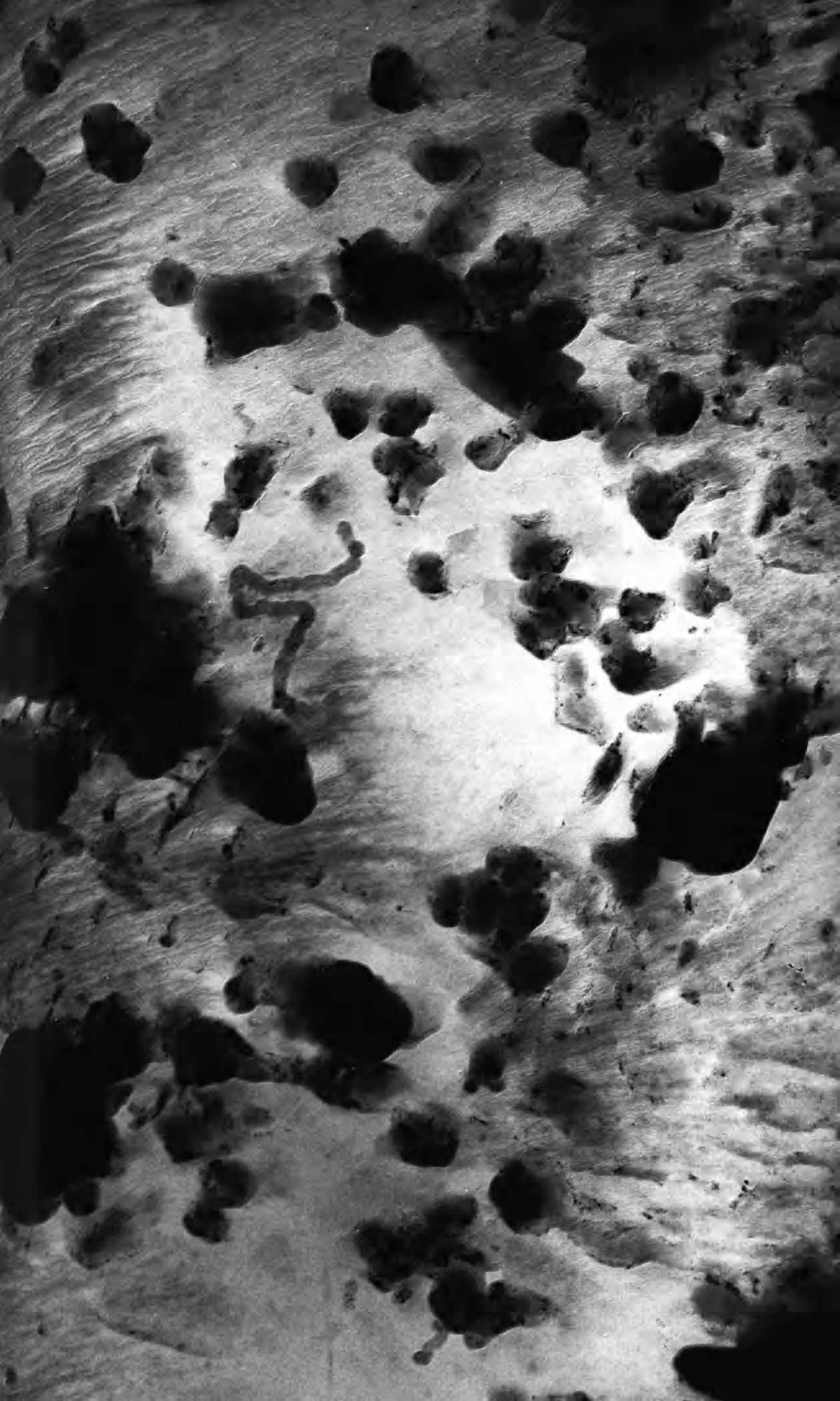

Separate nodules, similar to those constituting the boundary deposits are also scattered inside the metal grains. This micrograph shows the variations in appearance and thickness of the carbon product within single metal grains and also the presence of a small number of carbon filaments.

The first deposit formed was a thin film of oriented but not single crystal carbon such as that shown in Plate 3.35 from experiment 7F. The thick clumps appeared to form in a manner analogous to the growth of the graphite fibres, nucleating first as a carbon wall whose basal planes were circumferentially oriented. A stage in the growth of a group of clumps is given in Plate 3.36. It is suggested that these nodules were formed at the sites of emergent metal dislocations explaining the similarity between them and the nodules contained in grain boundary deposits. Both types of site also appeared to be sources of metal, allowing the transport of metal from the foil on to the deposit outer surface to continue the catalysis of hydrocarbon decomposition. Thicker carbon products had the appearance of Plate 3.37 from experiment 1Q and gave diffraction patterns which revealed the slight tendency for alignment of the basal planes parallel to the substrate surface.

The nodular material was normally the nucleation point for the growth of filamentous carbon similar to the

Plate 3.35

Initial form of deposit formed at foil edges, from experiment 7F. [NS 72 646].

magnification = 88,000X.

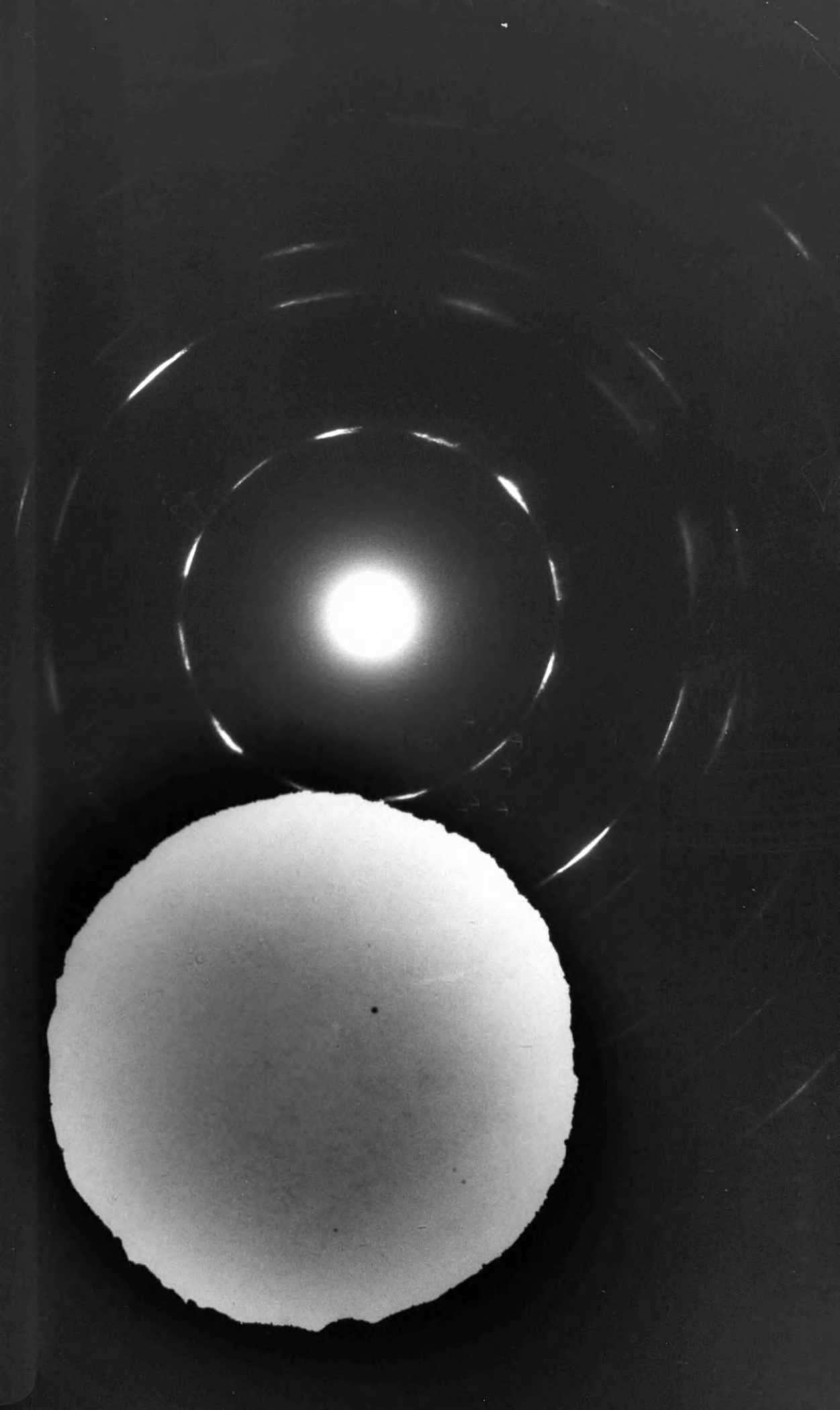

Plate 3.36

An early stage in the formation of a group of nodules from experiment 7K. [NS 72 746].

magnification = 88,000X.

Plate 3.37

Thicker edge carbon deposit from experiment 1Q. [1A 71 791].

magnification = 88,000X.

ones in Plate 3.38. The filaments were many microns in length but were invariably very thin with a constant diameter of about 300 Å, giving a length to width ratio of greater than one hundred. Filaments have been formed at the foil edge in all six interactions listed in Table 3.1 and all possessed an external carbon wall with a hollow or amorphous central zone. No Bragg diffraction effects were detected, suggesting that the carbon planes were not ordered, but metal particles were present at the tips and were frequently pear-shaped like the ones reported by Baker et al. (1972B). An example is given in Plate 3.39. The S.A.D. patterns of these filaments were polycrystalline and contained only (ol) and (hk) reflections indicating that they were non-graphitic.

3.2. In Situ Oxidation Studies

Oxidation of the pyrolytic carbons was undertaken in order to obtain more information concerning the characteristics of these materials and in particular to discover more about the metal content of the graphites, with a view to eventually establishing the role of the metal catalyst in the graphite formation.

A sample of graphite from experiment 12C was placed unsupported on an electron microscope specimen holder and oxidised at 800°C in dry oxygen. The course of the oxidation was followed by bright field microscopy and selected area diffraction. At 800°C molecular oxygen

Plate 3.38

Filamentary carbon showing its association with the nodular deposits, from experiment 7F. [NS 72 661].

magnification . 88,000X.

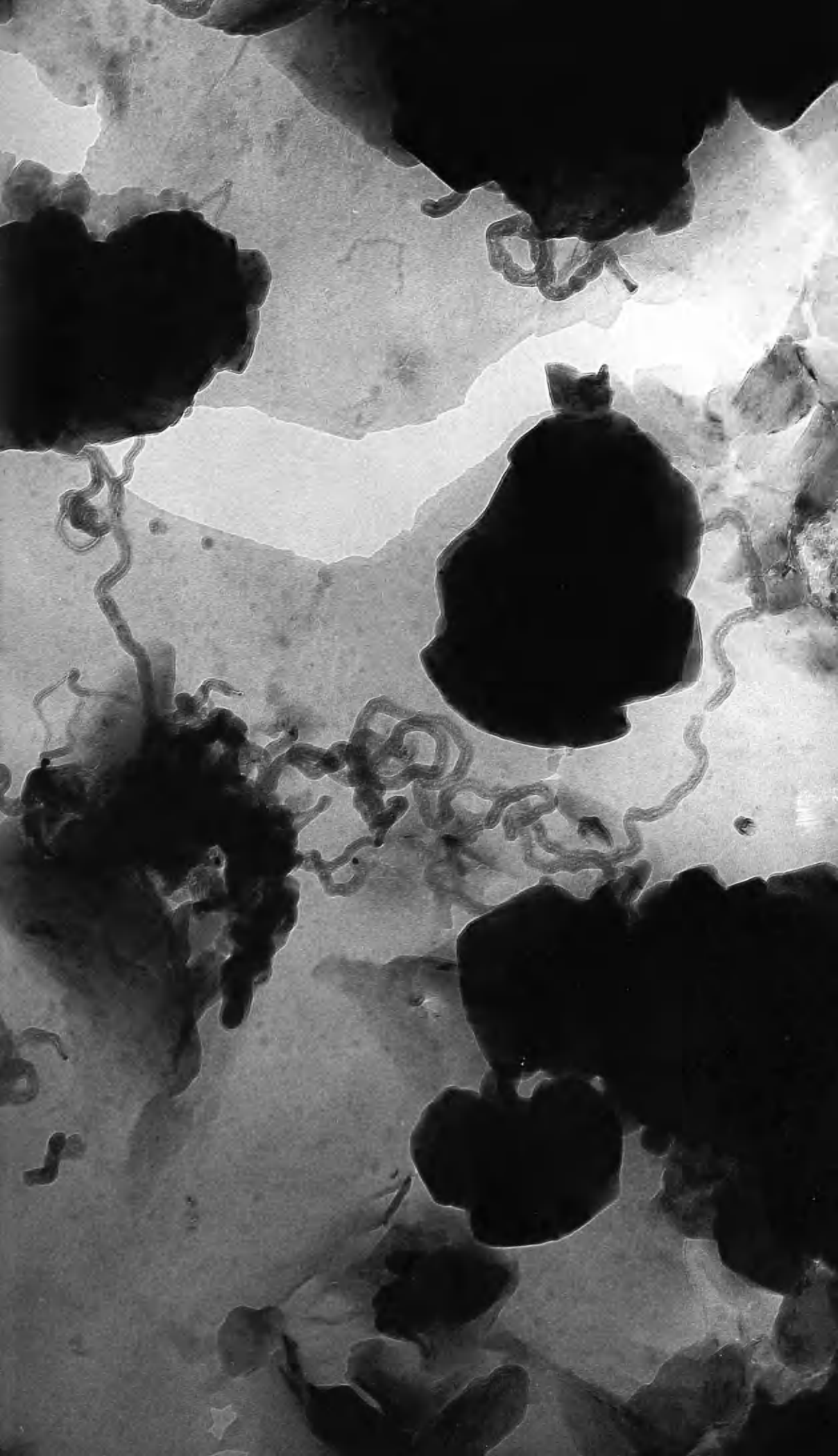

Plate 3.39

Filamentary carbon, several containing pear-shaped metal particles. [1A 72 230].

magnification = 120,000X.

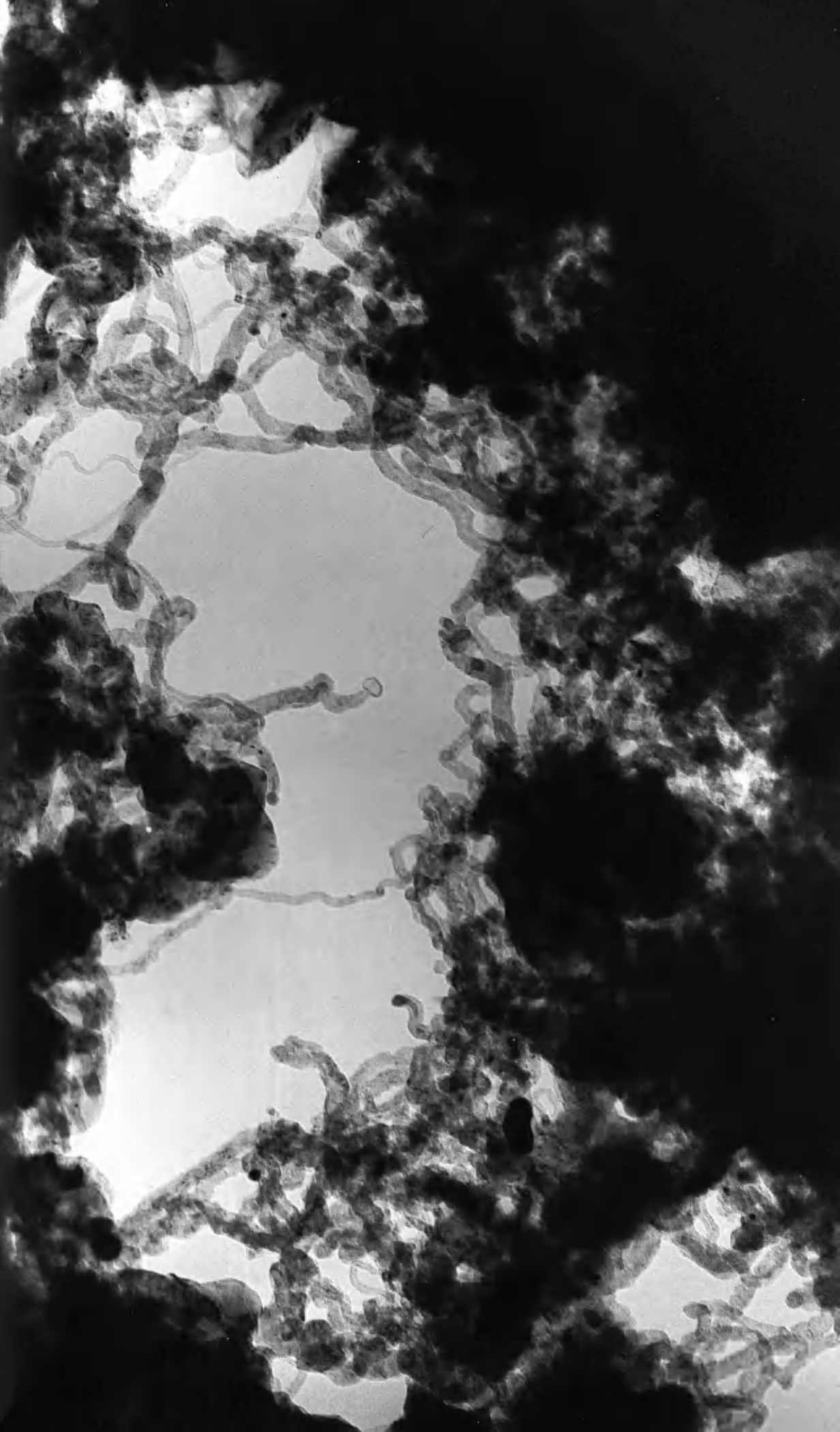

TABLE 3.6

d spacings, in Å, from the oxidation of experiment 12C deposit

graphite index	SP1 graphite	before oxidation	after 30 mins oxidation	after 300 mins oxidation	βNiOOH	βNiOOH index
		4.79	4.76	4.65	4.03	001
0002	3.355	3.39				
		2.48	2.38	2.44	2.41	100
$10\bar{1}1$	2.032	2.06	2.03	2.04		
0004	1.678	1.69	1.67	1.68		
		1.46	1.44	1.43	1.40	110
$11\bar{2}0$	1.229	1.21		1.24		
$11\bar{2}2$	1.154	1.13		1.17		

etches graphite, reflecting the greater reactivity of the edge carbon atoms (Thomas,1966). The etch pits observed here were mostly regular hexagons and contained metal particles which coalesced gradually while catalysing the gasification of the carbon. As the intensity of the graphite rings in the diffraction patterns became weaker a second material, βNiOOH, appeared. Table 3.6 summarises the changes in the diffraction patterns during the oxidation.

Graphite from experiment 70 was oxidised, as seen in Table 3.6, and as the oxidation progressed the S.A.D. pattern of NiO gradually replaced that of carbon, as shown by Table 3.7.

Table 3.7

d spacings, in Å, from the oxidation of experiment 70 deposit.

SP1 graphite	before oxidation	after 20 mins. oxidation	after 40 mins. oxidation	NiO
3.355	3.38	3.45		
		2.423	2.421	2.410
2.128	2.100	2.094	2.082	2.088
1.678	1.711	1.705		
		1.479	1.477	
			1.262	1.259
1.229	1.233	1.226		
			1.200	1.206
1.153	1.154	1.154		

The oxidation at 600°C of a grain boundary deposit from the same experiment was performed and Plate 3.40 shows the appearance of a partially oxidised area. The deposit proved to be an oriented polycrystalline carbon whose (0002) planes were parallel to the direction of the grain boundary line. This confirms the conclusion reached in section 3.1.6.

The flake graphite formed in experiment 16A was also examined by the oxidation technique. At 600°C in the electron microscope edge oxidation and pit formation occurred. Metal particles intrinsic to the graphite lattice were prominent in the catalysis of the oxidation and some degree of channelling by the metal was observed. The metal moved around the crystals of graphite and on contact with one another individual particles tended to coalesce. Studies on the orientation of the sides of the etch pits using the S.A.D. method indicated that oxidation took place parallel to the $\langle 10\bar{1}0 \rangle$ direction. This is termed "parallel oxidation" and is the type normally occurring at 600°C (Thomas, 1966). The etch pits in Plate 3.41 all have sides corresponding to $(11\bar{2}0)$ planes.

Oxidation of platelet graphite from experiment 1L at 800°C led to similar results. Pitting of the graphite was very evident. However, with few exceptions, the sides of the etch pits were not hexagonal and tended to be irregular, as Plate 3.42 shows. Oxidation proceeded along different (0002) planes independently,

Plate 3.40

Grain boundary deposit from experiment 7C partially oxidised at 600°C in order to show the alignment of the (0002) layer planes relative to the grain boundary line. [NS 70 2050].

magnification = 92,000X.

Plate 3.41

Platelet graphite from experiment 16A partially oxidised at 600°C showing the orientation of the sides of the etch pits. [NS 70 2089].

magnification = 106,000X.

Plate 3.42

Partially oxidised platelet graphite from experiment 1L showing irregular pits containing small metal catalyst particles. [NS 71 460].

magnification = 17,600X.

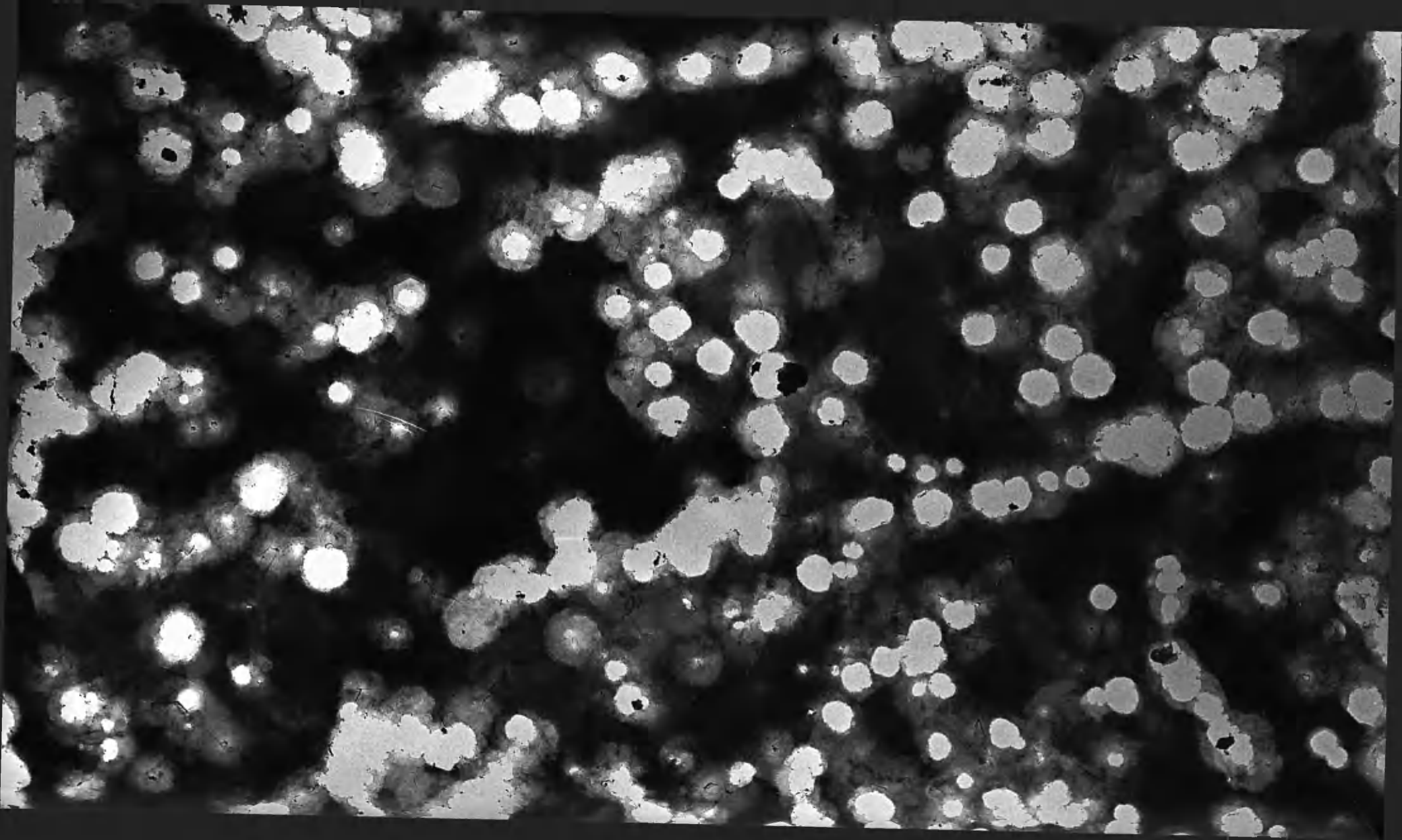

resulting in a gradual decrease in thickness of the graphite around each etch pit, and was undoubtedly catalysed by the small metal particles which were noticeably active around the edges of the pits. These metal particles were not present before the onset of oxidation and were seen to coagulate during this oxidation and during previous oxidation studies. They varied in size but ones are small as 20 Å in diameter were detected.

By calculating the amount of metal involved in the oxidation process an estimate for the proportion of metal contained in the platelet graphite of 0.1% by weight was arrived at. A value of 2% nickel present in the overall carbon deposit of experiment 23I was obtained by gasification of a weighed quantity of product and reweighing the metal residue. These figures indicate that most of the metal distributed among the deposit exists as free metal or as metal attached to fibres rather than as metal associated with the platelet graphite lattice.

A piece of deposit from experiment 1L was used as a substrate for the evaporation of a film of nickel. The combined specimen was then oxidised in the electron microscope. A micrograph of a partially oxidised area is shown in Plate 3.43. The more opaque parts are sintered nickel which is catalysing the graphite oxidation. The gasification is being catalysed uniformly

Plate 3.43

Oxidation of platelet graphite being catalysed by an evaporated film of nickel. [NS 71 658].

magnification = 88,000X.

throughout the thickness of the graphite film in contrast with the mode of catalysis when intrinsic nickel particles were utilised. This and other evidence contributed to the view that the metal which previously catalysed the oxidation originated from the graphite lattice itself.

Fibrous graphite from experiment 1AF was placed on a silica support film and oxidised at between 540°C and 640°C. The course of the oxidation was recorded and a number of features concerning the mechanism were revealed. Plate 3.44 was taken before the commencement of oxidation and Plate 3.45, 3.46 and 3.47 are from this same area after 10, 32 and 58 minutes oxidation respectively. At 540°C the initial change was the inward movement of the metal at the tips of fibre branches. This indicated that the inner region of the fibre clusters were not wholly filled with metal and hollow areas must have been present. The mobility of the metal at 540°C was slightly surprising but helped to explain the manner in which the fibres were actually produced. Subsequently, the oxidation started at the outer graphite surface. This verified that there was no easy route by which gases could diffuse through the carbon wall to the catalyst particle, otherwise the oxidation would have occurred faster from the catalyst outwards. As with the platelet graphite, oxidation revealed the presence of metal among

Plate 3.44

Fibrous graphite from experiment 1AF before oxidation. [NS 72 354].

magnification = 40,000X.

Plate 3.45

The same area of deposit as in Plate 3.44 after 10 minutes oxidation. [NS 72 357].

magnification = 40,000X.

Plate 3.46

The same area as Plate 3.44 after 32 minutes oxidation. [NS 72 362].

magnification = 40,000X.

Plate 3.47

The same area as Plate 3.44 after 58 minutes oxidation. [NS 72 370].

magnification = 40,000X.

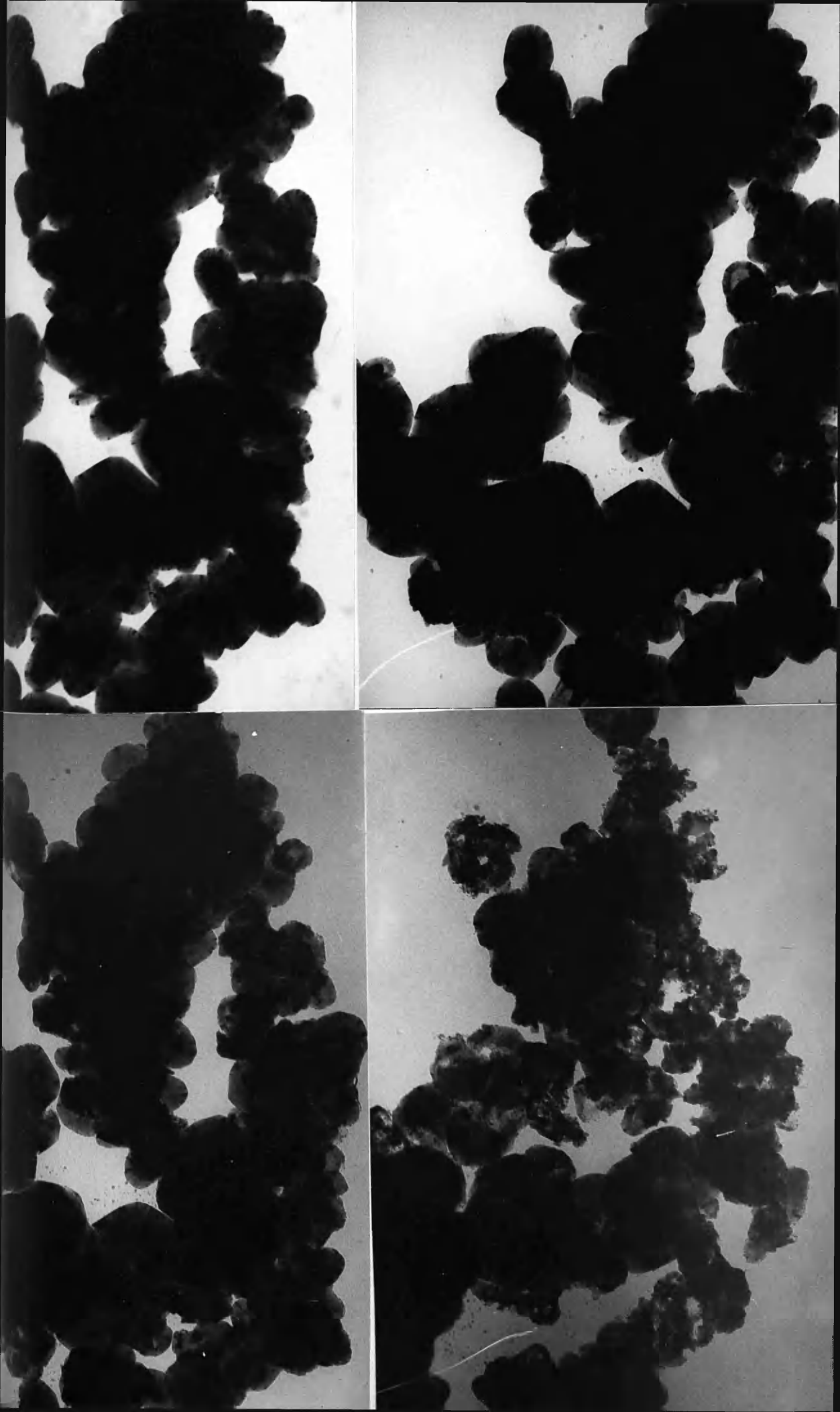

the fibrous graphite's lattice and the resulting small particles caused the formation of channels along the carbon wall parallel to the basal planes. Finally, when the central metal became exposed it catalysed the oxidation process.

3.3. Scanning Electron Microscopy

Examination of deposits by scanning electron microscopy indicated that on both iron and nickel substrates nucleation and growth was not simultaneous on all grains. Plate 3.48 from experiment 1H shows that after fairly short reactions some metal grains were still devoid of carbon whereas others were completely or partially covered. The variation in deposit rate with metal orientation has been discussed in the Introduction chapter. After longer reactions all grains finally became covered in deposit. The individual grains in Plate 3.48 are distinguishable but no signs of preferred grain boundary deposition are evident. Transmission electron microscopy examination of shadowed product indicated that boundary deposits were not raised far above the level of the general carbon product. Hence the degree of enhanced irradiation experienced by the boundary deposits in Plate 3.49 from experiment 1P implies that they contain a considerable amount of metal, as suggested in section 3.1.8.

Short duration experiments known to contain only platelet graphite with diffracting edge material were

Plate 3.48

Variation of deposit thickness on different nickel grains after experiment 1H.

magnification = 420X.

Plate 3.49

Metal-rich grain boundary deposits from experiment 1P.

magnification 2500X.

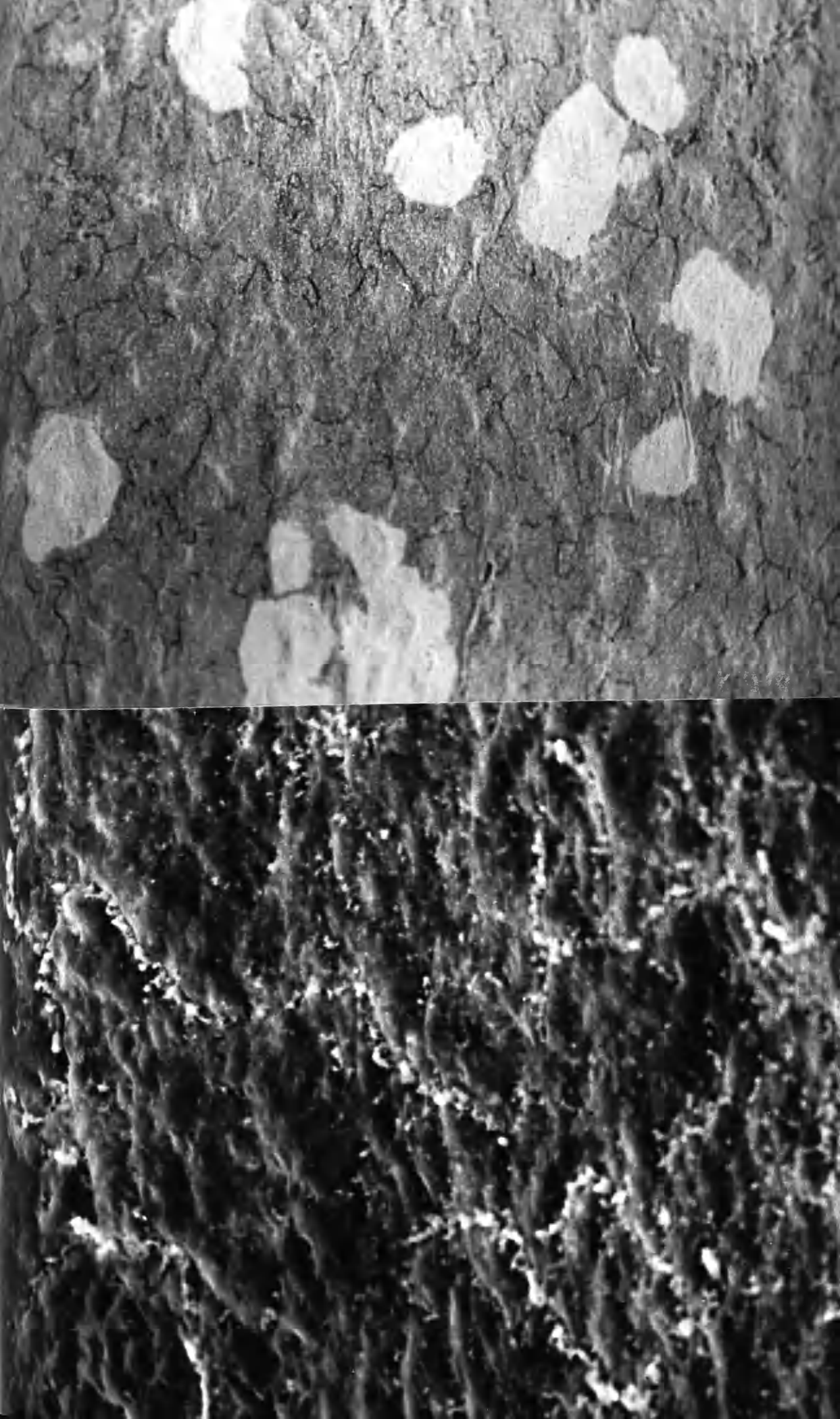

examined by S.E.M. and the flat, featureless appearance confirmed previously discussed ideas concerning the nature of the platelet deposit. The area in Plate 3.50 from experiment 1R reveals features consistent with those noted for diffraction edges. The bright spots are thought to be the raised areas containing metal corresponding to incipient fibres. The regular appearance of this latter deposit should be contrasted with the nodular, rougher outlines of the deposit from the longer reaction 1D in Plate 3.51. This outer surface corresponds to fibrous or non-oriented material. The lighter regions may be metal-rich particles carried outward by the growing carbon.

An area of deposit from the cooler edge region of experiment 1R is given in Plate 3.52. The surface features are much less regular than ones from the centre deposit of the same experiment in Plate 3.50. The clumps or nodules described in 3.1.8 are prominent, jutting out from the flatter regions. Also visible are smaller clusters perhaps containing the carbon filaments known to be present among the product of this experiment.

3.4. X-Ray Powder Analysis

Table 3.8(over) gives a comparison between the lattice spacings of SP1 graphite and graphite deposited in experiment 12C, both sets of data obtained from X-ray powder photographs.

Plate 3.50

Platelet graphite from experiment 1R containing diffraction edges.

modification 10,500X.

Plate 3.51

Rough deposit surface after a longer reaction, from experiment 1D.

magnification = 6,200X.

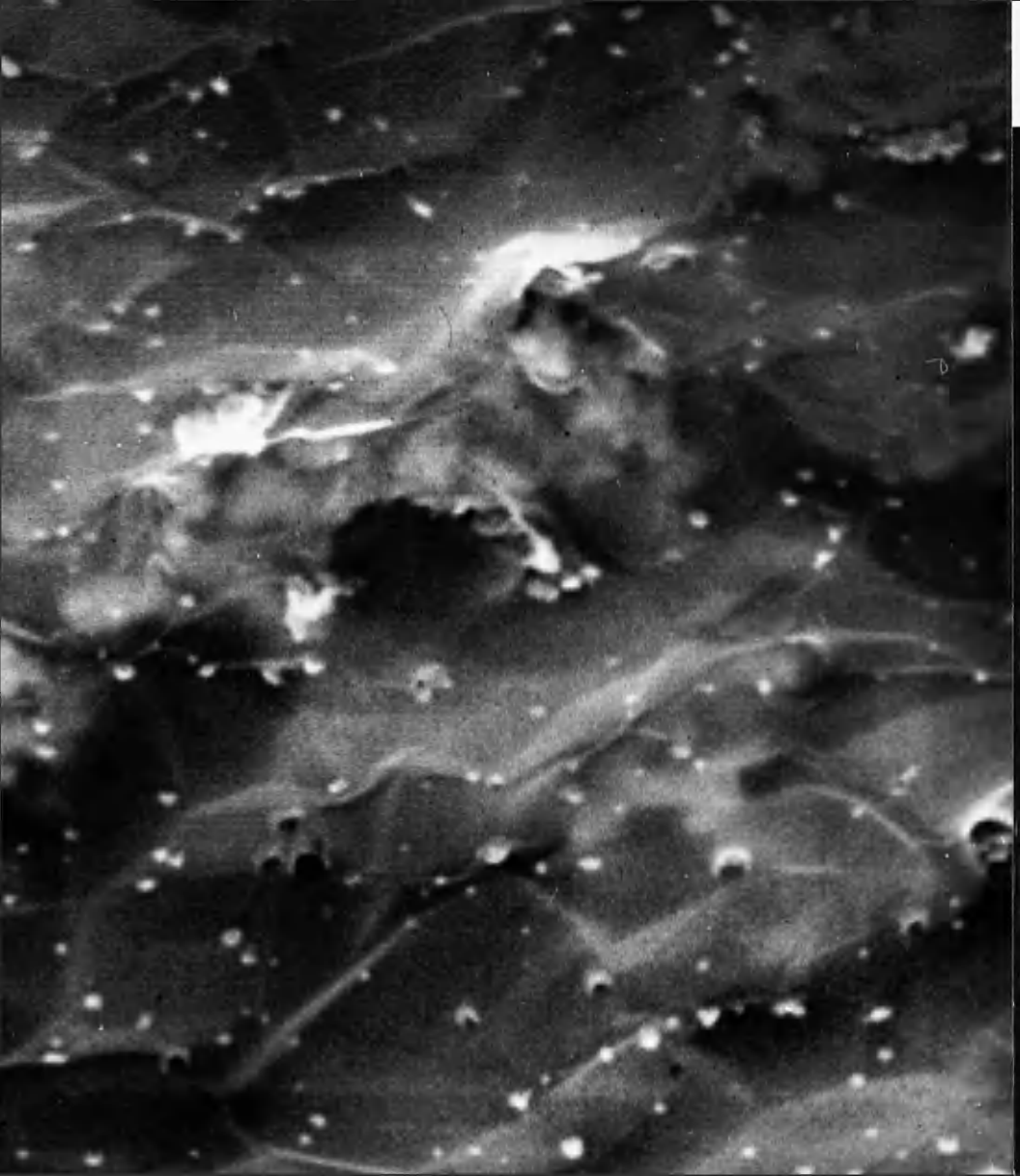

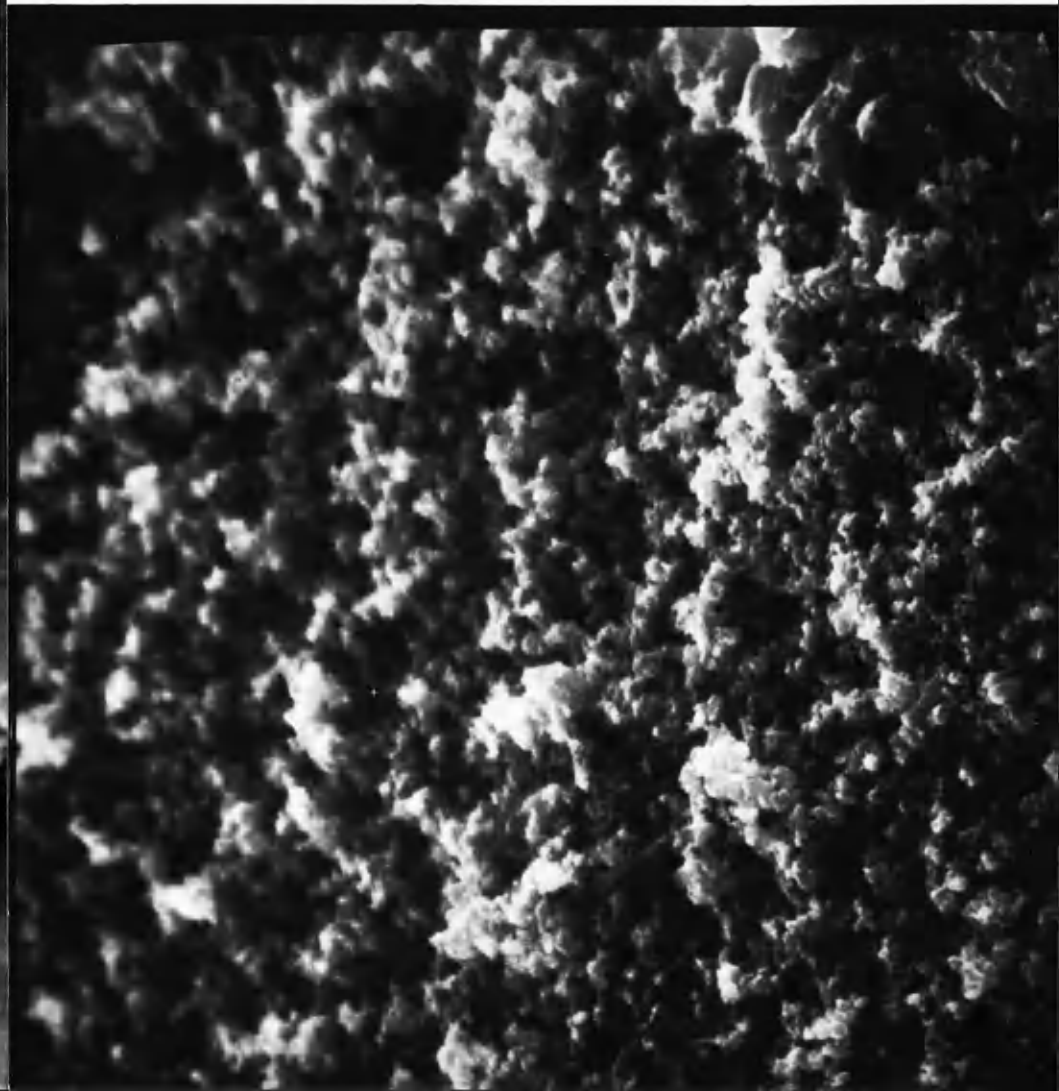

Plate 3.52

Appearance of the edge deposit features, from experiment 1R.

magnification = 4,500X.

Table 3.8

d spacings, in Å, from SP1 graphite and experiment 12C graphite.

Pyrolytic graphite	SP1 graphite	Index	Difference
3.355	3.357	0002	0.002
2.130	2.131	$10\bar{1}0$	0.001
2.032	2.029	$10\bar{1}1$	0.003
1.677	1.675	0004	0.002

It can be seen that there was excellent agreement between the lattice spacings of the two graphites. The most significant value determined was the inter-layer spacing of 3.355 Å which corresponded to 100% stacking order and therefore, according to Franklin's (1951B) p factor criterion, to perfect graphite. This result was important in establishing the high quality of the pyrolytic graphite formed at temperatures as low as 600°C and 700°C.

3.5 Mass Spectrometry

In order to obtain information on the mode of breakdown of the hydrocarbon molecules during the formation of carbon mass spectrometric analysis was employed. After experiments IV and IW much of the methane atmosphere used was found to have been converted to hydrogen. The percentage of higher hydrocarbon left after reaction was less than that

present as impurities in the unreacted methane. This was to be expected as any higher hydrocarbon formed would be at least as reactive as methane and would decompose comparatively readily to carbon.

In comparison the gaseous products of experiments 23C, 23D and 23I, 23J were complex and their compositions are listed in Table 3.9.

Table 3.9

Gaseous products (%) of butadiene decomposition.

Gas	Expt. 23C, 23D	Expt. 23I, 23J
H_2	60	30
CH_4	10	30
C_2H_4	10	30
C_2H_6	7	2
C_6H_6	-	7
C_5H_8	4	1
C_4H_8	4	-
C_4H_{10}	2	-
C_3H_8	2	-

In both sets of experiments, of the weight of carbon contained in the butadiene approximately 20% has been deposited as carbon and the remainder was left in the gas phase as various hydrocarbon species. From the point of view of butadiene decomposition the reaction had gone to completion as no butadiene remained among the gas mixture but from the standpoint of carbon

deposition only 20% reaction had taken place and undoubtedly a longer reaction would have led to further deposition occurring via decomposition of the intermediate gases. The much faster rate of carbon formation when butadiene was employed (see section 3.6) would be expected to be possible only for part of the deposition process when hydrocarbon molecules of low thermal stability were available in the gas phase to continue the fast decomposition. When only CH_4 and C_2H_6 were left the reaction rate would decrease appreciably. This conclusion is only valid in the absence of other effects such as changes in the availability of catalyst surfaces.

3.6. Kinetics

Any mechanism which attempts to explain comprehensively the processes involved in carbon deposition has to be able to interpret the observed reaction kinetics. The weight of carbon deposited during a wide variety of interactions was measured and the importance of several parameters in controlling the reaction rate was studied. The accuracy of the measurements taken was not high because of the limitations of the apparatus used and the reproducibility depended on such factors as the temperature gradient along the reacting foil, which was not easily controllable. In spite of the difficulties encountered several conclusions about the nature of the reactions can be drawn from the kinetic data obtained.

Experiments on the nickel/methane system at 700°C and 600 torr have shown that the rate of carbon deposition decreased as the reaction time was increased. Figure 3.1 indicates the extent of the drop in rate with time. Other workers (Baukloh et al., 1950; Walker et al., 1959B; Tesner et al., 1970; Tamai et al., 1968), studying the interaction of iron, cobalt and nickel on carbon monoxide and hydrocarbons, have found a similar rate dependence on time. The first three groups of workers mentioned also detected after the start of the reaction a temporary increase in rate which they ascribed to a catalytic induction period. Lobo (1971) working with nickel / hydrocarbon interactions found the reaction rate to be totally independent of time over considerable periods. However, his procedure involved passing a heated gas over a foil rather than the more usual resistance heating. Because of the temperature gradient outwards from a foil which is heated by the resistance method the transfer of active metal to the exposed surface of the growing carbon becomes gradually more difficult as the thickness of deposits increases. The method of heating the gas avoids this factor, explaining why no drop in rate with time was found by Lobo.

At a constant reaction duration of two hours and at a temperature of 700°C a pressure change from 1 torr to 600 torr in the nickel methane system resulted in a doubling of the deposition rate, approximately.

FIGURE 3·1

RATE v TIME (C_4H_6/Ni)

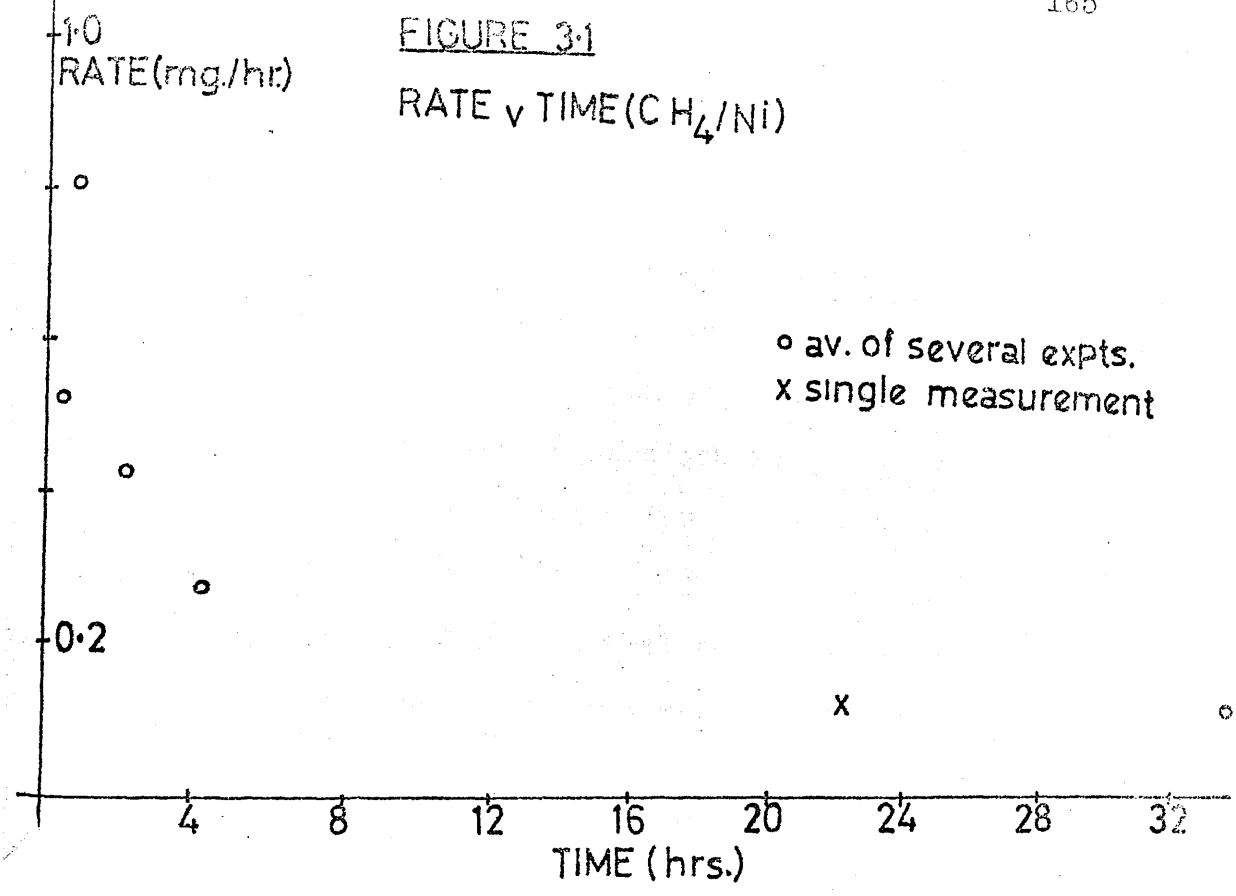

FIGURE 3·2

RATE v PRESSURE (C_4H_6/Ni)

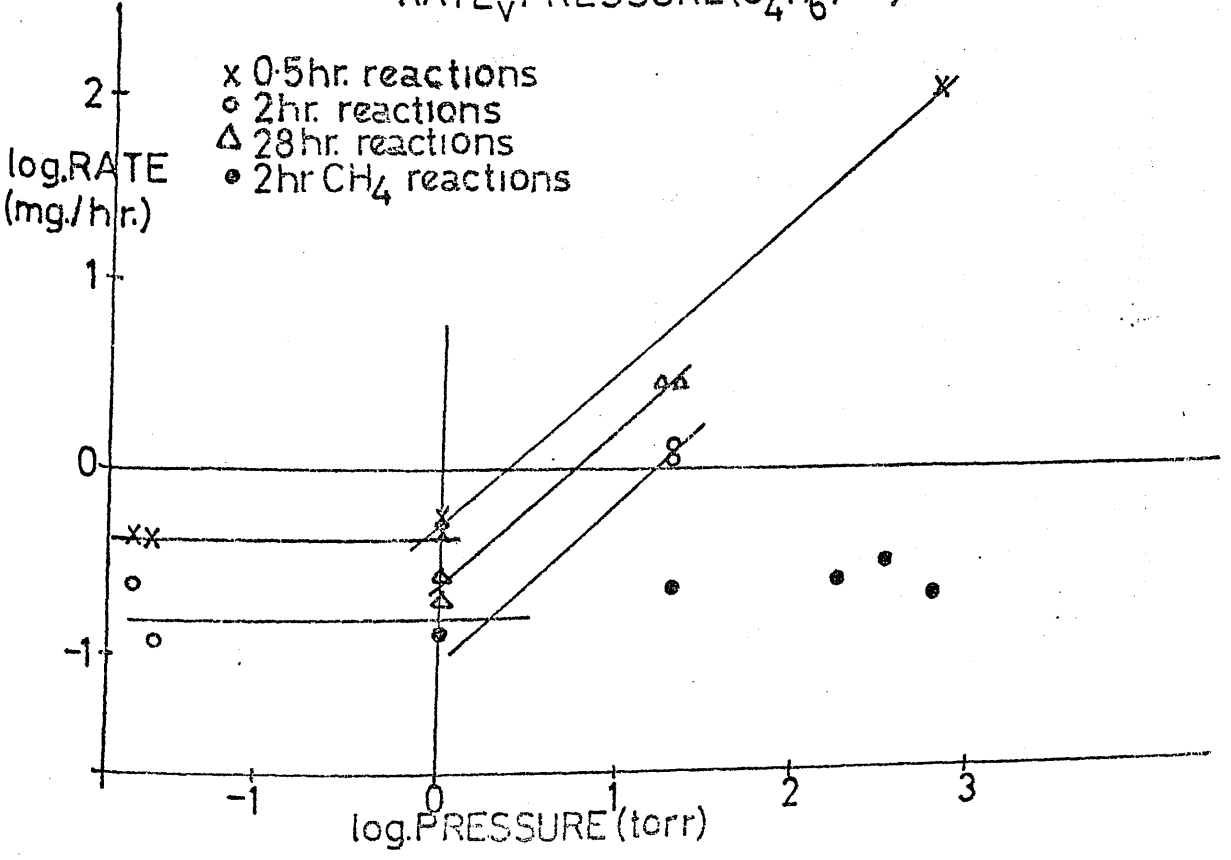

With methane/iron interactions an increase in rate by a factor of about three was caused by the 600-fold increase in pressure. Tamai and co-workers (1968) found that at 900°C and 1000°C the rate of the methane/nickel reaction was nearly independent of pressure between 60 torr and 600 torr while the methane/iron reaction rate altered by a factor of between five and ten for the same change in pressure.

Work performed with nickel powder of particle diameter approximately 5μ (experiment 1F) showed that the reaction rate (and deposit morphology) was proportional to the surface area of the metal but independent of particle size in the range 5 to 100μ.

Experiments involving methane under a wide variety of conditions have shown that the reaction rate using iron was between two and three times that obtained with nickel, this in spite of the fact that purer conditions were required for iron to function as a carbon deposition catalyst. Tamai (1968) quoted an average iron to nickel efficiency ratio of 5, claiming that the difference in activity was mainly due to the greater ability of iron to permeate into carbon layers.

The rate of reaction of propane with nickel was found to be similar to that of the methane reaction, both giving rates below those observed for the three unsaturated gases employed. Thus the effect of chain length or number of carbon atoms was much less than that

produced by the presence of a double bond in the decomposing molecule. At 20 torr CH_4 and C_3H_8 were slightly slower than C_3H_6 and acetone and much slower than C_4H_6. At higher pressures, as mentioned, the increase in rate of CH_4, and presumably C_3H_8, decomposition was minimal but with C_4H_6 the variation was much greater. Figure 3.2 describes the rate changes caused by a range of pressures covering more than 4 orders of magnitude. The average values of CH_4 reaction rates are included for comparison. At lower pressures the rates of carbon deposition from C_4H_6 and CH_4 were fairly similar but as the pressure was increased the disparity in rates widened until at 600 torr a more than 100-fold difference existed. The rate of reaction of C_3H_6 also increased considerably with pressure.

Lobo (1971) found that with C_3H_6/H_2 mixtures at 715°C the order of reaction with respect to the hydrocarbon was one between 100 and 150 torr but approached zero at lower pressures. This is similar to the viariation shown in Figure 3.2 for butadiene. Below approx. 1 torr C_4H_6 gave a carbon product identical to that from saturated gases, indicating that under those conditions its carbon deposition mechanism was similar.
At higher pressures, corresponding to faster deposition, some solid phase carbon was observed as detailed in section 3.1.3.

CHAPTER 4

DISCUSSION

4. DISCUSSION

Contents

4. Discussion

4.1. General Considerations

Part of the reason for the degree of confusion in the literature regarding the chemical nature of carbon deposition catalysts lies in the different criteria proposed for judging catalyst performance. It is known that Fe, Co and Ni increase the rate of formation of carbon from gaseous precursors and also increase the crystalline perfection of the carbon formed at any given temperature (see Introduction). These two aspects are undoubtedly inter-related but require to be carefully distinguished. Conditions which will favour a very high rate of carbon deposition will not be ideal for the formation of large platelets of "perfect" graphite. One example is the auto-catalytic behaviour of the product carbon reported by several authors (Bromley et al., 1960; Lobo, 1971). As the carbon is deposited it increases the rate of further deposition although it is known that crystallinity decreases with amount of deposit (Walker et al., 1959A) and Hirai and Yajima (1967) have shown that crystalline graphite will not grow on top of a graphite substrate.

Carbon mobility and diffusion. The carbon species which is the immediate precursor of the graphite lattice formed in deposition studies is not known for certain. The work of Matsumoto, mentioned previously, suggests that

C_1 species are important. These C_1 species, or surface "C atoms", would be expected to have a higher mobility than larger hydrocarbon fragments and would fit into the growing graphite lattice more easily than the larger species. For these reasons the following section deals exclusively with the situation encountered by individual carbon atoms.

Robertson (1968) has given the values for diffusion rates of carbon atoms on various surfaces. They are:

αFe	5.3×10^{-7} cm.^{2} sec.$^{-1}$	at 672°C
	12.1×10^{-7} cm.^{2} sec.$^{-1}$	at 761°C
Ni	5.0×10^{-7} cm.^{2} sec.$^{-1}$	at 750°C
graphite (a direction)	1.35×10^{-13} cm.^{2} sec.$^{-1}$	at 2185°C
	2.7×10^{-13} cm.^{2} sec.$^{-1}$	at 2200°C

The high values of carbon mobility on Fe and Ni may explain why the build up of graphite crystals can occur at these low temperatures, but strictly they only apply to the first graphite layer on the metal surface. Additional layers are formed on a graphite film and the lower mobility values for diffusion of carbon on graphite should apply. To explain the continued ordered growth it is believed that metal has to be available at the growth sites to aid the decomposition of the gas and to allow a sufficiently high carbon atom mobility for graphite formation.

At 700°C the solubility of carbon in nickel is, $S = 7.05 \times 10^{-5} g.cm.^{-3}$ (Lander et al., 1952) and the diffusion rate, D, is 3.28×10^{-9} $cm.^2 sec.^{-1}$ (Diamond, 1965). The feasilibity of forming a film of carbon almost 100 Å thick on the nickel surface due to dissolved carbon coming out of solution as the foil is cooled after reaction can be calculated.

The time taken for cooling from 700°C to 100°C is approx. 5 seconds and the distance through which carbon atoms can diffuse in this time is $\sqrt{Dt} = 1.28 \times 10^{-4}$ cm. Assuming that for this distance into the foil a saturated solution exists then the amount of carbon per unit area arriving at the surface is 9.02×10^{-7} g., corresponding to a film over 200 Å thick. Taking into account the approximations and assumptions made it is reasonable to conclude that a carbon film of the thickness observed could be formed by the dissolution method described. The appearance of the film was similar to that formed by Derbyshire, Presland and Trimm (1972) using a dissolution-precipitation technique.

Metal mobility and diffusion. The mobility of various metals on graphite has been observed by many workers during the course of graphite oxidation studies (Sears et al., 1963; Presland et al., 1963; Thomas et al., 1964). During this present work several graphite oxidations were followed and the mobility of nickel particles noted. The ability of nickel to move easily

over graphite surfaces is therefore an advantage for carbon deposition catalysis, being necessary to explain the presence of the nickel among the carbon deposit. However, the diffusion of nickel through bulk pyrographite, as investigated by Wolfe and Borg (1964), is considerably more difficult. For diffusion parallel to the a- and c-axes the diffusion coefficients D_a and D_c, respectively, are given by,

$D_a = 1.76 \times 10^2 \exp(-48.1 \times 10^3/RT)$, and

$D_c = 2.43 \exp(-53.2 \times 10^3/RT)$

No diffusion at all through the graphite layer planes was detected in graphite annealed at a temperature above 3300°C, proving that the sole diffusion mechanism in an imperfect lattice is via defects.

Presence of Sulphur and Carbon Impurities. The precise effect of the sulphur impurity in nickel foils is uncertain. It is known that sulphur segregates to the nickel (110) surface during thermal treatment and inhibits carbon formation on metals (see sections 1.2.1 and 1.2.2) but its exact mechanism remains obscure. It is possible that the sulphur presence on the surface retards the (110) reactivity, explaining the faster rate of reaction of the (111) and related planes. The uneven coverage of the metal surface within any one grain, often encountered in carbon deposition experiments, may be due to outcrops of metal sulphide formed from the sulphur impurity.

Carbon also segregates to the nickel surface on heating and the previous presence of trace amounts is necessary for carbon deposition catalysis (Blakely et al., 1970; Coad et al., 1971). Since carbon-bearing gases adsorb on free metal rather than on metal carbides (section 1.1.3.2) the need for having carbon already on the surface is surprising. The surface carbon may aid the dehydrogenation of adsorbed hydrocarbon species.

4.2. Filamentary Carbon.

In section 3.1.4 the growth of the graphite fibres at 700°C was discussed. Metal for the catalysis of fibre growth was obtained by distortion of the foil surface due to the stresses incurred by the platelet graphite growth processes. This effect is similar to the release of compressive stresses during deposition reactions by the formation of metal and metal oxide whiskers reported by Gulbransen and Copan (1959) and encountered during the in situ work described in Chapter 5. Metal at the junction of several graphite crystals is forced into adopting a nodular shape at the surface and if the compression is sufficiently great a column of metal is extruded until the compressive forces are released. As the metal is being forced outwards the graphitic diffracting edge region is growing alongside and gradually forms a graphite fibre. If the stress is not large then the metal nodule may not separate from

the substrate surface and a hemispherical fibre will result. In the former case, however, once the stress is released by extrusion the metal contained in the fibre "necks" and finally separates from the parent foil. Further growth of the fibre generally carries the catalyst particle with it, though from time to time some of the metal is left along the body of the fibre (see, for example, Plate 3.20). It appears likely that if any additional stress is experienced by the foil near the root of the fibre then this can be released by the removal of further amounts of metal along the centre of the fibre, since fibre centres are normally hollow except for areas containing metal.

The oxidation work performed on the graphite fibres has established that the metal within the fibres is mobile at temperatures well below 700°C and the mobility is also shown by the amount of branching and clustering which occurs whenever there is a plentiful supply of metal within the fibres. The oxidation work indicated the existence of small particles of metal among the graphite wall in addition to the large particle at the fibre tip. The manner in which this material became incorporated into the graphite matrix will now be described.

High resolution studies have revealed that at the fibre tip the carbon wall narrows, meaning that the graphite planes furthest away from the metal core are

behind the inner ones in growth sequence. In this region the planes still remain parallel to the fibre surface and therefore only the innermost one is in actual contact with the metal particle and no other ones have ever been adjacent to the metal. This is apparent when the growth scheme outlines in section 3.1.4 is recalled; the outer carbon layers are the ones which were originally at the upper surface of the platelet graphite. For this reason the growth of the fibre wall by the insertion of layer planes on to the surface of the metallic particle, involving either gaseous diffusion through the carbon on to the metal or diffusion of carbon through the particle, cannot explain the observed fibre fine structure.

Even if a fibre of the type described is formed in isolation it cannot grow by carbon deposition directly on to the central particle's surface as this process will not give rise to parallel-oriented basal planes. This can be understood by reference to Figures 4.1 to 4.7. Figure 4.1 represents an early stage of fibre growth when one carbon layer plane has partially formed on the metal. Only if this particle does not move can successive planes form on the metal surface to give Figure 4.2. For most types of fibre this simple picture is not valid. The appearance of the second (inner) layer plane means that the first one has to separate from the metal surface either at the top

FIBRE GROWTH MECHANISMS

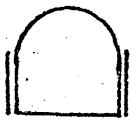

FIGURE 4·1

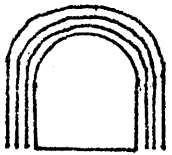

FIGURE 4·2

FIGURE 4·3

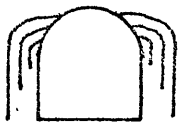

FIGURE 4·4

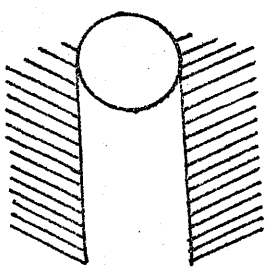

FIGURE 4·5

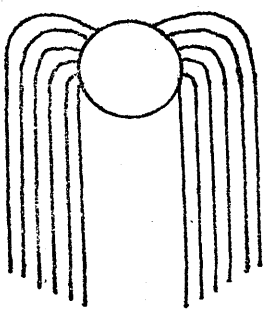

FIGURE 4·6

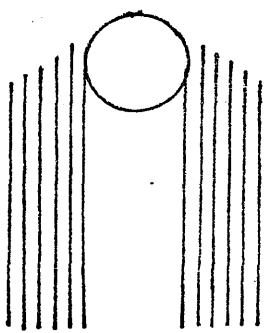

FIGURE 4·7

or at the bottom of the contact area. In both cases this separation will cause the planes to lose their parallel orientation, as indicated by Figures 4.3 and 4.4, respectively. Continued growth will produce fibres with the forms of Figures 4.5 and 4.6, respectively. Neither of these types have been observed in this work, the true fibre characteristics being summarised by Figure 4.7.which is an idealised representation of the fibre in Plate 3.30.

It should be noted that the fibres formed by Lieberman et al. (1971) have a structure similar to that described in Figure 4.5, implying that they were formed during carbonisation by a build-up of the basal planes from the inside.

To explain the observed features of the fibres it is necessary to postulate that the active species migrate to the exposed growing graphite planes. This is in accord with the oxidation evidence of small metal particles in the graphite walls. Since each fibre has a constant diameter bulk diffusion of catalyst through the carbon wall to the surface, which would lead to a gradual thickening of the wall with increasing distance from the fibre tip, does not occur to any significant extent. This is true even of fibres which have metal particles distributed along their centres, for example the fibres in Plate 3.20.

The only other means of transferring metal from the catalyst particle to the carbon surface involves the

release of mobile metal species from the catalyst surface to the growing carbon faces by surface diffusion. Since these metal species although present in the graphite lattice are not visible even under the resolution of Plate 3.30 they must consist of no more than two or three atoms and it is suggested that they exist as individual atoms. The transportation of the atoms to the carbon may be aided by the formation of organo-metallic species from partially decomposed hydrocarbon molecules. McCarroll et al. (1969) have argued that, for example, the adsorption of an ethylene molecule by a nickel atom will allow the atom to travel across the nickel surface more easily. The metal atoms will jump from the central particle on to the first carbon layer and act as " keying agents" for the positioning of the individual carbon atoms into the graphite lattice. Some will move on to higher planes while others will be incorporated into the growing carbon structure. The role of the large metallic particle is to act as a source of atoms for the propagation of the catalytic process by this means.

This growth mechanism is valid even if the central particle contains a metal compound rather than the free metal, as suggested by electron diffraction evidence, as long as the removal of small amounts of metal can be achieved. Since transition metal compounds, especially oxides, are non-stoichiometric this condition should not be too stringent.

The cessation of fibre growth occurs whenever the carbon deposition overtakes the translational motion of the central particle. It is likely that the carbon deposition is not uniform in speed or direction in any given fibre and as soon as the metal becomes coated in a layer of carbon its outward movement is blocked and the fibre stops growing after completely encapsulating the metal. That the metal is encapsulated was shown by the oxidation studies as no gasification of the inner planes occurred until oxygen had access, considerably after the onset of oxidation. The other possible reasons for termination of fibre growth, namely chemical deactivation or cooling at the fibre tip (discussed in Chapter 5) are not applicable to this type of filament.

Encapsulation occurs when the innermost layer plane covers the whole of the metal particle. This cuts off the supply of metal to the other graphite planes which are still growing and would be expected to slow down their rate of growth, although it appears that normally sufficient metal atoms are already available among them to allow completion of growth.

The metal required for the formation of filamentary carbon grown at 450°C is obtained rather differently from the manner just described for fibres. Normally filaments nucleated at the site of the nodular deposit which was common at this temperature.
As mentioned in section 3.1.8 the nodular deposit appeared

to contain large amounts of metal and the separation of metal particles allowed the growth of the filamentary carbon. Their appearance and the presence of pear-shaped metal particles at their tips suggest that these filaments are similar to the ones whose growth sequence has been described by Baker et al. (1972B). They have postulated that in the case of C_2H_2 on Fe, Co, Ni, decomposition on the exposed parts of the metal particle will cause a temperature gradient within the particle. The deposited carbon will dissolve in the metal, diffuse along the thermal gradient and be precipitated at the protected cooler region. Further, more crystalline carbon will be deposited at the exposed parts and will form an outer skin covering the inner region of rather amorphous carbon. In this case also total encapsulation of the particle accompanied the termination of filament growth.

4.3. Flake Graphite

The average thickness of the carbon product can be estimated from the weight of deposit on a known area of foil. For a weight increase of 1 mg. the average thickness is 7500 Å but after approx. 0.5 mg. of carbon has formed, the exact value depending on experimental conditions, non-oriented carbon begins to form in appreciable quantities. Hence the maximum Lc dimension for platelet graphite is about 4000 Å. For the production of larger crystals different experimental

conditions would be required; perhaps a temperature increase or use of lower pressures with purer metal would improve the crystal dimensions.

Several models for the course of hydrocarbon decomposition were listed by Presland and Walker (1969):

1. Chemical model. C_1 and C_2 species e.g. CH_3, C_2H_2 present on the metal surface polymerise and crystallise as carbon.
2. Thin film model. Dehydrogenation of the gas occurs, single carbon atoms move across the carbon surface and slot into position at growth fronts.
3. Metallurgical model. This mechanism is responsible for the dissolution-precipitation method of graphite formation and has been shown (section 4.1) to play only a minor part in producing carbon deposits during the present work. Presland and Walker considered that single crystal graphite would not be formed in the short time required to cool a metal foil to room temperature. A further possibility, not mentioned in their paper is,
4. Intermediate compound model. Deposited carbon enters the metal lattice forming an approximately stoichiometric carbide, such as Fe_3C, which can decompose especially at higher temperatures where carbides of Fe, Co, Ni are unstable, to give crystalline carbon. Little evidence for the existence of intermediate carbides was found during

these studies. However, Lobo (1971) detected several phases in his work which may have been intermediate carbides. Tamai et al.(1968) reported that Fe_3C and Ni_3C may be active in carbon formation from paraffins and olefins. This suggestion is fairly speculative as the main evidence for this conclusion is the presence of Fe_3C, detected by X-rays.

Blau and Presland (1970) formed laminar (platelet) graphite at low pressures from acetylene. They found that an increase in pressure led to poorer quality deposits and explained this fact by reasoning that a rise in pressure produced an increase in supersaturation which led to a higher nucleation density and therefore smaller and less oriented crystals. The effect of a rise in temperature was to improve the orientation of the crystals because of the higher mobility of the carbon atoms at increased temperatures which allowed a more ordered growth process. Their conclusions have in general been confirmed by these studies.

The presence of small amounts of metal among the flake graphite crystals suggests that the mechanism of growth may be analogous to the mechanism proposed in section 4.2 for fibre growth. No information on the feasibility of metal diffusion through platelet graphite has been obtained but it is reasonable to expect that if this is not possible with the fibrous material it would

also not occur with platelet graphite. It is proposed, therefore, that metal reaches the graphite lattice by surface diffusion, that individual metal atoms are free to move over the surface of the growing crystals on each plane and that their presence is sufficient to ensure the ordered arrangement of the succeeding layers throughout the whole crystal.

The orientation of the a-axis of the crystal is determined by the manner in which the first basal plane is deposited as succeeding planes have the same orientation. Any tendency of the graphite crystals within a given metal grain to align will be due to an epitaxial relationship between the metal and carbon lattices. The existence of epitaxy in pyrolytic carbon deposits is in dispute. Presland et al. (1970) found that graphite was laid down epitaxially on the (110) nickel faces at 1000°C with the graphite (0002) planes parallel to the nickel (110) surface, the directional relationship being unknown. This was in spite of the face that the (111) nickel face is geometrically more favourable for epitaxy and was found to react faster than the (110) plane, in disagreement with the findings of Cunningham et al. (1957), discussed in section 1.1.3.3. Little evidence for epitaxy was detected in this work.

CHAPTER 5

THE IN SITU REACTIONS OF IRON AND NICKEL CHAINS IN THE TRANSMISSION ELECTRON MICROSCOPE

5. THE IN SITU REACTIONS OF IRON AND NICKEL CHAINS IN THE ELECTRON MICROSCOPE.

Contents

5. The In Situ Reactions of Iron and Nickel Chains in the Transmission Electron Microscope.

5.1. Introduction

Metal and metal oxide " smoke particles" have been prepared by burning metals in air (Yeorian, 1935; Ehrardt et al., 1940) and by electric arcing between two electrodes of the same metal (Harvey et al., 1960). In the experiments by Harvey and co-workers metallic iron gave rise to γFe_2O_3 particles and nickel formed NiO particles, in each case the product being crystalline and showing a definite tendency to adhere together in chains. Particles of metallic iron and nickel can be prepared by evaporating the appropriate metal in argon at low pressures (Kimoto et al., 1963). On exposure to air the metals tend to form a thin coating of oxide (Kimoto et al., 1966) and if oxidised for a few seconds at 500°C in air iron particles initially form γFe_2O_3 which then change to αFe_2O_3 (Kaito et al., 1970).

The metal chains, when placed on specimen holders, form a self-supporting network which removes the need for the normal carbon or silica support film. They can therefore be used as substrates in the observation of reactions in the electron microscope without the attendant fear of any interaction with supporting media. A preliminary study of the changes effected by heating

the chains was carried out and was followed by work on the decomposition of hydrocarbons in the electron microscope employing the iron and nickel chains as catalysts for these reactions.

5.2 Experimental

5.2.1. Apparatus: The preliminary work was done in the Siemens Elmiskop I microscope using the hollow aperture drive described earlier. The carbon deposition experiments were carried out at the Applied Chemistry Group at A.E.R.E. Harwell in a Jeolco Jem 7A microscope fitted with a gas reaction cell for the observation of in situ high temperature reactions. It was designed by Hashimoto et al.(1966) and converted for use in this system by Feates et al.(1970).

5.2.2. Chemicals: The preliminary studies used the iron and nickel described in the first chapter. Later work used spectroscopically pure iron and nickel. The hydrogen and acetylene were 99% pure and the methane was 99.9% pure.

5.2.3. Procedure: To obtain the chains each metal was evaporated from a previously cleaned tungsten wire in a commercial coating unit under a pressure of between 50 torr and 100 torr argon or neon. The chains of evaporated metal fell on the base plate of the coating unit and were caught by mounts or grids placed there. The unsupported chains were subjected to heating and

chemical reaction in the electron microscope.

5.3 Results

5.3.1. Preliminary Studies using Iron

5.3.1.1. At Room Temperature: The chains were examined in the electron microscope. Particle sizes varied from 100 Å to 1500 Å. Their crystallinity was shown by dark field microscopy and selected area diffraction work, for example Plate 5.1. This plate contains α-iron d spacings and some diffuse rings due to γFe_2O_3 formed by air at room temperature acting on the chains over a period of several days.
Table 5.1 and Table 5.2 contain the measured d spacings of α-iron and γFe_2O_3, respectively.

Table 5.1

α-iron chains formed by evaporation of iron foil in argon.

Calculated d spacings (Å)	Literature α-iron d spacings (Å)	Index	Difference (Å)
2.036	2.0268	110	0.009
1.436	1.4332	200	0.003
1.172	1.1702	211	0.002
1.012	1.0134	220	0.001
0.908	0.9064	310	0.002
0.827	0.8275	222	0.001

Plate 5.1

Selected area diffraction pattern of iron chains at room temperature. [NS 70 1549].

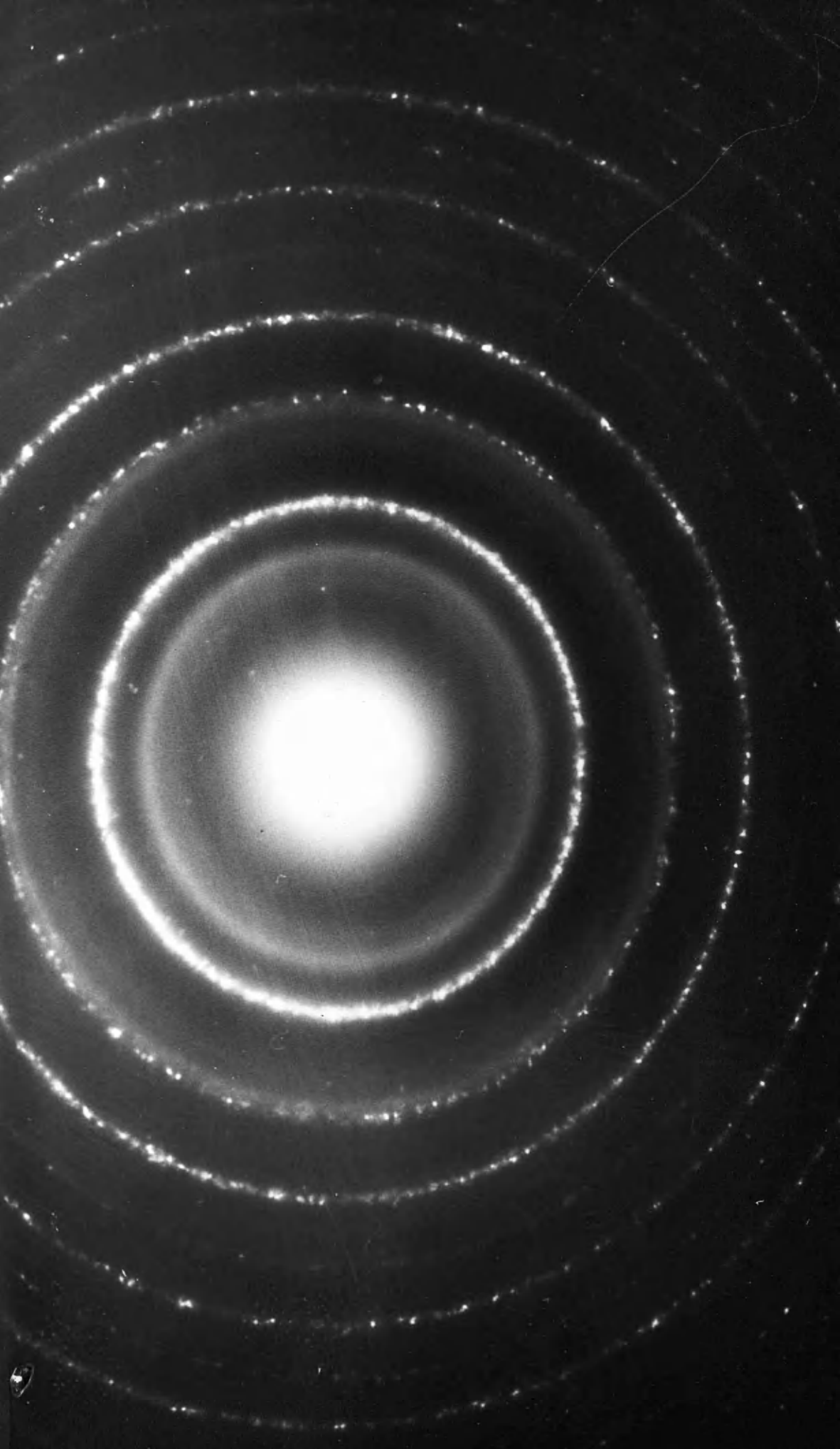

Plate 5.2

Single iron chain showing the surface γFe_2O_3 layer. [1A 70 619].

magnification = 350,000X.

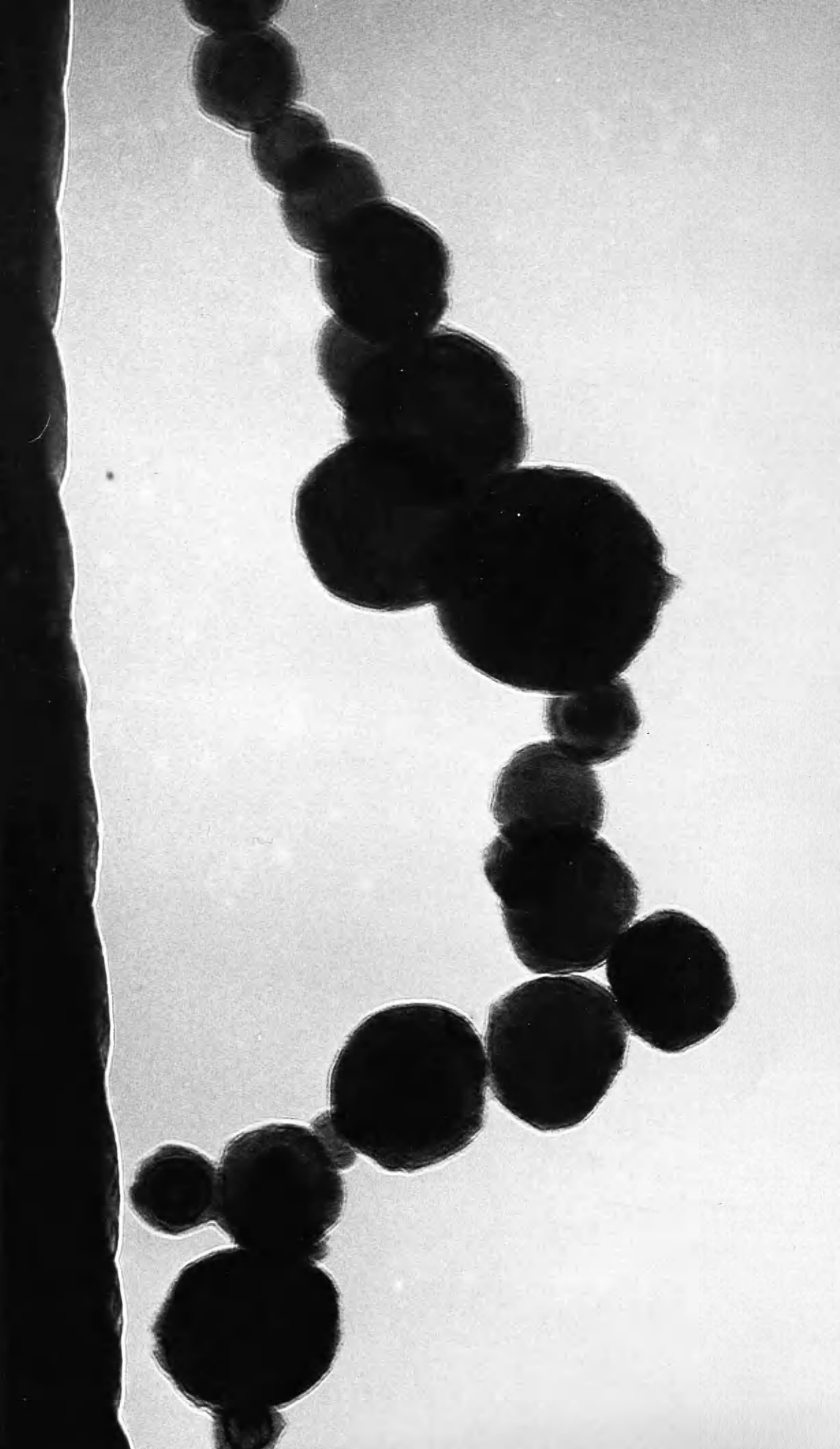

Table 5.2

γFe_2O_3 formed by exposure of α-iron chains to air

Calculated d spacings (Å)	Literature d spacings (Å)	Fe_2O_3 Relative Intensity	Difference (Å)
2.90	2.944	90	0.044
2.50	2.510	100	0.010
-	2.082	90	-
-	1.818	80	-
1.624	1.602	90	0.022
1.474	1.472	90	0.002

Plate 5.2 shows a small chain lying at the edge of a specimen holder. Many of the individual particles have a solid inner region with a definite termination followed by a more tenuous surface layer. This surface layer corresponds to the γFe_2O_3 formed by air oxidation. There appears to be a degree of alignment between some crystal planes of the oxide and the surface of the particle.

5.3.1.2. Heating in the Microscope. When iron chains were heated in the microscope two effects were noted:

1. The particle size increased due to sintering and caused alterations in the arrangements of the chains. Plates 5.3, 5.4 and 5.5 show the appearances of one chain at 350°C, 600°C and 700°C, respectively.

Plate 5.3

Iron chain at 350°C in the electron microscope. [NS 70 1552].

magnification = 30,000.

Plate 5.4

Same iron chain as above at 600°C. [NS 70 1562].

magnification = 30,000X.

Plate 5.5

Same iron chain as above at 700°C. [NS 70 1574].

magnification = 30,000X.

Plate 5.6

S.A.D. pattern of an area of chains at 350°C showing mostly Fe_3O_4 rings. [NS 70 1557].

Plate 5.7

S.A.D. pattern of an area of chains at 600°C showing Fe_3O_4 rings which denote a larger particle size than Plate 5.6. [NS 70 1567].

Plate 5.8

S.A.D. pattern of an area of chains at 700°C showing Fe_3O_4 and αFe_2O_3 reflections. [NS 70 1578].

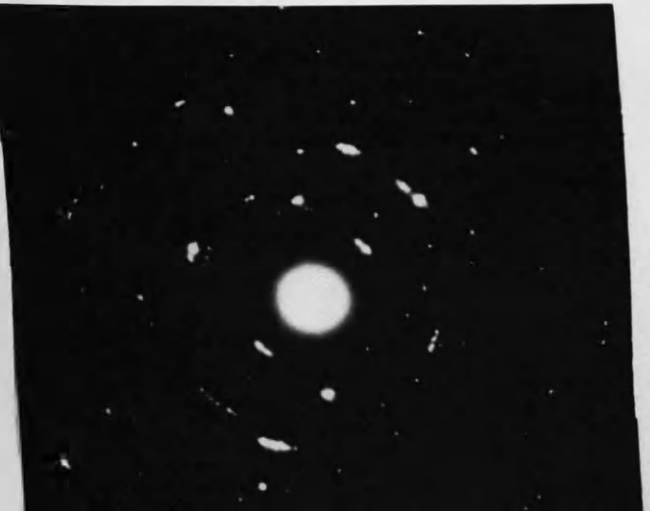

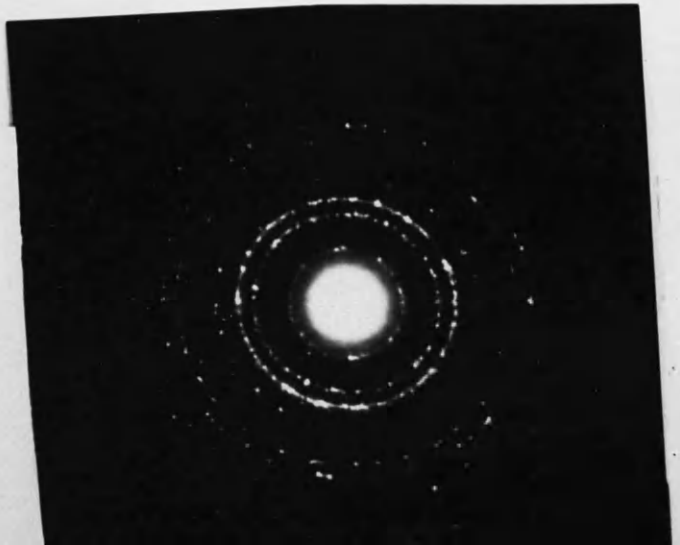

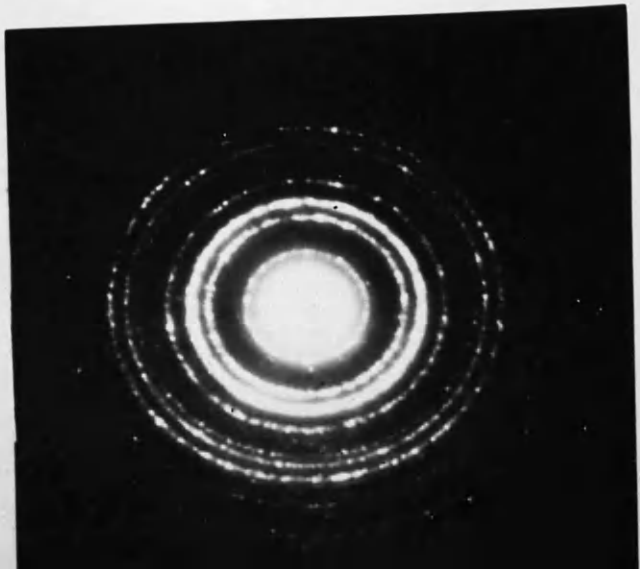

2. In spite of the vacuum of between 10^{-4} and 10^{-5} torr oxidation of the iron took place at elevated temperatures. Plates 5.6, 5.7 and 5.8 show the diffraction patterns of an area of chains at 350°C, 600°C and 700°C respectively. Plate 5.6 is almost completely Fe_3O_4 with negligible α-iron left intact. Plate 5.7 is due to Fe_3O_4 of larger particle size than at 350°C. Plate 5.8 is due to α Fe_2O_3 with traces of Fe_3O_4. The particle size has further increased. Table 5.3 and Table 5.4 give the d spacings of the Fe_3O_4 and α Fe_2O_3, respectively.

Table 5.3

Fe_3O_4 from oxidation of α-iron in the electron microscope

Calculated d spacings (Å)	Literature Fe_3O_4 d spacings (Å)	Relative Intensity	Difference (Å)
4.870	4.850	40	0.020
2.973	2.966	70	0.007
2.523	2.530	100	0.007
2.094	2.096	70	0.002
1.714	1.712	60	0.002
1.617	1.614	85	0.003
1.481	1.483	85	0.002
1.064	1.092	60	0.028
0.857	0.857	50	0

Table 5.4

α-Fe_2O_3 from oxidation of α-iron in the electron microscope

Calculated d spacings (Å)	Literature α-Fe_2O_3 d spacings (Å)	Relative Intensity	Difference (Å)
3.685	3.66	25	0.03
2.669	2.69	100	0.02
2.484	2.51	50	0.03
2.178	2.201	30	0.023
1.847	1.838	40	0.009
1.714	1.690	60	0.024

5.3.1.3 Heating in Hydrogen and Methane. The iron chains were heated to 600°C in hydrogen. The degree of sintering was reduced but the oxidation of the iron was not prevented. In the presence of hydrogen or methane the chains became coated in a layer of unknown material and some areas were seen to contain thin overgrowths. Plate 5.9 shows both of these features and Plate 5.10 taken ten minutes later indicates that the overgrowth material is susceptible to damage by the electron beam. The diffraction pattern of the area shown in Plates 5.9 and 5.10 gave no information about the nature of the deposits.

5.3.2. Preliminary Studies using Nickel

5.3.2.1. At Room Temperature. The particle sizes of the nickel chains lay between 100 Å and 2000 Å, approximately the same as the range found with iron chains.

Plate 5.9

Iron chains coated in the presence of hydrogen or methane. [NS 70 1894].

magnification = 180,000X

Plate 5.10

The same area as in Plate 5.9 showing the effect of the electron beam on the coating material. [NS 70 1896].

magnification = 180,000X.

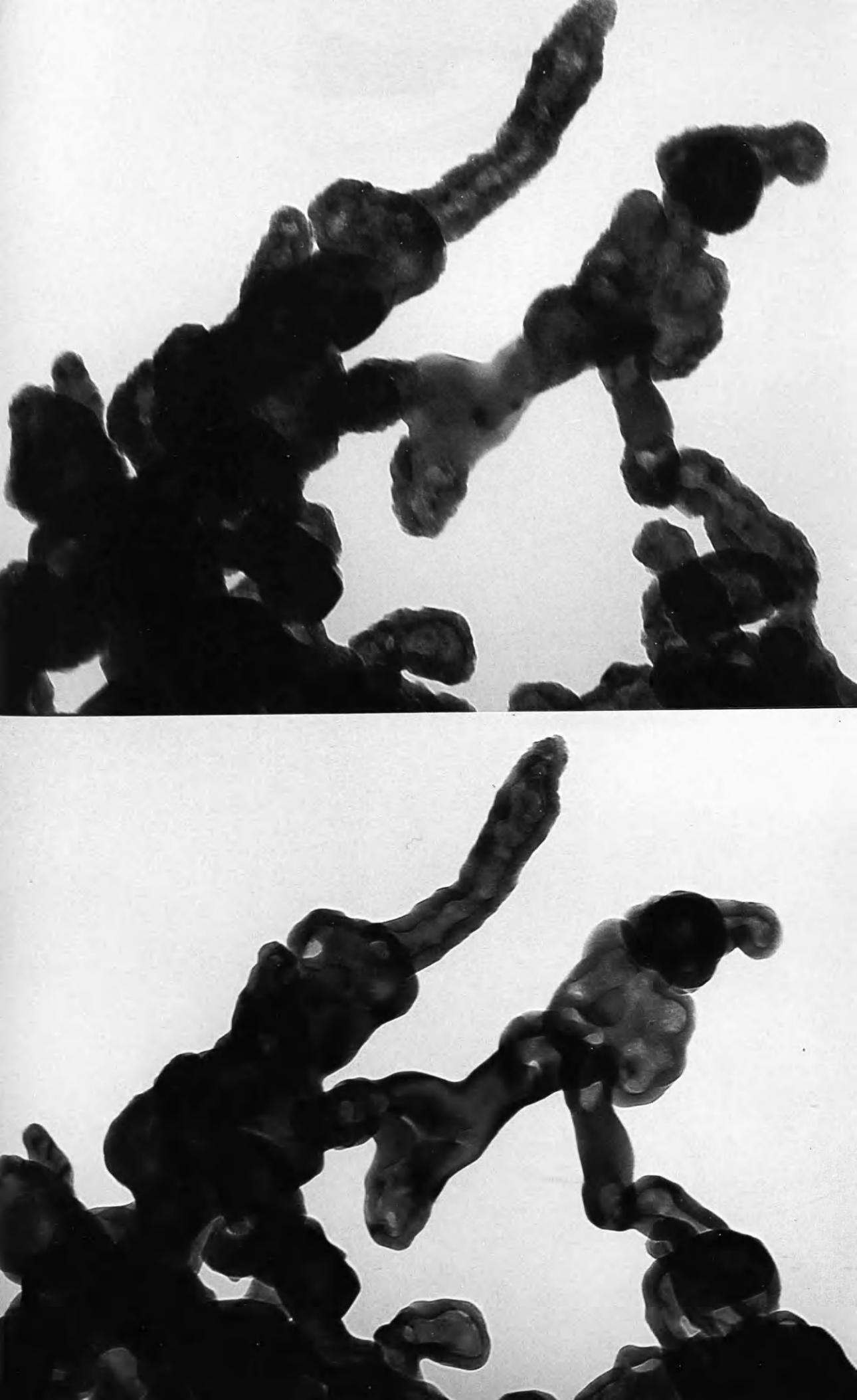

Plate 5.11 shows the typical appearance of the chains at room temperature and Plate 5.12 contains the diffraction pattern of the inset area. The d spacings found are listed in Table 5.5.

Table 5.5

Nickel chains formed by evaporation of nickel foil in argon

Calculated d spacings (Å)	Literature nickel d spacings (Å)	Index	Difference (Å)
2.036	2.034	111	0.002
1.757	1.762	200	0.005
1.252	1.246	220	0.006
1.061	1.0624	311	0.001
1.013	1.0172	222	0.004
0.890	0.8810	400	0.009
0.799	0.8084	331	0.009
0.776	0.7880	420	0.012

5.3.2.2. Heating in the Microscope. The same two effects noticed with the iron chains were observed with the nickel chains:

(1) The nickel sintered gradually as the temperature was raised. Plates 5.13, 5.14 and 5.15 were taken at 350°C, 600°C and 700°C, respectively. They show

(2) The nickel, though more resistant to oxidation than iron, changes to nickel oxide, NiO, on prolonged heating. Plates 5.16, 5.17 and 5.18 at 350°C, 600°C and 700°C, respectively, show increasing amounts of

Plate 5.11

Appearance of the nickel chains at room temperature. [NS 70 1603].

magnification = 180,000X.

Plate 5.12

Selected area diffraction pattern from the inset area of nickel chains. [NS 70 1967].

magnification = 80,000X.

Plate 5.13

The area of chains shown in Plate 5.11 after sintering at 350°C. [NS 70 1613].

magnification = 30,000X

Plate 5.14

The same area as Plate 5.13 after further sintering at 600°C. [NS 70 1626].

magnification = 30,000X

Plate 5.15

The same area as Plate 5.13 after sintering at 700°C [NS 70 1639].

magnification = 30,000X

Plate 5.16

S.A.D. pattern of nickel chains at 350°C showing a trace of NiO. [NS 70 1612].

Plate 5.17

S.A.D. pattern at 600°C showing Ni and NiO rings. [NS 70 1627].

Plate 5.18

S.A.D. pattern at 700°C showing further conversion of nickel to nickel oxide.

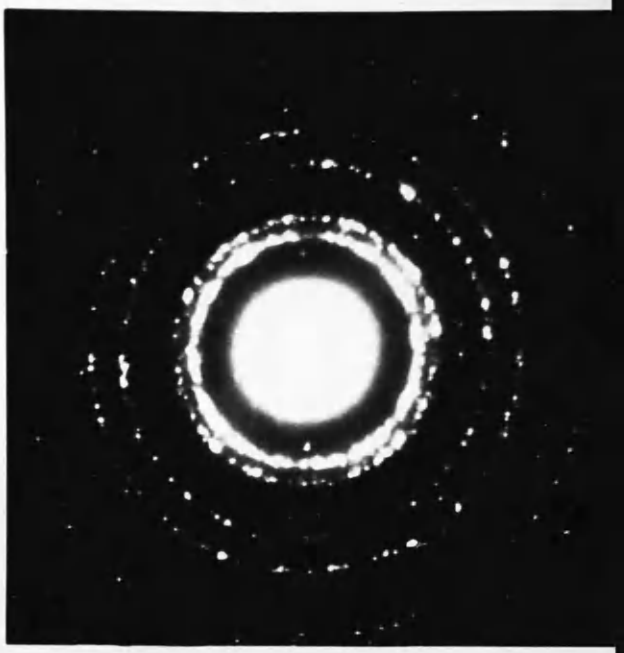

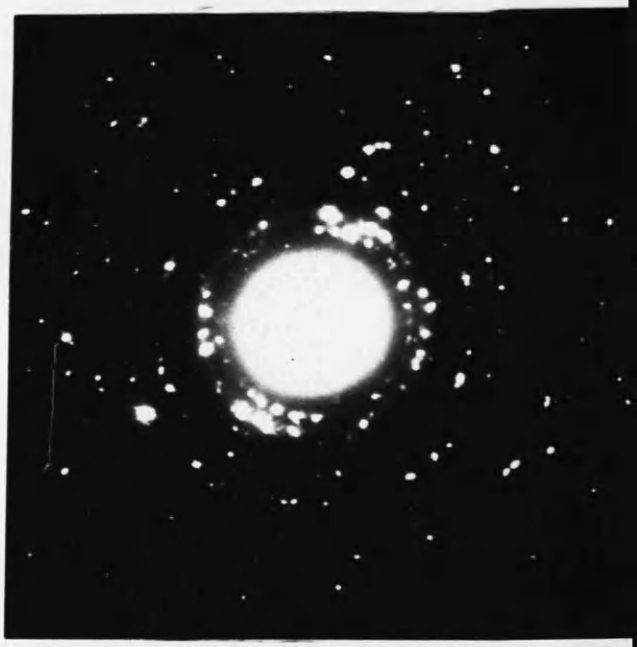

nickel oxide and also an increase in crystal size. Table 5.6 gives the d spacings of the nickel oxide.

Table 5.6

Nickel oxide from oxidation of nickel in the electron microscope.

Calculated d spacings (Å)	Literature nickel oxide d spacings (Å)	Index	Difference
2.385	2.410	111	0.025
2.060	2.088	200	0.028
1.472	1.476	220	0.004
1.262	1.259	311	0.003
1.190	1.206	222	0.016
1.035	1.0441	400	0.009

5.3.2.3. Heating in Hydrogen and Methane. Heating the nickel chains in hydrogen or methane did not prevent nickel oxide formation though sintering was noticeably inhibited in the presence of hydrogen. Plate 5.19 shows an area of chains which has been allowed to complete the sintering process in hydrogen at 600°C.

5.3.3. Carbon Deposition on Iron

5.3.3.1. Reaction with Acetylene. The iron chains were left at 825°C for 15 minutes when it was found that the iron was covered in a thick layer of polycrystalline carbon.

Plate 5.19

Nickel chains sintered in hydrogen at 600°C.
[NS 70 1909].

magnification = 80,000X.

On top of this layer a large number of filaments of length 2500 Å or less were observed, many of them having definite metal particles at their tips. A typical area of deposit is shown in Plate 5.20. Selected area electron diffraction work on this deposit showed the presence of carbon and Fe_3O_4 on the reaction products. The d spacings measured are summarised in Table 5.7.

Table 5.7

Fe_3O_4 and polycrystalline carbon formed by reacting acetylene with iron chains.

SP1 graphite d spacings (Å)	Calculated d spacings (Å)	Fe_3O_4 d spacings (Å)
	5.085	4.850
3.355	3.45	
	2.910	2.966
	2.471	2.530
2.128	2.110	
	2.087	2.096
	1.719	1.712
	1.607	1.614
	1.483	1.483
1.229	1.230	

5.3.3.2. Reaction with Methane. Iron chains in 2 torr methane again formed a layer of carbon at 825°C. After a period of one or two minutes at this temperature very straight filaments grew out from the iron matrix,

Plate 5.21

Iron oxide, Fe_3C_4, whiskers formed by action of methane on iron chains at 825°C.

magnification = 150,000X.

Plate 5.20

Polycrystalline and filamentous carbon formed by action of acetylene on iron chains at 825°C.

magnification = 50,000X.

Plate 5.23

Carbon filaments formed on nickel chains by reaction with acetylene at 825°C.

magnification = 150,000X.

Plate 5.22

Polycrystalline carbon layer formed on nickel by acetylene pyrolysis at 825°C.

magnification = 75,000X.

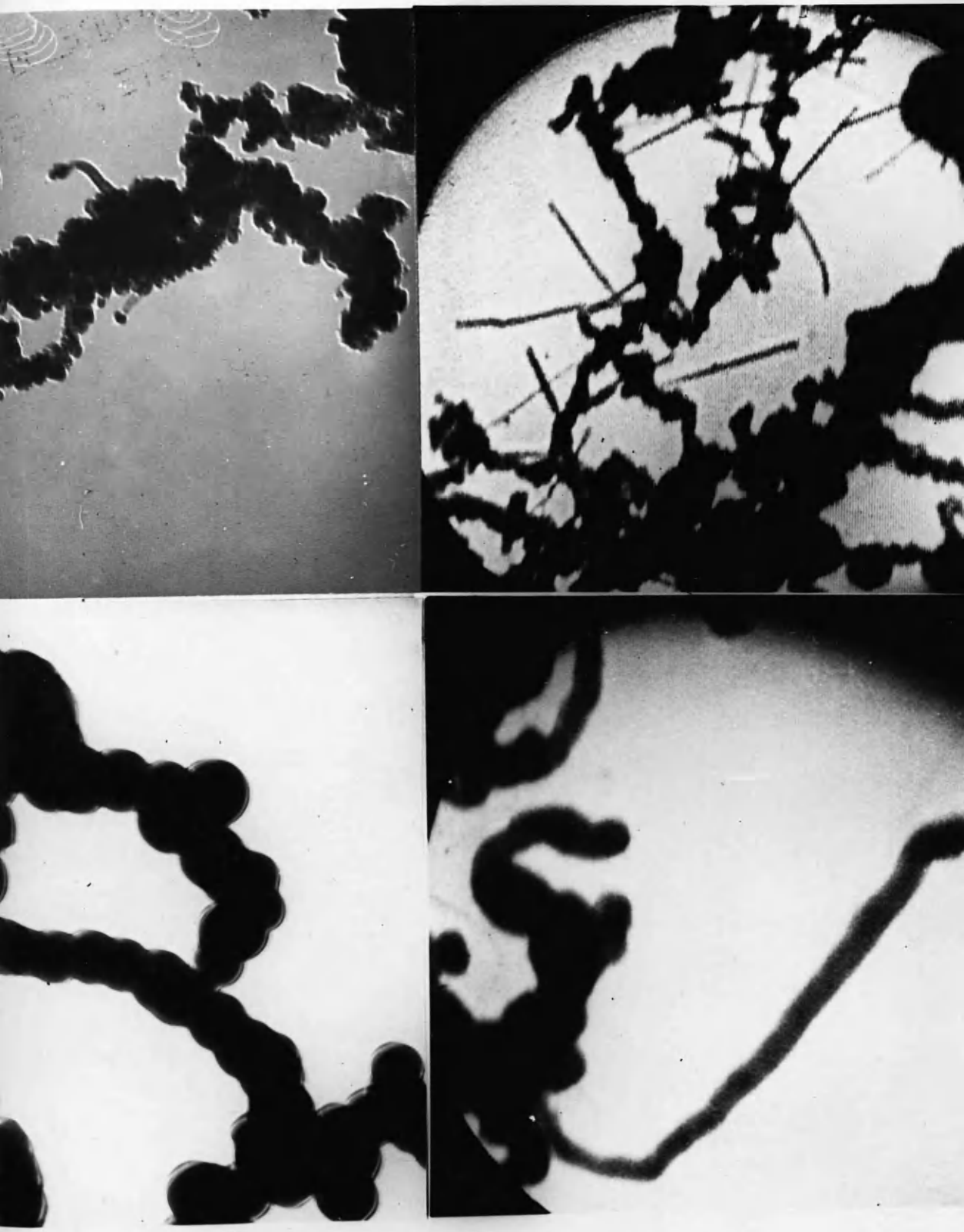

different areas of chains producing the filaments at slightly different times and thus implying a temperature variation in the system. In every case the filaments would grow only for periods of about 15 seconds and then cease growth completely. Plate 5.21 shows the features common to all of the filaments; a geometrical regularity of shape, either perfectly straight or with changes of direction of exactly 120°; an absence of internal markings such as a division into edge and central regions; no metal particle at the filament tip. Diffraction patterns from individual ones verified that they differed from the carbon filaments previously described and that they were in fact single crystal "whiskers" of Fe_3O_4. The d spacings from a single whisker are shown in Table 5.8.

Table 5.8

Fe_3O_4 whisker formed by the reaction of methane on iron chains.

Calculated d spacings (Å)	Literature Fe_3O_4 d spacings (Å)	Relative Intensity	Difference (Å)
5.15	4.85	40	0.30
2.978	2.966	70	0.012
2.516	2.530	100	0.014
2.068	2.096	70	0.028
1.639	1.614	85	0.025
1.482	1.483	85	0.001
1.268	1.279	30	0.009
1.193	1.211	20	0.018

An oxidation of the product of the methane/iron reaction had no effect on the Fe_3O_4 whiskers as would be expected but resulted in a general conversion of the iron chains to Fe_3O_4. Diffraction patterns of the product of the oxidation consisted entirely of Fe_3O_4 rings indicating that the carbon deposit layer has been completely removed.

5.3.4. Carbon Deposition on Nickel

5.3.4.1. Reaction with Acetylene. The nickel chains left reacting at 825°C with 2 torr acetylene produced a deposit layer as shown by Plate 5.22 which by diffraction was shown to be polycrystalline carbon. The d spacings obtained are given in Table 5.9.

Table 5.9

Polycrystalline carbon formed by reaction of acetylene with nickel chains.

Calculated d spacings (Å)	SP1 graphite d spacings (Å)	Index
3.4	3.355	0002
2.05	2.128	$10\bar{1}0$
1.74	1.688	0004

Carbon filaments, of length approximately 1μ, similar to those shown on Plate 5.23 were produced, though only at the edge of the specimen holder where the temperature was highest.

5.3.4.2. Reaction with Methane. Two methane/nickel experiments were carried out. The first gave exactly the same polycrystalline and filamentous carbon as found for nickel acetylene; the second gave angular filaments which were similar to the Fe_3O_4 whiskers previously discussed except that their diameters decreased slightly with growth. They were probably whiskers of NiO.

5.4. Discussion and Conclusion

The in situ work is of interest in the context of other metal chains phenomena (discussed in the introduction to this chapter) and also for the information it adds to our knowledge of carbon deposition processes.

5.4.1. Polycrystalline Carbon. The polycrystalline carbon deposited in almost all of the interactions is featureless and of low quality. The diffraction rings obtained from it were the (02), (10), (11) and (04) reflections, no general (hkl) reflections being observed.
No attempt was made to calculate crystallite sizes using ring half-width measurements but the deposit appeared to be little better than the amorphous, carbonaceous contamination formed on specimens in the electron microscope under normal operating conditions. (Hillier, 1948; Konig, 1951). Contamination is produced by the breakdown of hydrocarbon vacuum pump oil

giving rise to a hydrocarbon polymer which is carbonised by continued bombardment in the electron beam (Ennos, 1953, 1954; Heide, 1958, 1963). The mechanism of the formation of the polycrystalline carbon is probably similar to that of the contamination, the more controlled conditions of fixed gas pressure and elevated temperature resulting in a product with some degree of crystallinity. The appearance of this deposit was different on iron than on nickel indicating that the nature of the substrate played a limited role in determining the form which the polycrystalline carbon adopted. Baker et al.(1972A) found that " flocculent, amorphous" deposit can form on iron, silica or alumina indicating that the substrate particles acted purely as a nucleus for deposition above 900°K. The present work was performed mostly at 1100°K.

5.4.2. Filamentary Carbon. The carbon filaments formed in these studies were sufficiently ordered to give fibrous diffraction patterns and to exhibit what appeared to be edge and centre regions. They were probably most similar to the filaments formed in coating unit experiments on iron and nickel from a variety of gases at approximately 450°C. As expected, no platelet graphite was deposited in the in situ studies. Baker et al. (1972A) have shown that platelets do not normally form in experiments where the polycrystalline carbon has been deposited.

Two major facts emerge from the observation of the growth of the filamentous carbon. Firstly, the period of growth of each filament was very short compared with the total reaction time; secondly, in several instances filament growth occurred on different areas of substrate after slightly different times due (presumably) to temperature variations. Both of these pieces of information would have been very difficult to obtain by any means other than in situ studies.

The brevity of each filament's growth period suggests that growth cessation is due to chemical deactivation of the catalyst particle. This was found for carbon monoxide/iron interactions by Walker et al. (1959B), where the iron catalyst was gradually converted to the inactive Fe_3C. This argument is reinforced by the fact that other work in the present system (Baker, priv. comm.) has shown that the presence of hydrogen, which would replenish the catalyst by converting Fe_3C back to iron, causes the filaments to grow for longer periods. The observation that the initiation of filamentary growth is affected by temperature fluctuations may indicate that growth ceases suddenly due to a cooling down of the tip of the filament since heat transfer by conduction becomes more difficult with increasing filament length. However, the fibres grown by hydrocarbon decomposition in the coating unit reported in Chapter 1-4 and the

filaments discussed by Baker et al. (1972B) both ceased growth because of an impermeable carbon layer which prevented access of gas to the active sites, thereby inhibiting reaction and it is probable that these filaments stopped growing for the same reason.

Baker and co-workers (Priv. Comm.) have found using this reaction system that the existence of a polycrystalline carbon layer on top of the metal substrate is a prerequisite for filament nucleation. There is undoubtedly a direct analogy between this observation and the fact that in deposition experiments in the coating unit carbon fibres grew at 700°C only after a layer of platelet graphite had formed. Both features imply that the original carbon layer is needed in order to aid the separation of a metal particle from the metal substrate to form the catalyst at the tip of the growing fibre.

5.4.3. Oxide Whisker Growth

Whiskers are filamentous single crystals of near uniform cross-section with a high degree of structural perfection. Directional changes or " kinks" at crystallographic angles are frequently found and it has been shown that a facet common to both arms of the kink implies no change in orientation of the crystal (Baker, 1956; Courteney, 1957; Saimoto, 1960).

The growth of whiskers, being uni-directional, requires that the prevailing supersaturation must remain below $(p/pe)_{crit.}$, the critical supersaturation ratio, otherwise growth may occur spontaneously on all crystal faces (Evans, 1972). It is uncertain in these instances whether the oxide whiskers grew from the solid phase using the oxide coating known to form on the metal chains' surface or whether they grew from the vapour phase using " atmospheric " oxygen.

In a situation where a thin polycrystalline layer of material (in this case oxide) lies on a rigid substrate (metal) deposition processes (carbon formation) produce compressive stress in the surface layer which can be relieved by whisker growth. In these circumstances the whiskers are single crystals and often possess kinks, as found here. The growth rate is increased by high temperatures and the presence of oxygen or organic contaminants. Alternatively, the whiskers may have formed by a metal/oxygen chemical reaction at sites of screw dislocations in the solid.

The growth of iron whiskers by $Fe(CO)_5$ chemical vapour deposition has been observed in detail in the electron microscope (Gabor et al, 1969). Kittaka and Kaneko (1969) have used carbon black particles to catalyse the formation of iron whiskers from iron halides at 500°C-900°C.

REFERENCES

Agar, W.D., Brit. J. Appl. Phys., 11, 185, (1960).

Aggarwal, P.S., Goswani, A., J. Phys. Chem., 65, 2105, (1961).

Akamatsu, H., Sato, K., Bull. Chem. Soc. Japan, 22, 127, (1949).

Alderson, R.H., Holliday, J.S., " Techniques for Electron Microscopy" . (1965).

Allen, C.G., University of Glasgow, B.Sc. Thesis (1966).

Andrews, K.W., Dyson, D.J., Keown, S.R., " Interpretation of Electron Diffraction Patterns" , London (1967).

Bacon, G.E., Acta. Cryst., 3, 137, (1950).

Bacon, G.E., Acta. Cryst., 4, 558, (1951).

Bacon, G.E., Acta. Cryst., 5, 392, (1952).

Bacon, G.E., A.E.R.E. M R., 2702, 44, (1958).

Bahr, H.A., Bahr, T.H., Ber., 61B, 2465, (1928A).

Bahr, H.A., Bahr, T.H., Ber., 61B, 2177, (1928B).

Bahr, H.A., Jessen, V., Ber., 63, 2226, (1930).

Bahr, H.A., Jessen, V., Ber., 66, 1238, (1933).

Bailey, J.E., Hirsch, P.B., Proc. Roy. Soc., A267, 11, (1962).

Baker, C., Chou, Y.T., Kelly, A., Phil. Mag., 6, 1305, (1961).

Baker, G.S., J. Appl. Phys., 27, 1561, (1956).

Baker, R.T.K., Private Communication.

Baker R.T.K., Feates, F.S., Harris, P.S., Carbon, 10, 93, (1972A).

Baker, R.T.K., et al. J. Catal., 26, 51, (1972B).

Bannerjee, B.C., Hirt, T.J. Walker, P.L., Nature, 192, 450, (1961).

Barrett, C.S., " Structure of Metals" , McGraw Hill, N.Y., (1943).

Bartuska, P., Czech, J. Phys., 20, 1329, (1970).

Baukloh, W., Hieber, G., Z. Anorg. Allg. Chem., 226, (1936).

Basinski, Z.S., Hume-Rothery, W., Sutton, A.L., Proc. Roy. Soc., A229, 459, (1955).

Baukloh, W., Hillbruge, J., Arch. Eisen., 15, 163, (1941).

Baukloh, W., Edwin, B., Arch. Eisen., 16, 197, (1942).

Baukloh, W., Chatterjee, B., Das, P.P., Trans. Indian Inst. Metals, 4, 271, (1950).

Bell, L., Iron and Steel. Inst., 1, 85, (1871).

Bernal, J.D., Proc. Roy. Soc., A106, 749, (1924).

Berry, T.F., Ames, R.N., Snow, R.B., J. Amer. Ceram. Soc., 39, 308, (1956).

Biscoe, J., Warren, B.E., J. Appl. Phys., 13, 364, (1942).

Blakely, J.M., Kim, J.S., Potter, H,C., J. Appl. Phys., 41, 2693, (1970).

Blau, G., Presland, A.E.B., Soc. Chem. Ind.London, (1970).

Boehm, H.P., Hofman, U., Z. Anorg. Allg. Chem., 278, 58, (1955).

Bollman, W., J. Inst. Metals, 87, 438, (1958-59).

Boudouard, O., C.R. Acad. Sci., 128, 307, (1899A).

" " " " " 128, 98, (1899B).

" " " " " 128, 822, (1899C).

" " " " " 128, 824, (1899D).

" " " " " 128, 1522, (1899E).

" " " " " 128, 1524, (1899F).

Boudouard, O., C.R. Acad. Sci., 130, 132, (1900A).

" " " " 131, 1204, (1900B).

" " Ann. Chim. Phys., 24, 5, (1901).

Bradshaw, A.B., Pritchard, J. Proc. Roy. Soc., A316, 169, (1970).

Bromley, J., Strickland-Constable, R.F., Trans. Far. Soc., 56, 1492, (1960).

Chambard, G., Gregoire, P., Azou, P., Bastien, P., C.R. Acad. Sci., C272, 385, (1971).

Chatterjee, B., Das, P.P., Nature, 173, 1046, (1954).

Chemical Rubber Co., " Handbook of Phys. and Chem.," 50th ed. (1969-70).

Chufarov, G.I., Bull. Acad. Sci. URRS. C.S.T., 883, (1946).

Chufarov, G.I., Antonova, M.F., Bull. Acad. Sci. URSS., C.S.T., 381, (1947).

Coad, J.P., Riviere, J.C., Surf. Sci., 25, 609, (1971).

Colombo, V., Gazzarini, F., Lanzavecchia, G., Mater. Sci. Eng., 2, 125, (1967).

Conroy, J.S., Slysh, R.S., Murphy, D.B., Kinney, C.R., Proc. Conf. Carbon (3rd), 2, 395, (1959).

Cosslett, V.E., " Practical Electron Microscopy" , Butterworths, London, (1951).

Cosslett, V.E., Inst. Elect. Eng., 117, 1489, (1970).

Courtney, W.G., J. Chem. Phys., 27, 1347, (1957).

Crewe, A.V., New Scientist, July 9th, (1970).

Crewe, A.V.; Wall, J., Elect. Micros. Conf., 1, 35, (1970).

Cullis, C.F., Manton, J.E., Thomas, G.B., Wilman, H., Acta. Cryst., 12, 382, (1959).

Cullis, C.F., Presland, A.E.B., Read, I.A., Trimm, D.L., 2nd Conf. on Ind. C. and G., 195, (1965).

Cullis, C.F., Norris, A.C., 3rd Conf. on Ind. C. and G., 235, (1970).

Cullis, C.F., Norris, A.C., Carbon, 9, 517, (1971).

Cunningham, R.E., Gwathmey, A.T., Adv. Cat., 9, 25, (1971).

Davis, W.R., Slawson, R.J., Rigby, G.R., Nature, 171, 756, (1953).

Davis, W.R., Rigby, G.R., Trans. Brit. Ceram. Soc., 53, 511, (1954).

Davis, W.R., Slawson, R.J., Rigby, G.R., Trans. Brit. Ceram. Soc., 56, 70, (1957).

Debye, P., Scherrer, P., Z. Physik, 18, 291, (1917).

Derbyshire, F.J., Presland, A.E.B., Trimm, D.L., Carbon, 10, 114, (1972).

Diamond, S., Thesis, University of Illinois, (1965) from Lobo, (1971).

Diefendorf, R.J., J. Chim. Phys., 57, 815, (1960).

Dubovitskaya, N.V., Larikov, L.N., Uki. Fiz. Zh., 15, 493, (1970).

Durand, J.F., C.R. Acad. Sci., 117, 693, (1923).

Eckstrom, H.I., Adcock, W.A., J. Amer. Chem. Soc., 72, 1042, (1950).

Edmonds, T., McCarroll, J.J., Pitkethly, R.C., Nature, 223, 1260, (1969A).

Edmonds, T., Pitkethly, R.C., Surf. Sci., 15, 137, (1969B).

Edmonds, T., McCarroll, J.J., Pitkethly, R.C., J. Vac. Sci. Tech., 8, 68, (1971).

Ehrardt, A., Lark-Horowitz, B., Phys. Rev., 57, 603, (1940).

Ennos, A.E., Brit. J. Appl. Phys., 4, 101, (1953).

Ennos, A.E., Brit. J. Appl. Phys., 5, 27, (1954).

Ergun, S., Carbon, 6, 141, (1968).

Escombes, C., Baggioni, M., Quinson, J., Ejraind, C.H., Bull. Chim. Soc. France, 1967, 2435, (1967).

Evans, C.C., "Whiskers" Mills and Boon Ltd., London, (1972).

Everhart, T.E., Oatley, C.W., Wells, O.C., J. Electronics and Control, 7, 97, (1959).

Feates, F.S., Morley, H., Robinson, P.S., 7th Int. Cong. Elect. Micros., 295, (1970).

Finch, G.I., Wilman, H., Proc. Roy. Soc., A155, 345, (1936).

Fischer, F., Tropsch, H., Chem. Abs., 1526, (1925).

Fischer, F., Tropsch, H., TerNoddon, W., Brennstoff. Chem., 7, 97, (1926).

Fischer, F., Waughenheim, F., Brennstoff Chem., 9, 94, (1928A).

Fischer, F., Bahr, H.A., Ges. Abhandl Kenntris. Kohle, 8, 225, (1928B).

Fisher, R.M., Szirmae, A., McAlear, J.H., Anal. Chem., 42, 362R, (1970).

Fitzer, E., Fritz, W., Overhoff, D., 2nd Conf. Ind. C. and G. (1965).

Fleureau, B., C.R. Acad. Sci., 237, 330, (1953).

Flosken, J.W., Phys. Rev., 3, 1187, (1971).

Franklin, R.E., J. Chim. Phys., 47, 573, (1950).

Franklin, R.E., Proc. Roy. Soc., 209, 196, (1951A).

Franklin, R.E., Acta. Cryst., 4, 253, (1951B).

Frazee, J.D., Anderson, R.C., Proc. Conf. Carbon (3rd), 2, 405, (1959).

Frey, F.E., Hepp, H.J., Ind. Eng. Chem., 25, 441, (1933).

Frey, F.E., Ind. Eng. Chem., 26, 198, (1934).

Fruchart, R., Bull. Soc. Chim. Fr., 2652, (1963).

Fruchart, R., Senateur, J.P., Bouchard, J.P., Michel, A., Bull. Soc. Chim. Fr., 392, (1965).

Fryer, J.R., Siemens Review, 35, 13, (1968).

Fryer, J.R., Soc. Chem. Ind. London, (1970).

Fuks, M.Y., Palatnik, L.S., Koz Ma, A.A., Nechitailo, A.A., Semenenko, V.E., Fiz. Metal. Metalloved, 29, 271, (1970).

Gabor, T., Blockes, J.M., J. Appl. Phys., 40, 2696, (1969).

Gibson, J., Holohan, M., Riley, H.L., J. Chem. Soc., 1, 456, (1946).

Gillot, J., Lux, B., Cornault, P., du Chaffant, F., Carbon, 7, 710, (1969).

Glemser, Von O., Einerhand, J., Z. Anorg. Chem., 261, 26, (1950A).

Glemser, Von O., Einerhand, J., Z. Anorg. Chem., 261, 43, (1950B).

Gluud, W., Otto, K.V., Ritter, H., Ber., 62B, 8483, (1929).

Gomer, R., Mayer, L., J. Chem. Phys., 23, 1370, (1955).

Grenga, H.E., Lawless, K.R., 6th Int. Cong. Elect. Micros. (Tokyo), 551, (1966).

Grisdale, R.O., Pfister, A.C., Van Rosbroeck, W., Bell. System Tech. J., 30, 271, (1951).

Grisdale, R.O., J. Appl. Phys., 24, 1082, (1953).

Gulbransen, E.A., Copan, T.P., Disc. Far. Soc., 28, 229, (1959).

Haddon, W., B.Sc. Thesis Glasgow University, (1972).

Hagg, Von G. Jernkontorets Ann., 118, 173, (1934A).

Hagg, Von G., Z. Krist, 89, 92, (1934B).

Hall, C.E., J. Appl. Phys., 19, 271, (1948).

Hall, C.E., " Introduction to Electron Microscopy" , McGraw-Hill N.Y., (1953).

Hansen, M., " Constitution of Binary Alloys" , McGraw-Hill N.Y., (1958).

Harvey, J., Matthews, H.I., Wilman, H., Disc. Far. Soc., 30, 113, (1960).

Hashimoto, H., Naiki, T., Eko, T., Fujiwara, K., Watanabe, M., Nagahama, Y., 6th Conf. on Elect. Micros., 181, (1966).

Hassel, O., Mark, H., Z. Physik, 25, 317, (1924).

Heckman, F.A., Harling, D.F., Rubber Chem. and Tech., 39, 1, (1966).

Heckman, F.A., Harling, D.F., Int. Conf. Mat. Plast. Elast., 35, 80, (1969).

Heide, H.G., Proc. 4th Int. Cong. Elect. Micros., 1, 82 Berlin, (1958).

Heide, H.G., Z. Ang. Phys., 15, 116, (1963).

Heidenreich, R.D., " Fundamentals of Transmission Electron Microscopy",John Wiley N.Y., (1964).

Heidenreich, R.D., Siemens Review, 34, 4, (1967).

Henry, T.F., Bull. Soc. Chim. Belg., 72, 740, (1963).

Hillier, J., J. Appl. Phys., 19, 226, (1948).

Hilpert, S., Dieckmann, T., Ber., 48, 1281, (1915).

Hirai, T., Yajima, S., J. Mat. Sci., 2, 18, (1967).

Hirsch., P.B., Howie, A., Nicholson, R.B., Pashley, D.W., Whelan, M.J., " Electron Microscopy of Thin Crystals" , Butterworths London, (1965).

Hofer, L.J.E., Cohn, E.M., Peebles, W.C., J. Amer. Chem. Soc., 71, 189, (1948).

Hofman, U., Ber., 61B, 1180, (1928).

Hofman, U., Groll, E., Z. Anorg. Allg. Chem., 191, 414, (1930).

Hofman, U., Wilm, D., Z. Electrochem., 42, 504, (1936).

Hoppe, W., Naturwiss., 48, 736, (1961).

Hoppe, W., Optik, 20, 599, (1963).

Hoppe, W., Hill, H.C., " Introduction to Mass Spectrometry" , Heydon London, (1966).

Hoppe, W., Katerbau, K.-H., Langer, R., Mollenstedt, G., Spiedel, R., Thon, F., Siemens Review, 36, 24, (1969).

Hughes, E.E.G., Thomas, J.M., Fuel, 41, 297, (1962).

Imperial, G.R., Walker, P.L., Nature, 180, 1184, (1957).

Jack, K.H., Nature, 158, 60, (1946).

Jack, K.H., Proc. Roy. Soc., A195, 56, (1948).

Jacobson, B., Westgren, A., Z. Phys. Chem., B20, 361, (1933).

Janssen, M.M.P., J. Appl. Phys., 40, 3055, (1969).

Jenkins, F.A., White, H.E., " Fundamentals of Optics" , McGraw-Hill N.Y., (1951).

Juliard, A., Rayet, R., Ludo, A., Disc. Far. Soc., 4, 1930, (1948).

Kaito, C., Fusita, K., Naiki, T., Jap. J. Appl. Phys., 9, 151, (1970).

Kammlott, G.W., Surf. Sci., 25, 120, (1971).

Karcher, W., Glaude, P., Carbon, 9, 617, (1971).

Karu, A.E., Beer,M., J. Appl. Phys., 37, 2179, (1966).

Kay, D., " Techniques for Electron Microscopy" , Alden Press, Oxford, (1965).

Kearby, K.K., " Catalysis III" Chapter 10, Emmett, Reinhold N.Y., (1955).

Kehrer, V.J., Leidheiser, H., J. Phys. Chem., 58, 550, (1954).

Kimmer, J.T., Browning, L.C., Emmett, P.H., J. Chem. Phys., 16, 739, (1948A).

Kimmer, J.T., de Witt, T.W., Emmett, P.H., J. Amer. Chem. Soc., 70, 3632, (1948B).

Kimoto, K., Kamiyo, Y., Nonoyama, M., Uyeda, R., Jap. J. Appl. Phys., 2, 702, (1963).

Kimoto, K., Nisida, I., Uyeda, R., 6th Conf. on Elect. Micros., 531, (1966).

Kittaka, S., Kaneko, T., Jap. J. Appl. Phys., 8, 860, (1969).

Knoll, M., Ruska, E., Ann. de Physik, 12, 307, (1932).

Kohlhaas, R., Meyer, W.F., Metalwirt Metallwiss Metalltech, 17, 786, (1938).

Konig, H., Z. Phys., 129, 483, (1951).

Kryukov, Y.B., Bashkirov, A.N., Liberov, L.G., Fridman, R.A., Kinet. Katal., 12, 107, (1970).

Kuo, K., J. Iron Steel Inst., 173, 363, (1959).

Kuteliya, E.R., Utevskii, L.M., Metall. Term. Olvab. Metal, 161, 4, (1969A).

Kuteliya, E.R., Utevskii, L.M., Fiz. Metal Metalloved, 28, 129, (1969B).

Kuteliya, E.R., Fiz. Metal Metalloved, 28, 833, (1969).

Laidler, D., Taylor, A., Nature, 146, 130, (1940).

Lander, J.J., Kern, H.E., Beach, A.L., J. Appl. Phys., 23, 1305, (1952).

Larikov, L.N., Dubovitskaya, N.V., Strukt. Svoytra. Teks. Metal Splavov Mater. Soveshch, 160, (1965).

Leidheiser, H., Gwathmey, A.T., J. Amer. Chem. Soc., 70, 1206, (1948).

Le Poole, J.B., Philips Techn. Rundsch., 9, 633, (1971).

Lieberman, M.L., Hills, C.R., Miglionico, C.J., Carbon, 9, 633, (1971).

Lipson, H., Petch, N.J., J. Iron Steel Inst., 142, 95, (1940).

Lipson, H., Stokes, A.R., Nature, 149, 328, (1942).

Lobo, L.S. Ph.D. Thesis, London University, (1971).

Lobo, L.S., Trimm, D.L., Nature, 234, 15, (1971).

Maahs, H.G., Carbon, 7, 509, (1969).

Mackowsky, M.Th., Nemetschek, Th., Naturw., 43, 442, (1956).

Maire, G., Anderson, J., Johnson, B.B., Proc. Roy. Soc., A320, 227, (1970).

Maire, J., Mehring, J., Proc. Conf. on Carbon (4th), 345, (1960).

Margot, E., Oudar, J., Benard, J., C.R. Acad. Sci., 270, 1261 (1970).

Marsh, H., Warburton, A.P., J. Appl. Chem., 20, 133, (1970).

Matsumoto, H., Saito, Y., Yoneda, Y., J. Catal., 19, 101, (1970).

McCarroll, J.J., Edmonds, T.E. Pitkethly, R.C., Nature, 223, 1260, (1969).

McLellan, R.B., Dunn, W.W., Met. Trans., 1, 535, (1970).

McRae, D.R., J. Metals, 17, 1391, (1965).

Mellor, J.W., " Comprehensive Treatise on Inorg. and Theor. Chem." , Longmans, (1922).

Mizushima, S. Proc. Conf. on Carbon (4th), 3, 417, (1959).

Mollenstedt, G., Spiedel, R., Hoppe, W., Langer, R., Katerbau, K.-H., Thon, F., 4th Eur. Reg. Conf. Elect. Micros. Rome, (1968).

Nagakura, S., Jap. J. Phys. Soc., 12, 482, (1957).

Nagakura, S. Jap. J. Phys. Soc., 13, 1105, (1958).

Nagakura, S., Jap. J. Phys. Soc., 14, 186, (1959).

Nelson, J.B., Riley, D.P., Proc. Roy. Soc., 57, 477, (1945).

Nemetschekt, T., Arch. Eisen., 30, 519, (1959).

Notz, K.J., J. Phys. Chem., 71, 1965, (1967).

Oberlin, A., Rouchy, J.P., Carbon, 9, 39, (1971).

O'Harra, B.M., Darby, W.J., J.Amer. Chem. Soc., 6, 904, (1923).

Olmer, J.F., J. Phys. Chem., 46, 405, (1942).

Otvos, J.W., Stevenson, D.P., J. Amer. Chem. Soc., 78, 546, (1956).

Parkes, G.D., Mellor, J.W., " Modern Inorganic Chemistry" , Chapter 35, Longmans London, (1951).

Parks, G.S., Huffman, H.M., " Free Energy of Some Organic Compounds" , Reinhold, (1932).

Phillips, R., Brit. J. Appl. Phys., 11, 504, (1960).

Pinnick, H.T., J. Chem. Phys., 20, 276, (1952).

Pinsker, Z.G., Kaverin, S.V., Krist., 2, 386, (1957).

Podgurski, H.H., Kimmer, J.T., de Witt, T.W., Emmett, P.H., J. Amer. Chem. Soc., 72, 5382, (1950).

Portele, F., Z. Naturforsch. A., 24, 1268, (1969).

Presland, A.E.B., Hedley, J.A., J. Nucl. Mater. 10, 99, (1963).

Presland, A.E.B., Walker, P.L., Carbon, 7, 1, (1969).

Presland, A.E.B., Roscoe, C., Walker, P.L., Soc. Chem. Ind. London, (1970).

Pugh, H.L.D., Lees, J., Bland, J.A., Nature, 191, 865, (1961).

Renshaw, G.D., Roscoe, C., Walker, P.L., J. Catal., 18, 164, (1970).

Renshaw, G.D., Roscoe, C., Walker, P.L., J. Catal., 22, 394, (1971).

Richardson, F.D., Jeffes, J.H.E., J. Iron and Steel Inst., 163, 397, (1949).

Richardson, J.T., J. Catal., 21, 130, (1971).

Riegar, W., 3rd Conf. Ind. C. and G., (1970).

Rieke, W.D., Optik, 18, 278, (1961).

Riwan, R., Surf. Sci., 27, 267, (1971).

Robertson, S.D., Ph.D. Thesis, Glasgow University, (1968).

Robertson, S.D., Nature, 221, 1044, (1969).

Robertson, S.D., Carbon, 8, 365, (1970).

Robertson, S.D., Carbon, 10, 221, (1972).

Robinovich, E.Y., Rodionov, A.V., Trudy. Vsosoyuz. Mauch. Issl. Inst. Prirod. Gazev, 37, (1959).

Ron, M., Schechter, H., Niedzweidz, S., J. Appl. Phys., 39, 265, (1968).

Roscoe, C., Kline, D.E., Taylor, R.E., Carbon, 8, 95, (1970).

Rostrup-Nielsen, J.R., J. Catal., 21, 171, (1971).

Rudee, M.L., Carbon, 5, 155, (1967).

Saimoto, S., Griffiths, V., Teghfsooman, E., J. Appl. Phys., 31, 1693, (1960).

Saito, T., Gejyo, T., Carbon, 9, 93, (1971).

Schenk, H., Mashlanka, W., Arch. Eisen, 31, 271, (1960).

Schenk, R., Zimmerman, F., Ber., 36, 1232, (1903).

Schenk, R., Stahl, u. Eisen, 46, 665, (1926).

Schenk, R., Z. Anorg. Allg. Chem., 164, 313, (1927A).

Schenk, R., Z. Anorg. Allg. Chem., 164, 145, (1927B).

Schenk, R., Stenkhoff, R., Z. Anorg. Allg. Chem., 161, 287, (1927C).

Schwartz, A.S., Bokros, J.C., Carbon, 5, 325, (1967).

Sears, G.W., Hudson, J.B., J. Chem. Phys., 39, 2380, (1963).

Shalasov, V.A., Zhukov, A.A., Tomas, V.K., Fiz. Mettaloved, 21, 623, (1966).

Shiraski, T., Kitahara, A., Sakamoto, S., Morikawa, K., Kogyo, Kagaku, Zasshi., 68, 596, (1965).

Sidgewick, N.V., " The Chem. Elements and their Compounds" , Clarendon, Oxford, (1962).

Tamai, Y., Nishiyama, Y., Takahashi, M., Kogyo. Kagaku, Zasshi, 70, 889, (1967).

Tamai, Y., Nishiyama, Y., Takahashi, M., Carbon, 6, 593, (1968).

Taylor, A.J., " X-Ray Metallography" , Wiley N.Y., (1961).

Taylor, J.J., Iron Steel Inst., 184, 1, (1956).

Tebboth, J.A., J. Soc. Chem. Ind., 67, 62, (1948).

Tesner, P.A., Robinovich, E.Y., Rafalkes, I.S., Arefieva, E.F., Carbon, 8, 435, (1970).

Thomas, J.M., Walker, P.L., J. Chem. Phys., 41, 587, (1964).

Thon, F., Z. Naturforschg., 21a, 476, (1966A).

Thon, F., 6th Int. Cong. Elect. Micros. Kyoto, (1966B).

Thon, F., Siegal, B.M., 7th Int. Cong. Elect. Micros. Grenoble, (1970).

Trillat, J.J., Oketani, S., C.R. Acad. Sci., 232, 1116, (1951A).

Trillat, J.J., Oketani, S., Metaux Corr. Ind., 26, 145, (1951B).

Tropsch, A., Von Phillopovitch, A., Abhandl. Kennt. Kohle, 7, 44, (1925).

Tutiya, H., Sci. Papers Inst. Phys. Chem. Research (Tokyo), 10, 69, (1929).

Tutiya, H., Bull. Inst. Phys., Chem. Research (Tokyo), 8, 609, (1930A).

Tutiya, H., Bull. Inst. Phys. Chem. Research (Tokyo), 10, 556, (1930B).

Tutiya, H., Bull. Inst. Phys. Chem. Research (Tokyo), 10, 951, (1931).

Van Nostrand Ltd., " Inter. Encyc. of Chem. Science" , (1964).

Venkatachalam, R., Kuriacose, J.C., J. Indian Chem. Soc., 48, 206, (1971).

Walker, P.L., Rakszowski, J.F., Imperial, G.R., J. Phys. Chem., 63, 133, (1959A).

Walker, P.L., Rakzowski, J.F., Imperial, G.R., J. Phys. Chem., 63, 140, (1959B).

Walker, P.L., Thomas, J.M., Carbon, 8, 103, (1970).

Warren, B.E., J. Chem. Phys., 2, 551, (1934).

Warren, B.E., Phys. Rev., 59, 693, (1941).

Waughenheim, F., Brenn. Chem., 8, 385, (1927).

Weistweiler, W., High Temp.-High Press, 2, 187, (1970).

Weller S., Hofer, L.J.E., Anderson, R.B., J. Amer. Chem. Soc., 70, 799, (1948).

White, A.H., Germer, L.H., J. Chem. Phys., 9, 492, (1941).

Wolfe, J.R., Borg, J.R., Carbon, 1, 402, (1964).

Yeorian, Phys. Rev., 48, 631, (1935).

Zworykin, V.K., Morton, G.A., Ramberg, E.G., Hillier, J., Vance, A.W., " Electron Optics and the Electron Microscope" , Wiley N.Y., (1945).